



Durham E-Theses

Intrinsic quarks and heavy flavour production

Spiller, Timothy P

How to cite:

Spiller, Timothy P (1984) *Intrinsic quarks and heavy flavour production*, Durham theses, Durham University. Available at Durham E-Theses Online: <http://etheses.dur.ac.uk/7466/>

Use policy

The full-text may be used and/or reproduced, and given to third parties in any format or medium, without prior permission or charge, for personal research or study, educational, or not-for-profit purposes provided that:

- a full bibliographic reference is made to the original source
- a [link](#) is made to the metadata record in Durham E-Theses
- the full-text is not changed in any way

The full-text must not be sold in any format or medium without the formal permission of the copyright holders.

Please consult the [full Durham E-Theses policy](#) for further details.

Intrinsic Quarks and Heavy Flavour Production

Thesis submitted to the University of Durham
for the degree of Doctor of Philosophy by

Timothy P Spiller, BA (Oxford)

May 1984

The copyright of this thesis rests with the author.
No quotation from it should be published without
his prior written consent and information derived
from it should be acknowledged.



13. AUG. 1984

CONTENTS

ABSTRACT	i
ACKNOWLEDGEMENTS	ii
CHAPTER 1: MOTIVATION, BACKGROUND AND MODEL	
1.1 MOTIVATION	
1.1.1 Recent Experimental Data	1
1.1.2 Failure of Old Models	1
1.2 NEW MODELS FOR HEAVY FLAVOUR PRODUCTION	2
1.3 OUR MODEL: AIM AND CONSTRUCTION	6
1.4 STANDARD THEORY	
1.4.1 Cross-Sections and Widths	8
1.4.2 QED, QCD and Regge Theory	9
1.4.3 The Optical Theorem	10
1.5 LIGHT CONE VARIABLES	11
1.6 THE PARTON MODEL	12
1.7 DIMENSIONAL COUNTING RULES	18
CHAPTER 2: VALENCE QUARK DISTRIBUTIONS	
2.1 INTRODUCTION	25
2.2 MESON WAVEFUNCTION	28
2.3 BARYON WAVEFUNCTION	31
2.4 GENERAL CALCULATION	36
2.5 TRANSVERSE MOMENTUM	39
2.6 RESULTS	43
2.7 COMMENTS AND COMPARISON WITH EXPERIMENT	45
CHAPTER 3: HEAVY QUARK FRAGMENTATION FUNCTIONS	
3.1 DISTRIBUTION OF TWO SPINLESS CONSTITUENTS	
3.1.1 Introduction	59

3.1.2	Wavefunction Model and Calculation	63
3.2	FRAGMENTATION FUNCTIONS	65
3.3	WAVEFUNCTION MODEL	69
3.4	CALCULATION	71
3.5	COMPARISON WITH EXPERIMENT	75
CHAPTER 4: INTRINSIC HEAVY QUARKS		
4.1	INTRODUCTION	81
4.2	WAVEFUNCTION MODEL MOTIVATED BY PERTURBATIVE QCD	82
4.3	GENERAL CALCULATION	84
4.4	EXPLICIT SOLUTIONS FOR PION AND NUCLEON	89
4.5	COMMENTS	92
4.6	RELATION OF DISTRIBUTION FUNCTIONS TO OBSERVABLES	95
4.7	NUCLEON INTRINSIC CHARM VERSUS THE DATA	97
CHAPTER 5: THE SCATTERING PROCESS		
5.1	INTRODUCTION	102
5.2	EFFECTIVE HADRON-QUARK CROSS-SECTIONS	106
5.3	THRESHOLD RISE	
5.3.1	Counting Rule Suppression (Dynamics)	112
5.3.2	Limited Availability of Phase-space (Kinematics)	116
5.4	CHARM PRODUCTION IN γp INTERACTIONS	122
5.5	COMPARISON WITH THE DATA	126
CHAPTER 6: HADRONIC HEAVY FLAVOUR PRODUCTION		
6.1	THE MODEL	131
6.2	RECOMBINATION FUNCTIONS	135
6.3	RESULTS AND COMPARISON WITH EXPERIMENT	138
6.4	LEPTONS FROM TOP QUARKS AT THE COLLIDER	158
CHAPTER 7: SUMMARY AND CONCLUSIONS		
		170
REFERENCES		
		176

INTRINSIC QUARKS AND HEAVY FLAVOUR PRODUCTION

Timothy P Spiller

ABSTRACT

A model is constructed for the diffractive production of heavy flavours in hadron-hadron interactions, based on the presence of an intrinsic heavy quark component in the hadron wavefunction. It requires three ingredients; the heavy quark content of the initial hadron, the probability that these heavy quarks are scattered, and the probability that they form heavy flavoured hadrons afterwards.

The initial heavy quark distributions are calculated, using lowest order perturbative QCD, starting from the valence constituent quark distributions, and compared with deep inelastic charm production data. The valence distributions are designed to reproduce the dimensional counting rules, and, via reciprocity, to be consistent with the heavy quark fragmentation functions.

The light quark-hadron scattering cross-section is parametrized by Pomeron exchange, and extended to heavy quarks using the f-dominance hypothesis for the Pomeron-quark coupling. Dynamical and kinematical factors which control the rise of these cross-sections from threshold are built in. The validity of these ideas is tested against charm photo-production data, by using a vector dominance model for the photon-hadron scattering.

The probability that the scattered quarks recombine to produce heavy flavoured hadrons is assumed to be given by the overlap of the initial distribution of quarks with the distribution in a heavy hadron. We compare the predictions of our model with strangeness and charm production data, and make predictions for bottom and top production. In particular, the magnitude of the leptonic signal to be expected from the decay of top quarks produced at the CERN $p\bar{p}$ -Collider is given.

We conclude that all aspects of this model are consistent with present experimental data, and that the top quark should be observed at the Collider if its mass is around 35 GeV.

ACKNOWLEDGEMENTS

It has been my pleasure to pursue this research under the supervision of Peter Collins, who provided numerous ideas and much advice. I thank him, the other staff members at Durham, Alan Martin, Mike Pennington and Fred Gault, and the many research students; in particular Tony Rimmer, Phil Done, James Webb and Anthony Worrall, with whom I overlapped in space as well as time. They all contributed to the friendly stimulating environment in which what follows was concocted.

My thanks also to the SERC for a three year research studentship, and to Ruth Robson for her excellent typing.

There is a theory which states that if ever anyone discovers exactly what the Universe is for and why it is here, it will instantly disappear and be replaced by something even more bizarre and inexplicable.

There is another theory which states that this has already happened.

From *The Restaurant at the End of the Universe* by Douglas Adams.

CHAPTER 1

MOTIVATION, BACKGROUND AND MODEL

1.1 MOTIVATION

1.1.1 Recent Experimental Data

A lot of hadron-hadron scattering experiments have been done over the last decade, at various energies. It is found that heavy flavoured hadrons are produced quite frequently compared to light ones, roughly in the ratios

$$(u,d) : s : c \sim 1 : 1/4 : 10^{-2} \sim 10^{-3} \quad (1.1.1)$$

at the highest energies.

There appear to be two production mechanisms for heavy flavoured particles. Most are created "centrally", with small centre of mass (COM) momenta compared to that of the beams, but some (about 1/5) go "forward", with a sizeable momentum. The latter always have small transverse momentum (relative to the beam), so it is quite clear which initial hadron they came from. Such production is termed "diffractive".

1.2.1 Failure of Old Models

The older hadron production models fall into two categories.



(a) Statistical models⁽¹⁾, in which the probability of producing a hadron of mass m is $\sim \exp(\frac{-2m}{T})$ (a Boltzmann factor) where T is a universal temperature ~ 160 MeV.

This gives

$$(u,d) : s : c \sim 1 : 10^{-1} : 10^{-5} \quad (1.1.2)$$

(b) Tunnelling models⁽²⁾, in which the probability of producing a quark-antiquark pair (which then hadronize) is $\sim \exp(\frac{-\pi \langle m_{TQ}^2 \rangle}{K})$ where the string constant $K \sim 0.2$ GeV². $\langle m_{TQ}^2 \rangle$ is defined by $\langle m_{TQ}^2 \rangle \equiv m_Q^2 + \langle k_T^2 \rangle$, where m_Q is the quark mass and $\langle k_T^2 \rangle \sim 0.1$ GeV². This gives

$$(u,d) : s : c \sim 1 : 1/3 : 10^{-10} \quad (1.1.3)$$

Both give the right order of magnitude for strangeness production, but are far too small for charm, and neither explains the observed momentum distributions. Over the last few years there have been attempts to improve on these predictions.

1.2 NEW MODELS FOR HEAVY FLAVOUR PRODUCTION

Numerous predictions for hadronic charm production exist⁽³⁾, based on the expression

$$\sigma(AB \rightarrow c\bar{c}X) = \sum_{i,j} \int dx_i dx_j f_A^i(x_i) f_B^j(x_j) \theta(ij \rightarrow c\bar{c}) \quad (1.2.1)$$

for the cross-section. $f_A^i(x_i)$ is the probability density

for finding parton i in hadron A with longitudinal momentum fraction x_i . The parton amplitudes for the sub-process cross-section, $\hat{\sigma}$, come from perturbative QCD⁽⁴⁾, and are shown in figure 1.1. The $c\bar{c}$ pair are created centrally and assumed to fragment to form hadrons. The calculations use the measured x -distributions for light quarks and gluons, but assume values for the strong coupling α_s , the charmed quark mass m_c , and the threshold for the sub-process. For reasonable choices of these the predictions are generally too small to account for the central production of Section 1.1.1.

Barger et al⁽⁵⁾ also consider the excitation amplitudes of figure 1.2, as a possible explanation for the diffractive charm production. This requires additional assumptions for the magnitude and shape of $f_A^C(x_c)$. They argue this arises from QCD evolution, and that at $Q^2 \sim 4m_c^2$ is "hard", in order to fit the data, evolving to lower x_c at larger Q^2 to avoid conflict with deep inelastic scattering data. The charmed hadrons are produced by recombination with the valence quarks.

A model fusing a diquark from one hadron with a quark from the other has been proposed by Donnachie⁽⁶⁾, and tested against strange baryon production data. This requires assumptions for the magnitude and

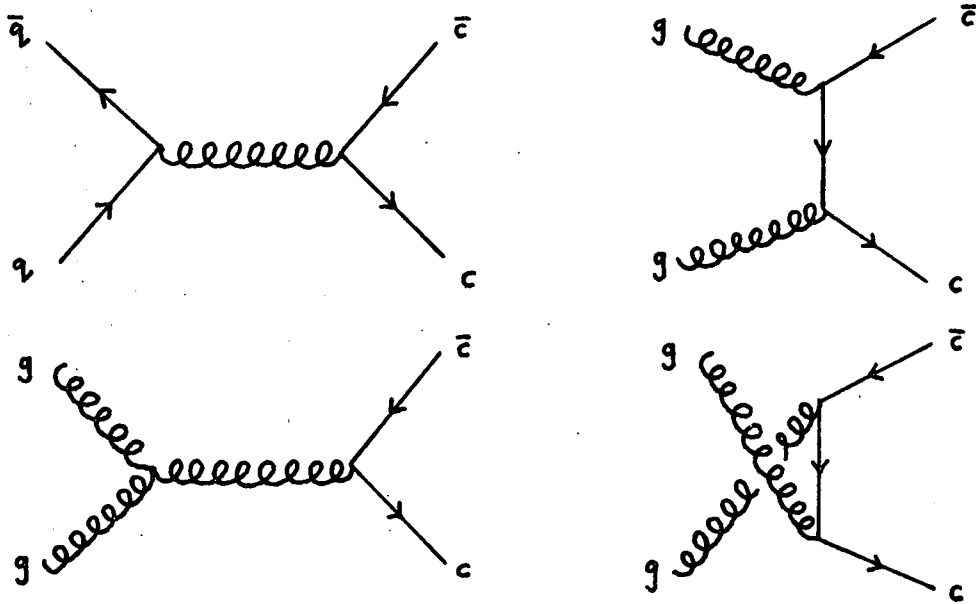


Figure 1.1: The parton amplitudes for $ij \rightarrow c\bar{c}$.

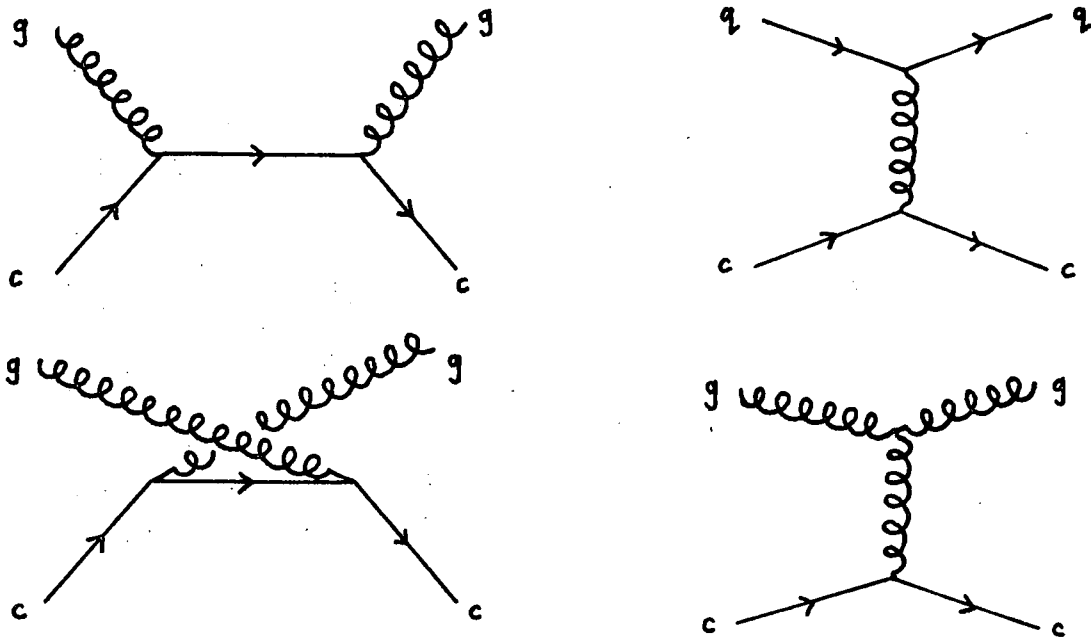


Figure 1.2: The parton amplitudes for $ic \rightarrow ic$.

shape of the diquark distribution.

Brodsky et al⁽⁷⁾ propose an explanation for diffractive charm production using the idea of "intrinsic" charm. They model the contribution to $f_p^C(x_c)$ from the $|uudc\bar{c}\rangle$ Fock state of the proton, and conclude that the heavy quarks carry most of the momentum. The final hadrons are again produced via a reformation process, the normalization being fixed from experiment.

These diffractive models contain uncertainties. Normalization to fit data is needed, and possible difficulties in recombining the quarks into hadrons are neglected. Extrapolation to heavier masses from charm is simply assumed to scale like m_c^2/m_i^2 ($i=b,t$), either in the intrinsic cross-section, or the inverse of the threshold for the diffractive excitation sub-process.

Insert A.

1.3 OUR MODEL: AIM AND CONSTRUCTION

We propose a model for diffractive heavy flavour production, based on the idea of intrinsic heavy quarks, and regard central production as a separate effect, still to be satisfactorily explained. We aim to avoid some of the uncertainties of the existing models. Using a proton as an example, the basic idea is that a heavy quark Q in the proton's $|uudQ\bar{Q}\rangle$ Fock state scatters "softly" on the other hadron, and the quarks then recombine to form heavy flavoured hadrons.

The $Q\bar{Q}$ are pair-created inside the proton. As they are heavy we model this by lowest order perturbative QCD. Consequently the relative normalization of the Fock states $|uud\rangle$ and $|uudQ\bar{Q}\rangle$ is predicted. The quarks in these states are constituents, as between them they carry all of the proton's momentum.

In Chapter 2 we model valence constituent quark distributions, ensuring they satisfy the dimensional counting rules (see Section 1.7), and support these in Chapter 3 by considering heavy quark fragmentation. Chapter 4 is devoted to the calculation of intrinsic heavy quark distributions in light hadrons.

Unlike deep inelastic scattering, diffractive scattering is soft, and so the appropriate framework is Regge theory⁽⁸⁾. We discuss this in Chapter 5, and calculate heavy quark-hadron cross-sections.

Since recombination functions are essentially valence distributions, we then have all the ingredients to predict hadronic heavy flavour production, which is the topic of Chapter 6. We present our conclusions in Chapter 7.

In the remainder of this chapter we introduce the background theory and ideas we need, and define our notation for the calculation of cross-sections, parton

densities etc. This may be omitted, and simply used for reference, by the reader familiar with this framework.

1.4 STANDARD THEORY

1.4.1 Cross-Sections and Widths

The cross-section for $AB \rightarrow N$ particles is given by

$$\frac{\sigma(AB \rightarrow N)}{|A_{AB \rightarrow N}|^2} = \frac{1}{h} \int \prod_{i=1}^N \left[\frac{d^3 p_i}{2(2\pi)^3 p_i^0} \right] (2\pi)^4 \delta^4(p_A + p_B - \sum_{i=1}^N p_i) \quad (1.4.1)$$

Similarly for a width

$$\frac{\Gamma(A \rightarrow N)}{|A_{A \rightarrow N}|^2} = \frac{1}{2p_A^0} \int \prod_{i=1}^N \left[\frac{d^3 p_i}{2(2\pi)^3 p_i^0} \right] (2\pi)^4 \delta^4(p_A - \sum_{i=1}^N p_i) \quad (1.4.2)$$

In both cases $|A|^2$ is the squared modulus of the amplitude for an N-particle final state, averaged over initial spins and summed over final ones, p_i are the relevant four-momenta, and h is the flux factor, defined by

$$h \equiv 4 [(p_A \cdot p_B)^2 - m_A^2 m_B^2]^{\frac{1}{2}} \quad (1.4.3)$$

σ is Lorentz invariant while Γ^{-1} transforms as the zeroth component of a four-vector, (hence the dilation of lifetimes).

1.4.2 QED, QCD and Regge Theory

Our work will require frequent evaluation of amplitudes, such as in (1.4.1). When these are unknown we resort to modelling, but also call on QED⁽⁹⁾, QCD⁽⁴⁾ and Regge theory⁽⁸⁾.

We use QED, the U(1) gauge theory of electromagnetism, when considering the scattering of leptons and quarks, and also need weak interactions⁽¹⁰⁾ (the other half of the SU(2) x U(1) electro-weak theory) when considering leptonic decays of heavy quarks.

When calculating amplitudes we employ these theories perturbatively. The Feynman rules are conveniently listed in the appendices of Itzykson and Zuber⁽⁹⁾, as are many other standard results (eg trace theorems) and we adopt their notation throughout, except for defining the normalization of Dirac spinors by

$$\bar{u}(p,s)u(p,s) \equiv 2m \quad (1.4.4)$$

The spin summation then reads

$$\sum_s u(p,s)\bar{u}(p,s) = \not{p} + m \quad (1.4.5)$$

with the advantage that (1.4.1) and (1.4.2) hold for any combination of bosons and fermions. In all our

diagrams a photon is represented by  and a gluon by .

The QCD approach to hadron physics has deficiencies. At present quark confinement is not proven, and many features of hadron structure and scattering, particularly at high energy and low momentum-transfer, remain to be explained. However Regge theory has far more success with the latter, and so this is the approach we introduce and use when considering such scattering.

1.4.3 The Optical Theorem

Summing (1.4.1) over all possible final states gives the total cross-section. Using unitarity the right hand side may be re-written in terms of the elastic scattering amplitude at zero momentum-transfer, giving the optical theorem

$$\sigma_{\text{tot}}(AB) = \frac{2}{\hbar} \text{Disc}(A_{AB \rightarrow AB}) \quad (1.4.6)$$

We employ this occasionally, but Mueller's generalization⁽¹¹⁾ will be more useful. This says

$$16\pi^3 E_C \frac{d^3\sigma}{d^3p_C}(AB \rightarrow CX) = \frac{2}{\hbar} \text{Disc}(A_{ABC \rightarrow ABC}) \quad (1.4.7)$$

where again the discontinuity is evaluated with the final momenta equal to the initial. X is any hadronic final state. The derivation of (1.4.7) is the same as that of

(1.4.6), with the crossing of the final C to an initial \bar{C} . As a result the amplitude is at an unphysical value of $p_{\bar{C}}$. We simply assume this analytic continuation can be made; for a discussion see Reference 8, Section 10.4.

To evaluate discontinuities we use the rules due to Cutkosky⁽¹²⁾.

1.5 LIGHT CONE VARIABLES

Usually we will treat four-momenta in terms of their light cone components, defined by

$$p_A^\pm \equiv p_A^0 \pm p_A^3 \quad ; \quad p_{TA} \equiv (p_A^1, p_A^2) \quad (1.5.1)$$

and use the projection operator P_μ^+ , defined by

$$P_\mu^+ p_A^\mu \equiv p_A^+ \quad (1.5.2)$$

Under a Lorentz boost (with velocity β , and $\gamma \equiv (1 - \beta^2)^{-\frac{1}{2}}$) along the 3-axis, $p_A^\mu \rightarrow p_A'^\mu$, where

$$p_A'^\pm = \gamma(1 \mp \beta)p_A^\pm \quad ; \quad p_{TA}' = p_{TA} \quad (1.5.3)$$

Therefore any ratios of the form

$$x_i \equiv \frac{k_i^+}{p_A^+} \quad (1.5.4)$$

are invariant. For example, p_A and k_i are our notation for hadron and quark momenta respectively. The Jacobian for the variable change of (1.5.1) is $\frac{1}{2}$, so, using (1.5.4),

$$d^4 k_i = \frac{1}{2} dk_i^+ d^2 \underline{k}_{Ti} dk_i^- = \frac{1}{2x_i} dx_i d^2 \underline{k}_{Ti} d(k_i^2) \quad (1.5.5)$$

In terms of these variables dot products read

$$2p_A \cdot k_i = x_i (p_A^2 + p_{TA}^2) + \frac{1}{x_i} (k_i^2 + k_{Ti}^2) - 2p_{TA} \cdot \underline{k}_{Ti}$$

$$2k_i \cdot k_j = \frac{x_i}{x_j} (k_j^2 + k_{Tj}^2) + \frac{x_j}{x_i} (k_i^2 + k_{Ti}^2) - 2\underline{k}_{Ti} \cdot \underline{k}_{Tj} \quad (1.5.6)$$

1.6 THE PARTON MODEL

Whenever a hadron is probed sufficiently hard for its structure to be resolved, it is found to consist of almost free "current" quarks and gluons (collectively, partons)^(13,14). This is in agreement with QCD, since the strong coupling $\alpha_s(Q^2) \rightarrow 0$ as $Q^2 \rightarrow \infty$ ⁽⁴⁾. An interaction involves the scattering of one or more partons, which then hadronize in some way. An example is shown in figure 1.3.

We define the standard variables Bjorken- x and v by

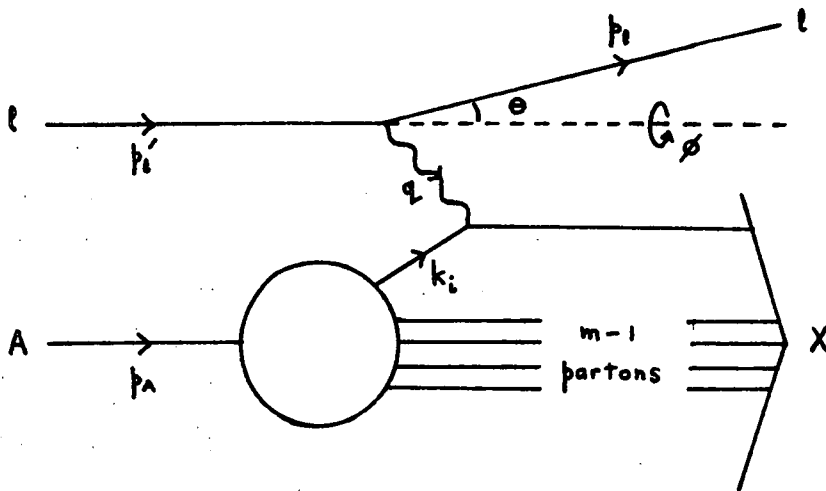


Figure 1.3: The parton diagram for deep inelastic electromagnetic lepton (l) - hadron (A) scattering, showing the four-momenta of the particles. In the hadron rest frame, $(p_A = (m_A, \underline{0}))$, we define $p_l \equiv (E_l, \underline{p}_l)$ and $p_l' \equiv (E_l', \underline{p}_l')$, and the angles θ, ϕ as shown.

$$x \equiv \frac{-q^2}{2p_A \cdot q} \quad ; \quad v \equiv p_A \cdot q \quad (1.6.1)$$

and $f_A^i(x_i)$ as the probability density of a quark i being in hadron A with light cone momentum fraction x_i , defined by (1.5.4). The cross-section for the process in figure 1.3 is

$$16\pi^3 E_1 \frac{d^3\sigma}{d^3p_1} (1A \rightarrow 1X) \equiv \sum_{m \geq n} \sum_{i=1}^m \int_0^1 dx_i f_A^i(x_i) 16\pi^3 E_1 \frac{d^3\sigma}{d^3p_1} (1q_i \rightarrow 1q_i) \quad (1.6.2)$$

where n is the number of valence quarks in A , and X is any hadronic final state. This assumes an incoherent sum over all possible parton final states is equivalent to the same for hadrons.

However our parton model will differ from the standard one, since when deriving f 's we will consider only the lowest possible value of m . The distributions are then considered to be those of constituent quarks, which can be thought of as bare current quarks surrounded by a sea of $q\bar{q}$ pairs and gluons. We use light cone variables, but we shall not neglect masses (except those \ll hadron masses) or off mass-shell effects. If we do, though, the usual results emerge, which we demonstrate as a check, and to introduce our notation.

The hadron tensor, $W_{\mu\nu}$, is defined by

$$16\pi^3 E_1 \frac{d^3\sigma}{d^3 p_1} (1A \rightarrow 1X) \equiv \frac{8\pi^3 \alpha^2}{E_1' q^4} L^{\mu\nu} W_{\mu\nu} \quad (1.6.3)$$

Neglecting the lepton mass, the lepton tensor is

$$L^{\mu\nu} \equiv \text{Tr}\{\not{p}_1' \gamma^\mu \not{p}_1 \gamma^\nu\} \quad (1.6.4)$$

while

$$\alpha \equiv \frac{e^2}{4\pi} \approx \frac{1}{137} \quad (1.6.5)$$

e being the lepton charge. The most general gauge-invariant expression for $W_{\mu\nu}$ is⁽¹⁵⁾

$$\begin{aligned} W_{\mu\nu} = & W_1(\nu, q^2) \left(-g_{\mu\nu} + \frac{q_\mu q_\nu}{q^2} \right) + \frac{W_2(\nu, q^2)}{m_A^2} \\ & \left(p_{A\mu} - \frac{q \cdot p_A}{q^2} q_\mu \right) \left(p_{A\nu} - \frac{q \cdot p_A}{q^2} q_\nu \right) \end{aligned} \quad (1.6.6)$$

Using the differential form of (1.4.1) with $N = 2$, the Feynman rules for QED, and integrating over the quark momentum gives

$$\begin{aligned} 16\pi^3 E_1 \frac{d^3\sigma}{d^3 p_1} (1q_i \rightarrow 1q_i) &= \frac{e^4 e_i^2 (2\pi)}{4hq^4} \theta((k_i+q)^0) \delta((k_i+q)^2 - m_i^2) \\ & L^{\mu\nu} T_{2\mu\nu}(k_i, k_i+q) \\ &= \frac{8\pi^3 \alpha^2 e_i^2}{hq^4} \theta((k_i+q)^0) \delta((k_i+q)^2 - m_i^2) \\ & L^{\mu\nu} T_{2\mu\nu}(k_i, k_i+q) \end{aligned} \quad (1.6.7)$$

where ee_i is the quark charge and

$$T_{2\mu\nu}(k_i, k_i+q) \equiv \text{Tr} \{ (k_i+m_i) \gamma_\mu (k_i+q+m_i) \gamma_\nu \} \quad (1.6.8)$$

Evaluating the trace gives

$$T_{2\mu\nu}(k_i, k_i+q) = 4 [k_{i\mu} (k_i+q)_\nu + k_{i\nu} (k_i+q)_\mu - g_{\mu\nu} (k_i \cdot (k_i+q) - m_i^2)] \quad (1.6.9)$$

Using (1.6.7) and (1.6.3), (1.6.2) becomes

$$\frac{W_{\mu\nu}}{E_1'} = \sum_{m \geq n} \sum_{i=1}^m \int_0^1 dx_i f_A^i(x_i) \frac{e_i^2}{h} \theta((k_i+q)^0) \delta((k_i+q)^2 - m_i^2) T_{2\mu\nu}(k_i, k_i+q) \quad (1.6.10)$$

We substitute in (1.6.9) and (1.6.6), and then operate with $P^{+\mu} P^{+\nu}$ (as defined by (1.5.2)) to obtain

$$\begin{aligned} & \frac{1}{E_1'} \left[\frac{W_1(\nu, q^2)}{q^2} q^{+2} + \frac{W_2(\nu, q^2)}{m_A^2} (p_A^+ - q \cdot p_A) q^{+2} \right] \\ &= \sum_{m \geq n} \sum_{i=1}^m \int_0^1 dx_i f_A^i(x_i) \frac{e_i^2}{h} \theta((k_i+q)^0) \\ & \delta((k_i+q)^2 - m_i^2) 8k_i^+ (k_i+q)^+ \quad (1.6.11) \end{aligned}$$

Neglecting the quark mass

$$\delta((k_i+q)^2 - m_i^2) = \frac{1}{2v} \delta(x_i - x) \quad (1.6.12)$$

and, from (1.4.3),

$$h = 4m_A x_i E_1' \quad (1.6.13)$$

Using (1.6.12) the integral in (1.6.11) is trivial, and defining $F_{1,2}$ by

$$F_1 \equiv m_A W_1(v, q^2) \quad ; \quad F_2 \equiv \frac{v}{m_A} W_2(v, q^2) \quad (1.6.14)$$

the result is

$$\frac{F_1 q^{+2}}{q^2} + \frac{F_2}{v} (p_A^+ - \frac{v}{q^2} q^+)^2 = \sum_{m \geq n} \sum_{i=1}^m f_A^i(x) \frac{e_i^2}{xv} k_i^+ (k_i+q)^+ \quad (1.6.15)$$

There is no q^{+2} coefficient on the right, so that on the left must vanish, giving

$$2xF_1 = F_2 = \sum_{m \geq n} \sum_{i=1}^m f_A^i(x) x e_i^2 \quad (1.6.16)$$

This is the familiar result for the structure functions $F_{1,2}$, showing they are functions of x only, obey the Callan-Gross relation⁽¹⁶⁾, and are related to the quark distribution functions in the usual way.

1.7 DIMENSIONAL COUNTING RULES

The dimensional counting rules⁽¹⁷⁾ describe the behaviour of the elastic cross-section at large $-q^2$, shown in figure 1.4 for lepton-baryon scattering. Consider the amplitude for reforming A (the elastic form factor, $G_A(q^2)$) containing n_g gluons, necessary to hold the hadron together. In QCD the fermion traces typically cancel the behaviour of the gluon propagators⁽¹⁸⁾, as we shall demonstrate in Chapter 2. The fermions labelled —X— in figure 1.4 have four-momenta² $\sim q^2$, and so their propagator denominators give the q^2 -dependence of $G_A(q^2)$,

$$G_A(q^2) \sim q^{-2n_g} \quad (1.7.1)$$

(1.4.1) with $N=2$ integrates to give

$$\sigma(1A \rightarrow 1A) = \frac{1}{h} \int \frac{d^3 p_1}{2E_1 (2\pi)^3} (2\pi) \theta((p_A+q)^0) \delta((p_A+q)^2 - m_A^2) \overline{|A_{1A \rightarrow 1A}|^2} \quad (1.7.2)$$

Neglecting the lepton mass

$$dq^2 \cong -2E_1 E_1' d(\cos\theta) \quad ; \quad d|p_1| \cong dE_1 \quad (1.7.3)$$

so

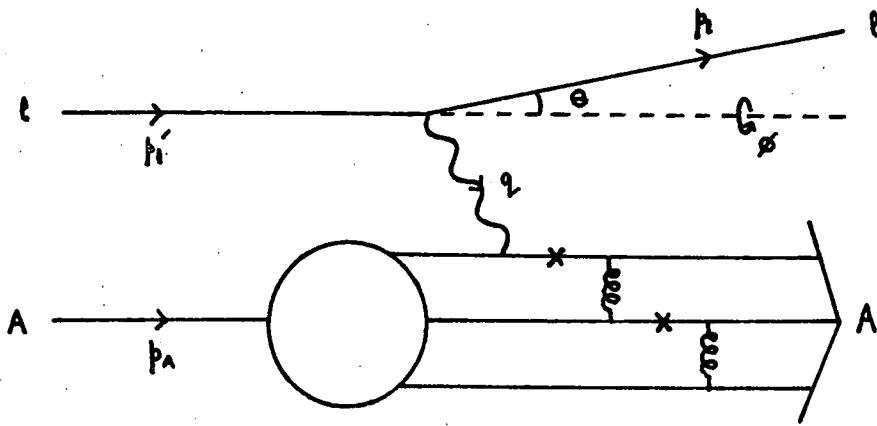


Figure 1.4: The parton diagram for elastic lepton (l) - hadron (A) scattering, with the same definitions for four-momenta as in figure 1.3.

$$\frac{d^3 p_1}{2E_1 (2\pi)^3} \delta((p_A+q)^2 - m_A^2) \cong \frac{dE_1 dq^2 d\phi}{8(2\pi)^3 E_1' m_A} \delta(E_1' - E_1 + \frac{q^2}{2m_A}) \quad (1.7.4)$$

and from (1.4.3)

$$h \cong 4E_1' m_A \quad (1.7.5)$$

We substitute these into (1.7.2) and integrate over E_1 and ϕ , but differentiate with respect to q^2 , obtaining

$$\frac{d\sigma(1A \rightarrow 1A)}{dq^2} \cong \frac{|A_{1A \rightarrow 1A}|^2}{64\pi E_1'^2 m_A^2} \quad (1.7.6)$$

a result that will also be of use later on. Including the photon propagator $A_{1A \rightarrow 1A} \sim q^{-2} G_A(q^2)$, so using (1.7.1), (1.7.6) gives

$$\frac{d\sigma(1A \rightarrow 1A)}{dq^2} \sim q^{-4(n_g+1)} \quad (1.7.7)$$

At large $-q^2$, the dominant contribution comes from the minimum n_g , which is $n-1$ (n being the number of valence quarks), giving for mesons (M) and baryons (B)

$$\frac{d\sigma(1M \rightarrow 1M)}{dq^2} \sim_{-q^2 \rightarrow \infty} q^{-8} \quad (1.7.8)$$

$$\frac{d\sigma(1B \rightarrow 1B)}{dq^2} \sim_{-q^2 \rightarrow \infty} q^{-12} \quad (1.7.9)$$

The large $-q^2$ form factor behaviour, (1.7.1), relates to that of the structure function $F_2(x)$ as $x \rightarrow 1$ if figure 1.3 goes over smoothly to figure 1.4 as $M_x^2 \rightarrow m_A^2$. To demonstrate this we require an expression for $\frac{d\sigma}{dq^2}(1A \rightarrow 1X)$, defined by

$$\frac{d\sigma}{dq^2}(1A \rightarrow 1X) \equiv \int dv \delta(v - \frac{1}{2}(M_x^2 - m_A^2 - q^2)) \frac{d^2\sigma}{dq^2 dv}(1A \rightarrow 1X) \quad (1.7.10)$$

to compare with (1.7.7).

The integrand derives from (1.6.2). Neglecting the lepton mass, (1.6.1) give

$$dx = \frac{-E_1 E_1'}{v} d(\cos\theta) \quad ; \quad dv = -m_A d|p_1| = -m_A dE_1 \quad (1.7.11)$$

and using these (1.6.2) becomes

$$\frac{d^3\sigma}{dx dv d\phi}(1A \rightarrow 1X) = \sum_{m \geq n} \sum_{i=1}^m \int_0^1 dx_i f_A^i(x_i) \frac{v E_1}{m_A E_1' d^3 p_1} \frac{d^3\sigma}{d^3 p_1}(1q_i \rightarrow 1q_i) \quad (1.7.12)$$

Substituting (1.6.7) and integrating over ϕ gives

$$\frac{d^2\sigma}{dx dv}(1A \rightarrow 1X) = \sum_{m \geq n} \sum_{i=1}^m \int_0^1 dx_i f_A^i(x_i) \frac{\pi \alpha^2}{m_A E_1' h q^4} \theta((k_i + q)^0) \delta((k_i + q)^2 - m_i^2) L^{\mu\nu} T_{2\mu\nu}(k_i, k_i + q) \quad (1.7.13)$$

Using (1.6.4), (1.6.8), (1.6.10), $p_1' = p_1 + q$, and neglecting the quark mass,

$$\frac{1}{16} L^{\mu\nu} T_{2\mu\nu}(k_i, k_i+q) = 2k_i \cdot p_1 [2k_i \cdot p_1 + 2q \cdot p_1 + 2k_i \cdot q + q^2] - 2q \cdot p_1 q \cdot (q+k_i) \quad (1.7.14)$$

and it is easy to show

$$k_i \cdot p_1 = 2x_i (m_A E_1' - v) \quad ; \quad q \cdot p_1 = xv \quad ; \quad k_i \cdot q = x_i v$$

$$q^2 = -2xv \quad (1.7.15)$$

We use these to re-write (1.7.14) and substitute it, along with (1.6.12) and (1.6.13), into (1.7.13).

Integrating, cancelling, and using (1.6.1) we get

$$\frac{d^2\sigma}{dx dv} (1A \rightarrow 1X) = \sum_{m \geq n} \sum_{i=1}^m f_A^i(x) e_i^2 \frac{2\pi\alpha^2}{x} \left[\frac{1}{v^2} - \frac{1}{vm_A E_1'} + \frac{1}{2m_A^2 E_1'^2} \right] \quad (1.7.16)$$

which is a familiar result⁽¹⁹⁾, in a slightly unfamiliar guise. We need this form in Chapter 4, but here re-write it, using (1.6.1) and (1.6.16), to that required by (1.7.10),

$$\frac{d^2\sigma}{dq^2 dv} (1A \rightarrow 1X) = \frac{-4\pi\alpha^2 v F_2}{q^4} \left[\frac{1}{v^2} - \frac{1}{vm_A E_1'} + \frac{1}{2m_A^2 E_1'^2} \right] \quad (1.7.17)$$

The invariant mass of the final state X is given by

$$M_X^2 \equiv (p_A + q)^2 = m_A^2 + q^2(1 - 1/x)$$

giving

$$-q^2 = \frac{x(M_X^2 - m_A^2)}{(1-x)} \quad (1.7.18)$$

and so for any $M_X^2 > m_A^2$

$$-q^2 \rightarrow \infty \equiv x \rightarrow 1 \quad (1.7.19)$$

All quark distribution functions $f_A^i(x_i) \rightarrow 0$ as $x_i \rightarrow 1$, because of the difficulty in transferring all the momentum to one quark. Suppose the least suppressed behaviour is

$$f_A^i(x_i) \underset{x_i \rightarrow 1}{\sim} (1-x_i)^N \quad (1.7.20)$$

From (1.6.16) and (1.7.19) we deduce

$$F_2 \underset{-q^2 \rightarrow \infty}{\sim} q^{-2N} \quad (1.7.21)$$

Substituting (1.7.17) into (1.7.10), integrating, letting $-q^2 \rightarrow \infty$, and using (1.7.21), we obtain

$$\frac{d\sigma(1A+1X)}{dq^2} \underset{-q^2 \rightarrow \infty}{\sim} q^{-2(N+3)} \quad (1.7.22)$$

This behaviour is for $M_x^2 > m_A^2$; if we assume that it connects smoothly to the elastic region, and compare with the most dominant form of (1.7.7) we get

$$N = 2n_{gmin} - 1 \quad (1.7.23)$$

the Drell-Yan-West relation⁽²⁰⁾.

CHAPTER 2

VALENCE QUARK DISTRIBUTIONS

2.1 INTRODUCTION

In this chapter we calculate the distribution of valence quarks in an arbitrary hadron A. More precisely we shall derive expressions for the x-distribution of the quark (or antiquark) in the $|q\bar{q}\rangle$ Fock state of a meson, and of the quarks in the $|qqq\rangle$ state of a baryon. For light hadrons these are the input for calculating the x-distributions of intrinsic heavy $Q\bar{Q}$ pairs, and for heavy hadrons (containing a valence Q or \bar{Q}) give their recombination functions, which are two of the ingredients for our diffractive model.

The calculations require several assumptions, which we introduce, along with their justification, as needed. At the end of this chapter we compare the results with experimental data.

In order to derive x-distributions without neglecting masses, or off mass-shell effects, we begin by considering the lepton-hadron inelastic scattering of figure 1.3. Probing the hadron with a photon is merely a calculational tool; during the course of our derivation the dependence on the photon four-momentum q will cancel. This must happen, because

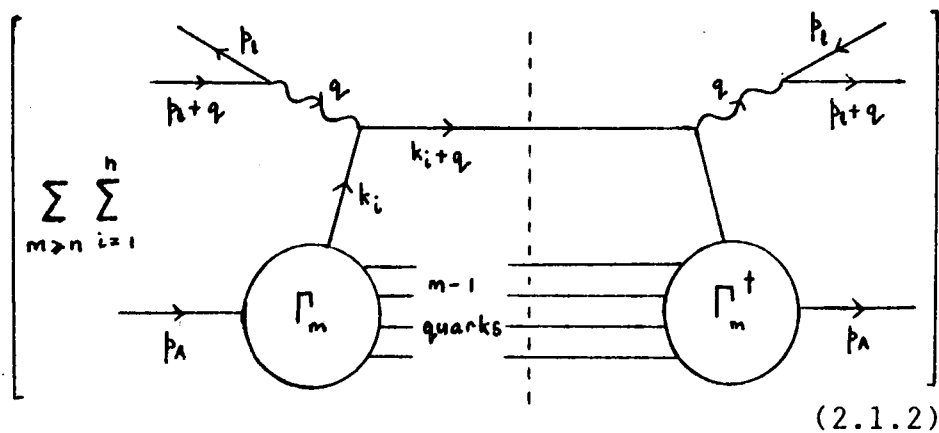
the final result is a property of the hadron alone.

Our starting point is Mueller's generalized optical theorem, (1.4.7), which applied to the process shown in figure 1.3 gives

$$16\pi^3 E_1 \frac{d^3\sigma}{d^3p_1} (1A \rightarrow 1X) = \frac{2}{h'} \text{Disc}(A_{1\bar{1}A \rightarrow 1\bar{1}A}) \quad (2.1.1)$$

$A_{1\bar{1}A \rightarrow 1\bar{1}A}$ is the three-particle elastic scattering amplitude, which is evaluated with all final state momenta equal to their corresponding initial values, and h' is the flux factor. In pictorial form

$$\text{Disc}(A_{1\bar{1}A \rightarrow 1\bar{1}A}) = \text{Disc}$$



where the discontinuity is evaluated at the dotted line,

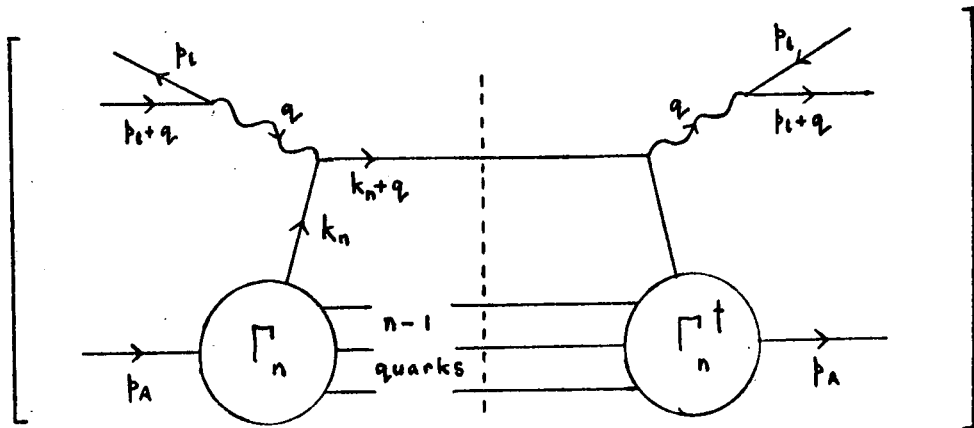
and Γ_m is the wavefunction for hadron A to be in an m -quark Fock state, (ie $\Gamma_m = \langle q_1 \dots q_m | A \rangle$). k_i are the quark four-momenta, and n is the number of valence quarks in A. The lepton and hadron four-momenta,

p_l and p_A respectively, satisfy their mass-shell constraints,

$$(p_i^2 = m_i^2 ; i = 1, A).$$

We now have two separate expressions ((1.6.2) and (2.1.1)) for the inclusive lepton-hadron differential cross-section, which are equal term by term in the summations. Picking out just the lowest term, and equating, we get

$$\int_0^1 dx_n f_A^n(x_n) 16\pi^3 E_1 \frac{d^3\sigma}{d^3p_1} (1q_n + 1\bar{q}_n) = \frac{2}{\hbar} \text{Disc}$$



(2.1.3)

where $n = 2$ for a meson and 3 for a baryon. $f_A^n(x_n)$ is the constituent quark distribution, because we only consider the Fock state where the valence quarks carry all of the momentum of the hadron between them.

The idea from here on is to feed in Γ_n , and derive an expression for $f_A^n(x_n)$. Unfortunately in the present state of hadron physics the Γ_n are still unknown, because we do not know how to calculate them from QCD. We therefore have to model them.

2.2 MESON WAVEFUNCTION

We observe experimentally that quarks are confined spatially within hadrons, although the theoretical proof of this does not yet exist. This tells us that the momenta of quarks must also be constrained in some way. Our model for the wavefunction Γ_n must incorporate this, and allow for the fermionic nature of the quarks. We therefore define the meson wavefunction, Γ_2 , by

$$\Gamma_2 \equiv C_2 g_2(x_1, x_2) G^{\frac{1}{2}}(\underline{k}_{T1}) G^{\frac{1}{2}}(\underline{k}_{T2}) u_2(\xi_2 p_A) \bar{u}_1(-\xi_1 p_A) \quad (2.2.1)$$

The spinors, (u_i with their spin labels suppressed) provide the Dirac space structure for two spin- $\frac{1}{2}$ quarks. The minus sign occurs because we choose label 1 for the antiquark, although the final result will not depend on this choice. ξ_i is the initial four-momentum fraction of quark i ; to conserve four-momentum $\xi_1 + \xi_2 = 1$.

The quark transverse momentum, \underline{k}_T , is defined relative to the beam axis, so $p_{TA} \equiv \underline{0}$. The hadronic binding is built into Γ_2 via its k_T -dependence. $G(\underline{k}_T)$ is a dimensionless function describing the k_T -distribution of a quark inside a hadron, whose properties we discuss in Section 2.5. Clearly in an $n = 2$ Fock state the quarks must have the same k_T -distribution, independent of their mass. We shall assume this holds for all higher Fock states, so a single function $G(\underline{k}_T)$ describes the k_T -distribution of

any quark in any Fock state, for a meson or a baryon.

The remaining momentum dependence of Γ_2 comes in $g_2(x_1, x_2)$, where x_1 and x_2 are defined by (1.5.4). This x -dependence is motivated by the minimum gluon exchange shown in figure 2.1, and fixed by appealing to the fact that (at least for equal mass quarks) it should be invariant under an interchange of the labels. Single gluon exchange generates the least suppressed behaviour of Γ_2 at the limits of x_i , ($0 \leq x_i \leq 1$; $i = 1, 2$). We treat the quark and antiquark on an equal footing in g_2 , and make no reference to which one is off mass-shell; this will be incorporated automatically in our calculation of $f_A^2(x_2)$. Both quarks cannot be on their respective mass-shells if bound within an on-shell meson.

The gluon propagator in figure 2.1 has the behaviour

$$\frac{1}{(k_1 - p_1)^2} = \frac{1}{(k_1^2 + p_1^2 - (x_1 p_A^+ p_1^- + \frac{(k_1^2 + k_{T1}^2) p_1^+}{x_1 p_A^+})} \stackrel{\sim}{x_1 \rightarrow 0} x_1 \quad (2.2.2)$$

using (1.5.6) to expand the dot product. Similarly, in terms of the other momenta instead

$$\frac{1}{(p_2 - k_2)^2} = \frac{1}{(p_2^2 + k_2^2 - (x_2 p_A^+ p_2^- + \frac{(k_2^2 + k_{T2}^2) p_2^+}{x_2 p_A^+})} \stackrel{\sim}{x_2 \rightarrow 0} x_2 \quad (2.2.3)$$

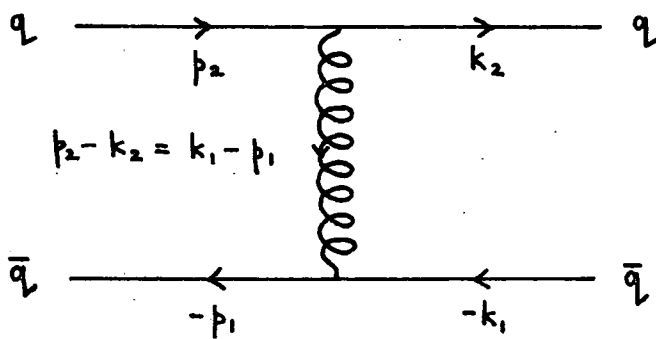


Figure 2.1: A single gluon exchange between the quark and antiquark in a meson, showing the four-momenta of the particles.

As the propagator appears twice in $|\Gamma_2|^2$ we choose

$$|g_2(x_1 x_2)|^2 = x_1 x_2 \quad (2.2.4)$$

which has the required invariance under label interchange. This choice ensures that $f_A^2(x_2)$ satisfies the dimensional counting rules, as we shall demonstrate having done the calculation.

The final ingredient in (2.2.1) is C_2 , which is a constant dependent upon the normalization chosen for $f_A^2(x_2)$. Any colour factors are absorbed into the definition of C_2 .

We now repeat this modelling process for three quarks in a baryon. This is more complicated, but employs the same basic ideas as here.

2.3 BARYON WAVEFUNCTION

The baryon wavefunction, Γ_3 , must have the same features as Γ_2 , so we define it by

$$\Gamma_3 \equiv C_3 g_3(x_1, x_2, x_3) \prod_{i=1}^3 G^{\frac{1}{2}}(\underline{k}_{Ti}) u_i(\xi_i p_A) \quad (2.3.1)$$

There are three quarks in a baryon, so we have three spinors for the Dirac space structure. As before, ξ_i is the initial four-momentum fraction of quark i , and $\sum_{i=1}^3 \xi_i = 1$ ensures the quarks carry all the four-momentum

of the baryon between them.

We again build the hadronic binding into Γ_3 through its k_T -dependence, using the same distribution function, $G(\underline{k}_T)$, as in the meson case.

The least suppressed behaviour for Γ_3 at the limits of x_i , ($0 \leq x_i \leq 1$; $i = 1, 2, 3$), arises from the minimal gluon exchange between the quarks. Unfortunately this time there are the six diagrams of figure 2.2, rather than one. We obtain the x -dependence of Γ_3 by considering these diagrams, and imposing invariance under the interchange of the labels of any two equal mass quarks.

There is an additional ingredient this time, the propagator of the quark which couples to both gluons, (labelled by ---X--- in figure 2.2). As well as contributing to the powers of x_i which damp Γ_3 for any of the $x_i \rightarrow 0$, this propagator depends on the quark mass, and exhibits a certain behaviour in the limit that one of the quarks becomes very massive.

Consider the denominators of these propagators for each of the diagrams in figure 2.2, in the limit $m_A, m_3 \rightarrow \infty$; m_1, m_2 fixed, (using four-momentum conservation

$$p_A = \sum_{i=1}^3 p_i = \sum_{i=1}^3 k_i).$$

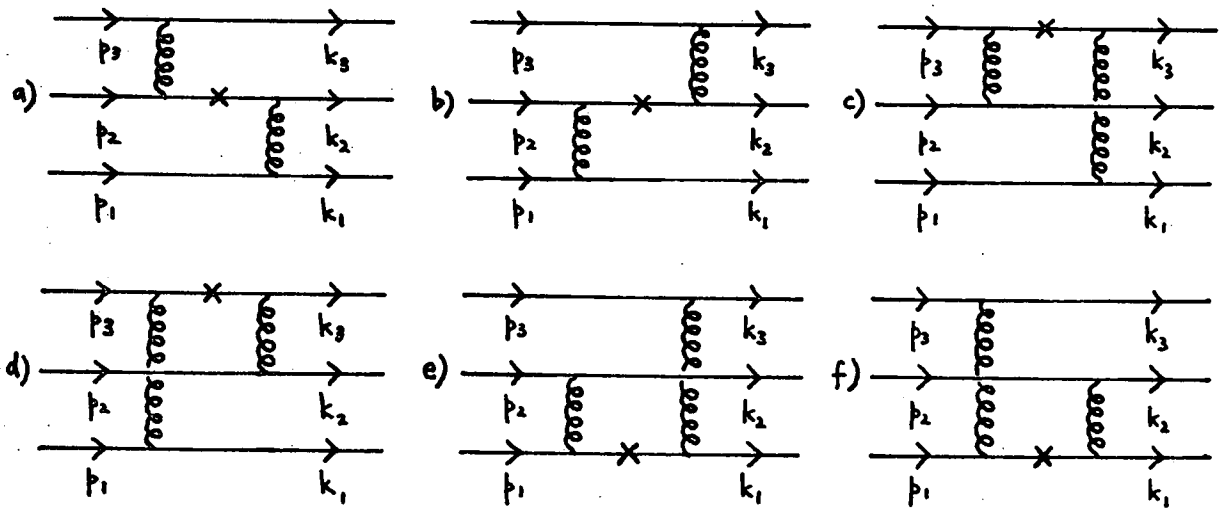


Figure 2.2: Two gluon exchange between the three quarks in a baryon, showing the four-momenta of the quarks.

- (a) $(p_A - p_1 - k_3)^2 - m_2^2 \cong (p_A - k_3) \cdot [p_A - k_3 - 2p_1]$
- (b) $(p_1 + p_2 - k_1)^2 - m_2^2 \cong (p_A - k_3) \cdot [p_A - k_3 - 2(p_1 + p_2 + k_2)]$
- (c) $(p_3 + p_2 - k_2)^2 - m_3^2 \cong k_3^2 - m_3^2$
- (d) $(p_1 + p_3 - k_1)^2 - m_3^2 \cong k_3^2 - m_3^2$
- (e) $(p_1 + p_2 - k_2)^2 - m_1^2 \cong (p_A - k_3) \cdot [p_A - k_3 - 2(p_1 + p_2 + k_1)]$
- (f) $(p_1 + p_3 - k_3)^2 - m_1^2 \cong (p_A - k_3) \cdot [p_A - k_3 - 2p_2]$ (2.3.2)

If we now let $k_3 + p_A (\cong k_3^2 + m_3^2 \cong x_3 + 1)$, all six of these expressions vanish like $(1 - x_3)$. We get an analogous result if we let m_1 or $m_2 \rightarrow \infty$ instead. We build this denominator behaviour into Γ_3 by choosing

$$g_3(x_1, x_2, x_3) \propto (m_A^2 - \sum_{i=1}^3 \frac{m_{Ti}^2}{x_i})^{-1} \quad (2.3.3)$$

where m_{Ti} is defined by

$$m_{Ti}^2 \cong m_i^2 + k_{Ti}^2 \quad (2.3.4)$$

(2.3.3) has the required symmetry for equal masses.

However we have not finished, because there are still the two gluon propagators and the numerator of the quark propagator to consider. In the limit

$x_3 \rightarrow 1$ (which forces $x_1, x_2 \rightarrow 0$) each gluon propagator gives a power of x_1 or x_2 , (which when integrated gives $(1-x_3)$), in a similar manner to the single gluon in r_2 . The quark propagator ($\frac{-\not{x}}{x}$) numerator contains a single power of its four-momentum, which when traced will always end up in a dot product. From (1.5.6) we see this cancels one power of x_1 or x_2 , and therefore $(1-x_3)$. The corresponding result arises if x_1 or $x_2 \rightarrow 1$, so our model for $|g_3(x_1, x_2, x_3)|^2$ must have a numerator which generates two powers of $(1-x_i)$ when integrated, if $x_i \rightarrow 1$; ($i=1,2,3$). There are four powers from the gluons minus two from the quark. The simplest symmetric choice is $x_1 x_2 x_3$, which, combined with (2.3.3), gives

$$|g_3(x_1, x_2, x_3)|^2 = \frac{x_1 x_2 x_3}{(m_A^2 - \sum_{i=1}^3 \frac{m_{Ti}^2}{x_i})^2} \quad (2.3.5)$$

Once again C_3 in (2.3.1) is a constant dependent upon the normalization of $f_A^3(x_3)$, and containing any colour factors.

In (2.2.1) and (2.3.1) we suppress the spin states of the quarks, because we shall average incoherently over them. We neglect correlations between these spins due to the spin state of the hadron, so the x -distributions we derive are for unpolarized quarks.

With our wavefunction modelling complete, we now

return to deriving valence quark x-distributions.

2.4 GENERAL CALCULATION

We derive an expression for $f_A^n(x_n)$ valid for both $n=2$ and $n=3$, which will avoid having to go through two virtually identical calculations. We take (2.1.3) and substitute our model for Γ_n from (2.n.1). Evaluating the discontinuity and averaging over the spins of the external fermions, we get

$$\int_0^1 dx_n f_A^n(x_n) 16\pi^3 E_1 \frac{d^3\sigma(1q_n+1q_n)}{d^3p_1} = \frac{1}{h} \prod_{i=1}^{n-1} \left[\frac{d^4k_i}{(2\pi)^4} \right. \\ \left. (2\pi)\theta(k_i^0)\delta(k_i^2-m_i^2)G(\underline{k}_{Ti}) \right] d^4k_n \\ \frac{\delta^4(p_A - \sum_{i=1}^n k_i) 2\pi\theta((k_n+q)^0)\delta((k_n+q)^2-m_n^2)G(\underline{k}_{Tn}) |g_n|^2 |C_n|^2 e^4 e_n^2}{(k_n^2-m_n^2+i\epsilon)(k_n^2-m_n^2-i\epsilon)(q^2+i\epsilon)(q^2-i\epsilon)} \\ \frac{1}{4} L^{\mu\nu} \frac{1}{2^n} \prod_{i=1}^{n-1} \left[\xi_i T_2(p_A, k_i) \right] \xi_n T_{4\mu\nu}(p_A, k_n, k_n+q, k_n) \quad (2.4.1)$$

where ee_n is the quark charge, and we have defined

$$T_2(p_A, k_i) \equiv \text{Tr} \{ (\not{p}_A + m_A) (\not{k}_i + m_i) \}$$

$$T_{4\mu\nu}(p_A, k_n, k_n+q, k_n) \equiv \text{Tr} \{ (\not{p}_A + m_A) (\not{k}_n + m_n) \gamma_\mu (\not{k}_n + \not{q} + m_n) \gamma_\nu (\not{k}_n + m_n) \} \quad (2.4.2)$$

$L^{\mu\nu}$ is defined by (1.6.4).

We replace the lepton-quark differential cross-section in (2.4.1) with the expression we derived in Chapter 1, (1.6.7), and also change to light cone variables, so

$$d^4k_n \delta^4(p_A - \sum_{i=1}^n k_i) = dx_n \delta(1 - \sum_{i=1}^n x_i) d^2k_{Tn} \delta^2(\sum_{i=1}^n k_{Ti})$$

$$d(k_n^2) \delta(x_n (m_A^2 - \sum_{i=1}^n \frac{k_i^2 + k_{Ti}^2}{x_i})) \quad (2.4.3)$$

The last δ -function is the origin of our earlier remark that the quark off-shellness will be built into this calculation automatically. Substituting (1.5.5) and (2.4.3) into (2.4.1), we obtain integrals over x_n on both sides of the expression. If we assume that the integrands are equal (which is equivalent to saying (2.4.1) holds in differential form), and cancel the lepton tensor ($L^{\mu\nu}$) and various other trimmings from both sides, the result is

$$f_A^n(x_n) T_{2\mu\nu}(k_n, k_n+q) = \frac{|C_n|^2 h}{h'} \int \prod_{i=1}^{n-1} \left[\frac{dx_i d^2k_{Ti} d(k_i^2)}{2(2\pi)^3 x_i} \right]$$

$$\left[\theta(k_i^0) \delta(k_i^2 - m_i^2) G(k_{Ti}) \right] d^2k_{Tn} d(k_n^2) \delta(1 - \sum_{i=1}^n x_i) G(k_{Tn})$$

$$\delta^2(\sum_{i=1}^n k_{Ti}) \delta(x_n (m_A^2 - \sum_{i=1}^n \frac{k_i^2 + k_{Ti}^2}{x_i})) \frac{|g_n|^2}{2^n} \prod_{i=1}^{n-1} \left[\xi_i T_2(p_A, k_i) \right]$$

$$\frac{\xi_n T_{4\mu\nu}(p_A k_n, k_n + q k_n)}{(k_n^2 - m_n^2)^2} \quad (2.4.4)$$

The traces in (2.4.2) can easily be evaluated to give

$$\begin{aligned} T_2(p_A k_i) &= 4(p_A \cdot k_i + m_A m_i) \\ T_{4\mu\nu}(p_A, k_n, k_n + q, k_n) &= 8(p_A \cdot k_n + m_A m_n) \left[k_{n\mu} (k_n + q)_\nu \right. \\ &+ k_{n\nu} (k_n + q)_\mu - 2k_n \cdot (k_n + q) g_{\mu\nu} \left. \right] + 4m_n^2 \left[(2p_A \cdot k_n - p_A \cdot (k_n + q)) g_{\mu\nu} \right. \\ &+ p_{A\mu} (k_n + q)_\nu + p_{A\nu} (k_n + q)_\mu \left. \right] + 4m_A m_n^3 g_{\mu\nu} \\ &+ 4k_n^2 \left[(p_A \cdot (k_n + q) + m_A m_n) g_{\mu\nu} - p_{A\mu} (k_n + q)_\nu - p_{A\nu} (k_n + q)_\mu \right] \end{aligned} \quad (2.4.5)$$

We substitute (1.6.9) and (2.4.5) into (2.4.4) and then employ the trick of operating on both sides with the projection operators $P^{+\mu} P^{+\nu}$ (defined by (1.5.2)). This leaves us free to cancel the remaining factors multiplying $f_A^n(x_n)$, and hence isolate it, giving

$$\begin{aligned} f_A^n(x_n) &= \frac{|C_n|^2 h}{h'} \int \prod_{i=1}^{n-1} \left[\frac{dx_i d^2 \underline{k}_{Ti} d(k_i^2)}{2(2\pi)^3 x_i} \delta(k_i^0) \delta(k_i^2 - m_i^2) G(\underline{k}_{Ti}) \right] \\ &d^2 \underline{k}_{Tn} d(k_n^2) \delta(1 - \sum_{i=1}^n x_i) \delta^2(\sum_{i=1}^n \underline{k}_{Ti}) \delta(x_n (m_A^2 - \sum_{i=1}^n \frac{k_i^2 + k_{Ti}^2}{x_i})) G(\underline{k}_{Tn}) \\ &|g_n|^2 \prod_{i=1}^{n-1} \left[\xi_i (2p_A \cdot k_i + 2m_A m_i) \right] \frac{2p_A \cdot k_n + 2m_A m_n - 1/x_n (k_n^2 - m_n^2)}{(k_n^2 - m_n^2)^2} \end{aligned} \quad (2.4.6)$$

To proceed any further we must integrate over the quark transverse momenta. It is possible to develop a general method for this, which applies to any k_T -integrals arising in this work.

2.5 TRANSVERSE MOMENTUM

In our wave function modelling we allowed for the hadronic binding by defining the dimensionless quark k_T -distribution function, $G(\underline{k}_T)$, such that

$$|\Gamma_n|^2 \propto \prod_{i=1}^n G(\underline{k}_{Ti}) \quad (2.5.1)$$

Rather than choose an explicit model for G , we need only assume it possesses certain properties in order to evaluate the k_T -integrals we encounter. With $|\Gamma_n|^2$ given by (2.5.1) they will always turn out to have the form

$$\int \prod_{i=1}^n [d^2\underline{k}_{Ti} G(\underline{k}_{Ti})] \delta^2(\sum_{i=1}^n \underline{k}_{Ti}) H_n(\{\underline{k}_{Ti} \cdot \underline{k}_{Tj}\}) \equiv I_n \quad (2.5.2)$$

where H_n is some function of all the possible dot products of the \underline{k}_{Ti} .

There is no preferred direction perpendicular to the hadron momentum, so we have rotational invariance about the beam axis, and therefore assume

$$G(\underline{k}_{Ti}) = G(k_{Ti}^2) \quad (2.5.3)$$

G is a dimensionless function, and so must contain a parameter with dimensions of momentum. Instead of worrying about what this is, and the actual form of G , we assume the k_T -integrals can be done, and concern ourselves with the resulting expectation values. For just one such integral we define $\langle k_T^2 \rangle$ by

$$\int d^2 \underline{k}_T G^2(k_T^2) H(k_T^2) \equiv \Pi \langle k_T^2 \rangle H(\langle k_T^2 \rangle) \quad (2.5.4)$$

the Π coming from the angular integral ($d^2 \underline{k}_T = \Pi d(k_T^2)$), and the $\langle k_T^2 \rangle$ out front keeping the dimensions correct. We then have to choose a suitable value for $\langle k_T^2 \rangle$. (We return to this point later).

Before we can apply (2.5.4) to (2.5.2) we need some further assumptions. The first is that G factorizes, so

$$G\left(\sum_{i=1}^{n-1} \underline{k}_{Ti}\right) = \prod_{i=1}^{n-1} G(\underline{k}_{Ti}) \quad (2.5.5)$$

We also have to worry about the cross terms, $\underline{k}_{Ti} \cdot \underline{k}_{Tj}$ ($i \neq j$), in H_n . These cannot average to zero, as we can see by considering

$$\begin{aligned} 0 \equiv \langle p_{TA}^2 \rangle &= \left\langle \left(\sum_{i=1}^n \underline{k}_{Ti} \right)^2 \right\rangle = \sum_{i=1}^n \langle k_{Ti}^2 \rangle + 2 \sum_{i>j}^n \langle \underline{k}_{Ti} \cdot \underline{k}_{Tj} \rangle \\ &= n \langle k_T^2 \rangle + 2 \sum_{i>j}^n \langle \underline{k}_{Ti} \cdot \underline{k}_{Tj} \rangle \end{aligned}$$

However this identity is satisfied for all n by choosing

$$\langle \underline{k}_{Ti} \cdot \underline{k}_{Tj} \rangle = \frac{-\langle k_T^2 \rangle}{n-1} \quad (i \neq j)$$

which may be written generally as

$$\langle \underline{k}_{Ti} \cdot \underline{k}_{Tj} \rangle = \frac{\langle k_T^2 \rangle}{n-1} (n \delta_{ij} - 1) \quad (2.5.6)$$

An example of both of these assumptions at work is an exponential of the form

$$G(\underline{k}_T) = \exp \left[\frac{\langle k_T^2 \rangle}{\Lambda_T^2} \right] \exp \left[\frac{-k_T^2}{\Lambda_T^2} \right]$$

where Λ_T is a constant with dimensions of momentum.

Substituting $\underline{k}_T = \sum_{i=1}^{n-1} \underline{k}_{Ti}$ we obtain

$$\begin{aligned} G\left(\sum_{i=1}^{n-1} \underline{k}_{Ti}\right) &= \exp \left[\frac{\langle k_T^2 \rangle}{\Lambda_T^2} \right] \exp \left[\frac{-\sum_{i=1}^{n-1} k_{Ti}^2}{\Lambda_T^2} \right] \exp \left[\frac{-2 \sum_{i>j}^{n-1} \underline{k}_{Ti} \cdot \underline{k}_{Tj}}{\Lambda_T^2} \right] \\ &= \exp \left[\frac{-(n-2) \langle k_T^2 \rangle}{\Lambda_T^2} \right] \exp \left[\frac{-2 \sum_{i>j}^{n-1} \underline{k}_{Ti} \cdot \underline{k}_{Tj}}{\Lambda_T^2} \right] \prod_{i=1}^{n-1} G(\underline{k}_{Ti}) \end{aligned}$$

The second exponential can be regarded as part of H_n when the k_T -integrals are done, and so the $\underline{k}_{Ti} \cdot \underline{k}_{Tj}$ are given by (2.5.6). This is exactly what is required, for then the two exponentials cancel to produce (2.5.5).

Returning to (2.5.2), we integrate over the δ -function, and build in (2.5.5) and (2.5.3). This gives

$$I_n = \int \prod_{i=1}^{n-1} \left[d^2 k_{Ti} G^2(k_{Ti}^2) \right] H_n(\{ k_{Ti} \cdot k_{Tj} \}) \quad (2.5.7)$$

We do the remaining integrals as in (2.5.4), adding the sophistication of (2.5.6), obtaining the final result

$$I_n = \pi^{n-1} \langle k_T^2 \rangle^{n-1} H_n \left(\left\{ \frac{\langle k_T^2 \rangle}{n-1} (n \delta_{ij} - 1) \right\} \right) \quad (2.5.8)$$

This prescription will enable us to do any k_T -integrals we come across from now on.

There is one further assumption that we make, that $\langle k_T^2 \rangle$ is independent of n , and so is the same for both baryons and mesons, and higher Fock states. This is clearly not exactly true, as H_n is different for each case, but it should be a reasonable approximation. The conjugate statement to this is that all hadrons have the same shape and size, and we know this is not a bad first approximation.

Anyway, armed with (2.5.8), we now return to deriving valence quark distributions.

2.6 RESULTS

If we expand the dot products in (2.4.6) using (1.5.6), the n k_i^2 -integrals over the δ -functions can be done trivially, and the n k_{Ti} -integrals done using the prescription of (2.5.8), to give

$$f_A^n(x_n) = \frac{|C_n|^{2h}}{2h'} \left[\frac{\Pi \langle k_T^2 \rangle}{2(2\Pi)^3} \right]^{n-1} \int_0^1 \prod_{i=1}^{n-1} \left[\frac{dx_i}{x_i} \right]$$

$$\frac{\delta(1 - \sum_{i=1}^n x_i) \langle |g_n|^2 \rangle}{x_n^2 (m_A^2 - \sum_{i=1}^n \frac{\langle m_{Ti}^2 \rangle}{x_i})^2} \prod_{i=1}^n \left[\xi_i \left(\frac{\langle m_{Ti}^2 \rangle}{x_i} + m_A^2 x_i + 2m_A m_i \right) \right] \quad (2.6.1)$$

where $\langle m_{Ti}^2 \rangle$ is defined by

$$\langle m_{Ti}^2 \rangle \equiv m_i^2 + \langle k_T^2 \rangle \quad (2.6.2)$$

Using the full expression for a flux factor, (1.4.3),

$$\frac{h}{h'} = \left[\frac{((p_1+q) \cdot k_n)^2 - m_1^2 k_n^2}{((p_1+q) \cdot p_A)^2 - m_1^2 m_A^2} \right]^{\frac{1}{2}} \quad (2.6.3)$$

Provided we work in a frame where all masses are negligible compared to momenta this can be greatly simplified. Putting $m_1=0$ and using (1.5.6) for the dot products, (2.6.3) becomes

$$\frac{h}{h'} \cong \frac{(p_1+q)^+ k_n^- + (p_1+q)^- k_n^+ - 2(p_{T1}+q_T) \cdot k_{Tn}}{(p_1+q)^+ p_A^- + (p_1+q)^- p_A^+}$$

$$\cong \frac{(p_1+q)^- k_n^+}{(p_1+q)^- p_A^+} = x_n \quad (2.6.4)$$

where to get the final result we picked the terms top and bottom which dominate in the large momentum limit.

If we make the definitions

$$V_n \cong \frac{1}{2} |C_n|^2 \langle k_T^2 \rangle \left[\frac{\Pi}{2(2\Pi)^3} \right]^{n-1} \prod_{i=1}^n \xi_i ;$$

$$\alpha \cong \frac{m_A^2}{\langle k_T^2 \rangle} ; \quad \beta_i \cong \frac{\langle m_{Ti}^2 \rangle}{\langle k_T^2 \rangle} ; \quad \gamma_i \cong \frac{m_A m_i}{\langle k_T^2 \rangle} \quad (2.6.5)$$

where V_n is now a dimensionless constant, we can simplify the expression for $f_A^n(x_n)$. Substituting (2.6.4) and (2.6.5) into (2.6.1) we obtain

$$f_A^n(x_n) = V_n \int_0^1 \prod_{i=1}^{n-1} \left[\frac{dx_i}{x_i} \right] \frac{\delta(1 - \sum_{i=1}^n x_i) \langle |g_n|^2 \rangle \langle k_T^2 \rangle^{2(n-2)}}{x_n \left(\alpha - \sum_{i=1}^n \frac{\beta_i}{x_i} \right)^2}$$

$$\prod_{i=1}^n \left[\frac{\beta_i}{x_i} + \alpha x_i + 2\gamma_i \right] \quad (2.6.6)$$

The final tidying up is done by using the definitions for $|g_n|^2$, (2.n.n+2), which give

$$f_A^n(x_n) = V_n \int_0^1 \prod_{i=1}^{n-1} [dx_i] \frac{\delta(1 - \sum_{i=1}^n x_i)}{(\alpha - \sum_{i=1}^n \frac{\beta_i}{x_i})^{2(n-1)}}$$

$$\prod_{i=1}^n \left[\frac{\beta_i}{x_i} + \alpha x_i + 2\gamma_i \right]$$

$$= \int_0^1 \prod_{i=1}^{n-1} [dx_i] \delta(1 - \sum_{i=1}^n x_i) f_A^n(\{x_n\}) \quad (2.6.7)$$

We now discuss the important features of this result, and compare it (although contrast might be a better word) with the experimental data.

2.7 COMMENTS AND COMPARISON WITH EXPERIMENT

We promised for the case $n=2$ that our choice of label 1 for the antiquark would have no effect on the result. The symmetry of the expression (2.6.7) shows this to be true.

We also promised that the results for both $n=2$ and 3 would satisfy the dimensional counting rules; (see Section 1.7). Consider the behaviour of (2.6.7) in the limit $x_n \rightarrow 1$. The denominator gives $2(n-1)$ powers of x_i ($i < n$), each of which generates a power of $(1-x_n)$ after integration. The integrals themselves give $(n-2)$ powers of $(1-x_n)$ (as there are $n-1$ integrals, and we lose one to the δ -function), but the fermion

traces (in the square brackets) knock off (n-1) powers of $(1-x_n)$. Therefore

$$f_A^n(x_n) \underset{x_n \rightarrow 1}{\sim} (1-x_n)^{2(n-1)-1} \quad (2.7.1)$$

in agreement with (1.7.23) since $n_{gmin} = n-1$. Our choices for the numerators of $|g_n|^2$ in (2.n.n+2) cancel the leading behaviour of the square brackets in (2.6.7), in agreement with Gunion's comment⁽¹⁸⁾ that fermion traces typically cancel against gluon propagators in QCD.

The expression for $f_A^n(x_n)$ has been derived with $n=2$ or 3 in mind, but clearly (2.6.7) could also be used for any integer $n > 3$. This is of little interest at the moment, since exotic hadrons (with, for example, $|q\bar{q}q\bar{q}\rangle$ as the valence Fock state) have yet to be observed.

The next topic of discussion is the denominator $(\alpha - \sum_{i=1}^n \frac{\beta_i}{x_i})$ and its effect on $f_A^n(x_n)$. We observe that if

$$m_A = \sum_{i=1}^n \langle m_{Ti}^2 \rangle^{\frac{1}{2}} \quad \text{and} \quad x_i = \frac{\langle m_{Ti}^2 \rangle^{\frac{1}{2}}}{m_A} \quad (2.7.2)$$

which using (2.6.5) can be written

$$\alpha^{\frac{1}{2}} = \sum_{i=1}^n \beta_i^{\frac{1}{2}} \quad \text{and} \quad x_i = \left(\frac{\beta_i}{\alpha}\right)^{\frac{1}{2}} \quad (2.7.3)$$

the denominator vanishes. If we divide $f_A^n(x_n)$ by its integral over x_n to normalize, and then take the limit $\alpha^{\frac{1}{2}} \rightarrow \sum_{i=1}^n \beta_i^{\frac{1}{2}}$, the result is

$$f_A^n(x_n) = \delta(x_n - (\frac{\beta_n}{\alpha})^{\frac{1}{2}}) \quad (2.7.4)$$

Defining the (dimensionless) binding Δ by

$$\langle k_T^2 \rangle^{\frac{1}{2}} \Delta \equiv \langle k_T^2 \rangle^{\frac{1}{2}} (\sum_{i=1}^n \beta_i^{\frac{1}{2}} - \alpha^{\frac{1}{2}}) = \sum_{i=1}^n \langle m_{Ti}^2 \rangle^{\frac{1}{2}} - m_A \quad (2.7.5)$$

we see that in order to avoid the unrealistic result of (2.7.4), (or worse, a zero in the denominator in (2.6.7)), we must always have

$$\Delta > 0 \equiv \sum_{i=1}^n \langle m_{Ti}^2 \rangle^{\frac{1}{2}} > m_A \quad (2.7.6)$$

It is therefore the quark transverse mass $\langle m_{Ti}^2 \rangle^{\frac{1}{2}}$ (defined by (2.6.2)), and not the current mass m_i (which appears in the propagator), that is the important quantity here.

For this reason, and also because all the momentum of the hadron is carried by the valence quarks, $f_A^n(x_n)$ must be thought of as a constituent (as opposed to current) quark distribution. This is clearly a problem when it comes to making comparisons with experiment.

Before we plot (2.6.7) for $n=2$ and 3 we need to

decide on the values of α , β_i and γ_i . In table 2a we list the masses we use, from which α , β_i and γ_i are calculated using (2.6.5). In all our calculations we

Flavour (Q)	m_Q	$\langle k_T^2 \rangle^{\frac{1}{2}}$	m_{M_Q}	$m_{M_Q}^*$	m_{Λ_Q}
u	0.0	0.450	0.140	0.769	0.938
d	0.0	0.450	(m_π)	(m_ρ)	(m_p)
s	0.355	0.573	0.494	0.892	1.116
c	1.627	1.688	1.869	2.010	2.282
b	5.078	5.098	5.270	5.412 [#]	5.684 [#]
(i)	25.00	25.00	25.18 [#]	25.32 [#]	25.59 [#]
t (ii)	35.00	35.00	35.18 [#]	35.32 [#]	35.59 [#]
(iii)	45.00	45.00	45.18 [#]	45.32 [#]	45.59 [#]

Table 2a: The hadron masses⁽²¹⁾ and quark masses used in all our calculations, in GeV.

take $\langle k_T^2 \rangle^{\frac{1}{2}} = 0.45$ GeV, because we shall find this gives the best results for hadron production later on. Figure 2.3 shows that the proton valence distribution is not particularly sensitive to this choice (provided we stay well away from $\langle k_T^2 \rangle^{\frac{1}{2}} = \frac{m_p}{3} = 0.313$ GeV).

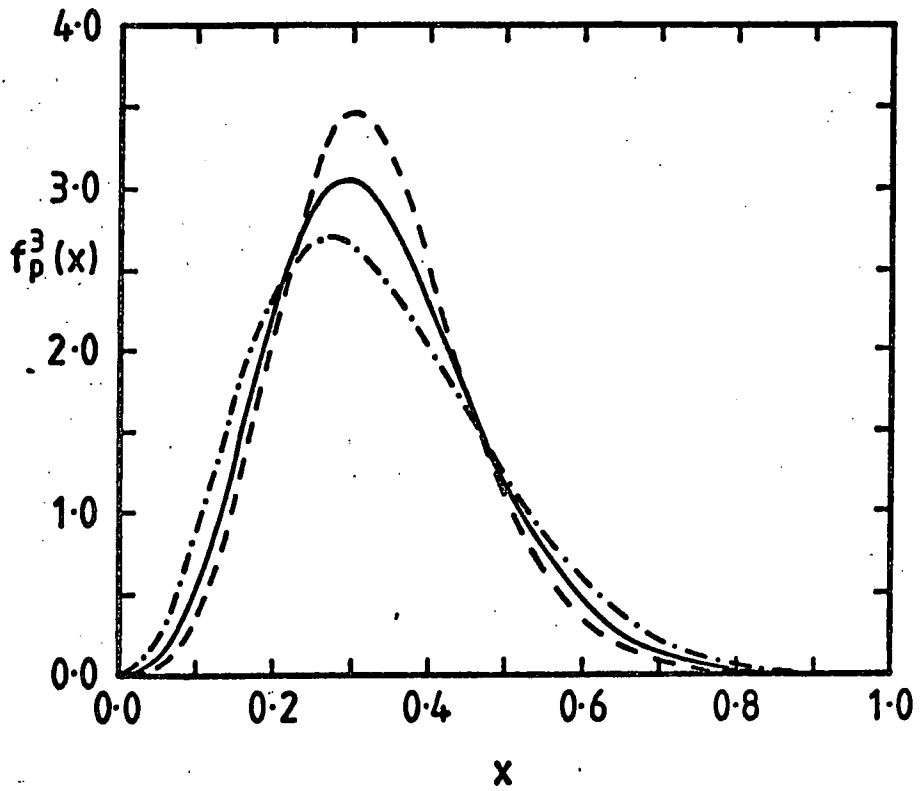


Figure 2.3: f_p^3 calculated from (2.6.7) for $\langle k_T^2 \rangle^{1/2} = 400$ (---), 450(—), and 600(-·-·-·-) MeV, normalized to unit area.

We choose the current masses of the up and down quarks to be zero, and consider three possible masses for the top quark. The other quark masses are chosen so that Δ (defined by (2.7.5)) is the same for the relevant vector meson as it is for the ρ . It is much better to consider the vector mesons for this, because Δ is anomalously large for the pion due to its very small mass, which presumably reflects its special role as a Goldstone boson. The unknown hadron masses (# in table 2a) are chosen to give the same Δ as for their known counterparts. Thus $m_{\Lambda_b^0}$ and $m_{\Lambda_t^+}$ are chosen so Δ is the same as for the Λ_c^+ , m_{B^*} and m_{T^*} are chosen so Δ is the same as for the other vector mesons, and the m_T are chosen so that

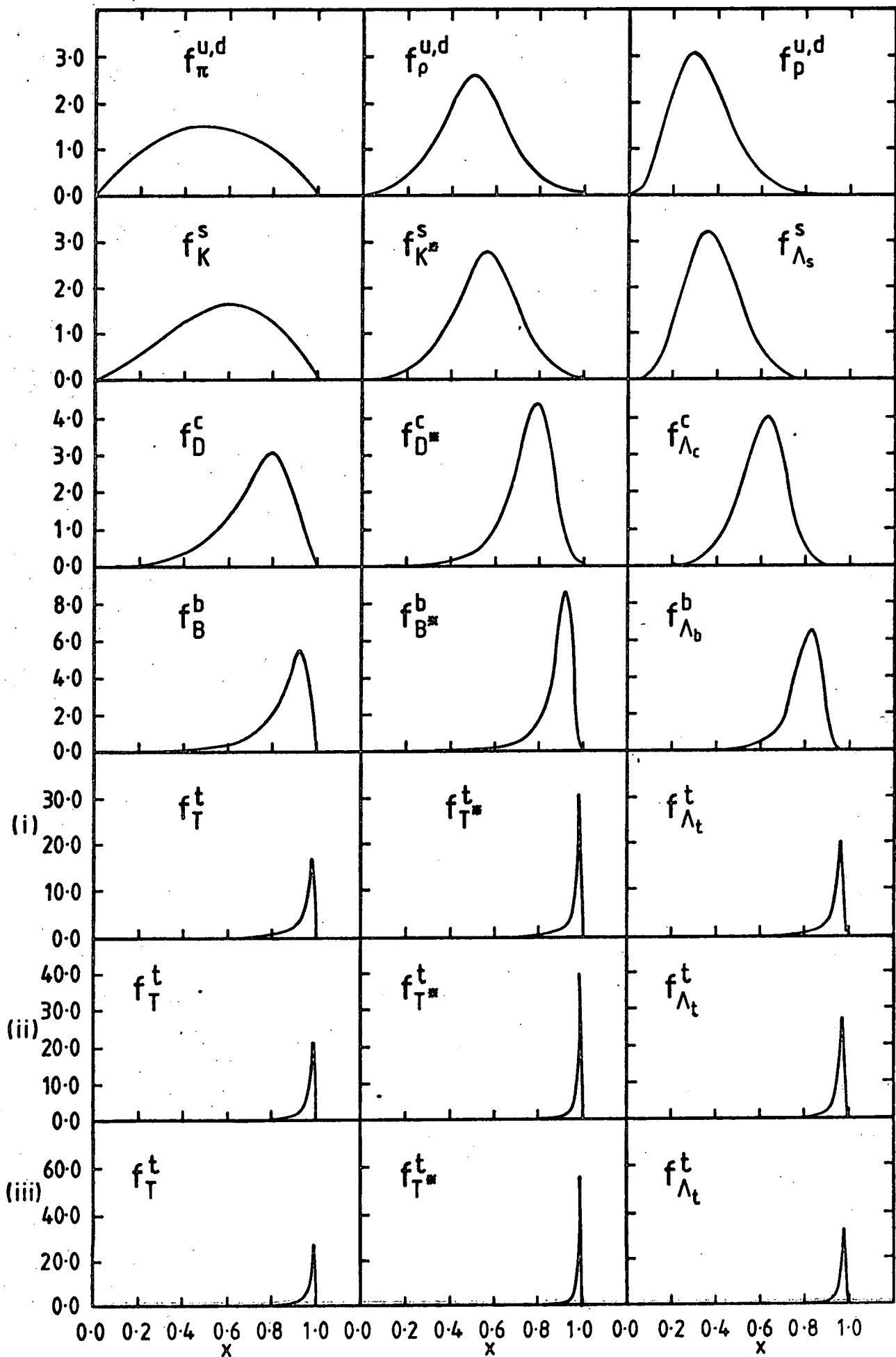
$$m_{T^*} - m_T = m_{B^*} - m_B = m_{D^*} - m_D \quad (2.7.7)$$

This last relation is reminiscent of the results derived from assuming a logarithmic interquark potential in potential model calculations⁽²²⁾.

The valence distributions calculated from (2.6.7) are shown in figure 2.4. For the baryons the one

Figure 2.4: The constituent valence quark distributions calculated from (2.6.7) with $n=2$ and 3 using the numbers from table 2a.(i), (ii) and (iii) correspond to $m_t = 25, 35$ and 45 GeV respectively.

Figure 2.4



non-trivial x -integral is done numerically; it is possible analytically, but difficult. Figure 2.4 shows that for both scalar and vector mesons, and baryons, as the quark mass increases (relative to the other constituents' masses) it carries an increasing fraction of the hadron's momentum. We can understand this result by the intuitive argument⁽⁷⁾ that in order to "hold together" in the hadron the quarks must have the same velocity. This simple (non-relativistic) picture works for valence distributions, but, as we shall see in Chapter 4, is not good enough when we come to consider the higher Fock states of hadrons.

For each flavour the scalar meson distribution is broader than that of its vector counterpart. This is due to the fact that Δ is always larger for the scalars, and increased binding results in a greater spread of momentum.

The origin of both the observations we have just made is the denominator $(\alpha - \sum_{i=1}^n \frac{\beta_i}{x_i})$. For this reason the results obtained are similar to those of Brodsky et al⁽⁷⁾, as they have such a denominator in their expression for the distribution function. However the rest of their ingredients are rather different to ours. They choose to omit the $1/x_i$'s from the phase-space, and always assume that Γ_n has no

x-dependence. As a consequence their distributions do not always obey the dimensional counting rules as $x \rightarrow 1$; (they obtain $(1-x)^2$ and $(1-x)^3$ for mesons and baryons respectively). These differences do not play much of a role here, because, as we have said, it is the denominator that matters most. However, when we consider higher Fock states in Chapter 4 we will find that the dimensional counting behaviour is more significant.

We should make one more comment on the choice of $\langle k_T^2 \rangle$. In Section 2.5 we made it the same for all baryons and mesons. This assumption must be qualified a bit, or problems could arise if we applied it to more excited mesons and baryons of greater spin; (to be precise mesons with spin > 1 and baryons with spin $> 3/2$). For then particles exist for which (2.7.6) does not hold if $\langle k_T^2 \rangle^{\frac{1}{2}} = 0.45$ GeV. These particles, in simple constituent quark models, are considered to be excitations of the lower spin ones, with some quark orbital angular momentum (l) so we would expect $\langle k_T^2 \rangle^{\frac{1}{2}}$ to be larger. We therefore need to choose a value of $\langle k_T^2 \rangle^{\frac{1}{2}}$ increasing with l , but since we only consider $l = 0$ hadrons in this work our single choice is sufficient.

To close this section we compare the predictions of (2.6.7) with experiment, to the extent that such a comparison is possible. As we have already stressed,

our distributions are of constituent rather than current quarks. Experiments measure the latter. For pions this is done via the Drell-Yan process, and for nucleons by deep inelastic scattering. In each case it is found that only a fraction of the hadron's momentum is carried by the valence quarks, the remainder being carried by $q\bar{q}$ pairs and gluons in the sea. These fractions are listed in table 2b.

π	0.4 ± 0.1
p,n	0.32 ± 0.01

Table 2b: The measured fraction of momentum carried by the valence quarks in a pion⁽²³⁾ and a nucleon⁽²⁴⁾.

We make the following definitions

$$F_{\pi}(x) \equiv \sum_2 x f_{\pi}^2(x) = 2x f_{\pi}^2(x) \quad (2.7.8)$$

$$F_2^A(x) \equiv \sum_3 e_3^2 x f_A^3(x) \quad (2.7.9)$$

as these are what experimentalists actually plot.

The final form of (2.7.8) follows because

$f_{\pi}^q(x) = f_{\pi}^{\bar{q}}(x)$. The x here is Bjorken- x , defined by

(1.6.1). (2.7.9) is the usual nucleon structure

function, (1.6.16), defined just for the valence Fock

state, and (2.7.8) is the same for a pion, except the

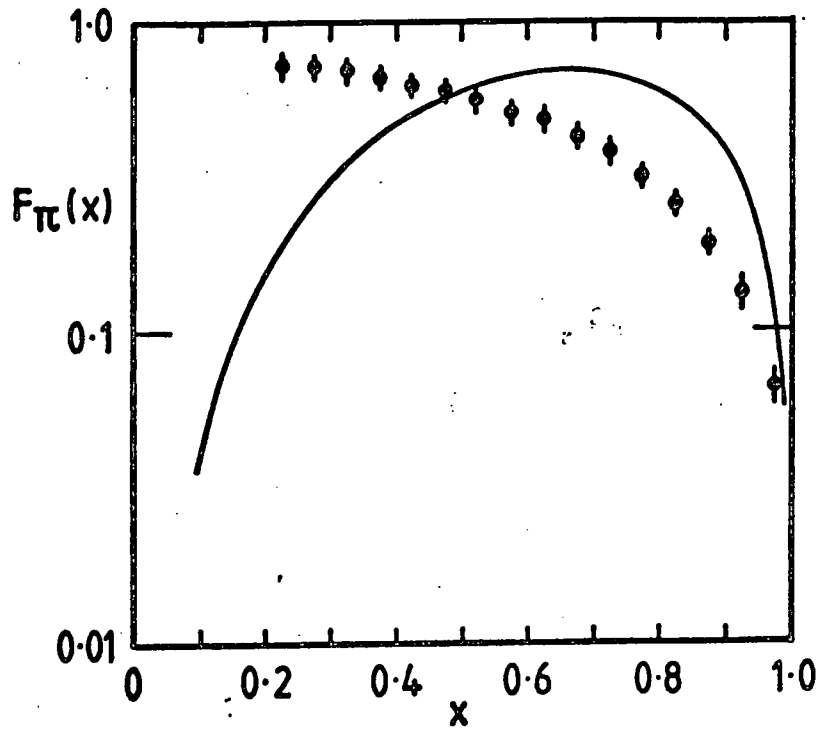


Figure 2.5: Our prediction for $F_{\pi}(x)$, calculated from (2.7.9) using (2.7.12) and the factor from table 2b, compared with the data⁽²³⁾.

quark charge is omitted. For nucleons in fact what is plotted is $F_2^p(x) - F_2^n(x)$ as the sea, being the same for both, then cancels. Using (2.7.9) this may be written

$$\begin{aligned} F_2^p(x) - F_2^n(x) &= \sum_3 e_u^2 f_p^3(x) x - \sum_3 e_d^2 f_n^3(x) x \\ &= \frac{x}{3} f_p^3(x) \end{aligned} \quad (2.7.10)$$

using the quark charges $e_u=2/3$, $e_d=-1/3$.

The normalizations of our distribution functions are

$$\int_0^1 dx x f_A^n(x) = 1/n \quad (2.7.11)$$

for $A = \pi$, p and $n=2,3$ respectively, as the constituent quarks carry all the momentum and have equal mass. To compare with the data we put in by hand the relevant factor from table 2b, which ensures the areas under the experimental and theoretical curves are equal. In figures 2.5 and 2.6 we plot (2.7.8) and (2.7.10) respectively.

In both cases the theoretical peak is at larger x than the experimental one. This is because if a constituent quark is probed at large momentum transfer squared (Q^2), as happens in the experiments, its structure is resolved, and its momentum distribution is suppressed to lower x by QCD evolution^(4,25). The

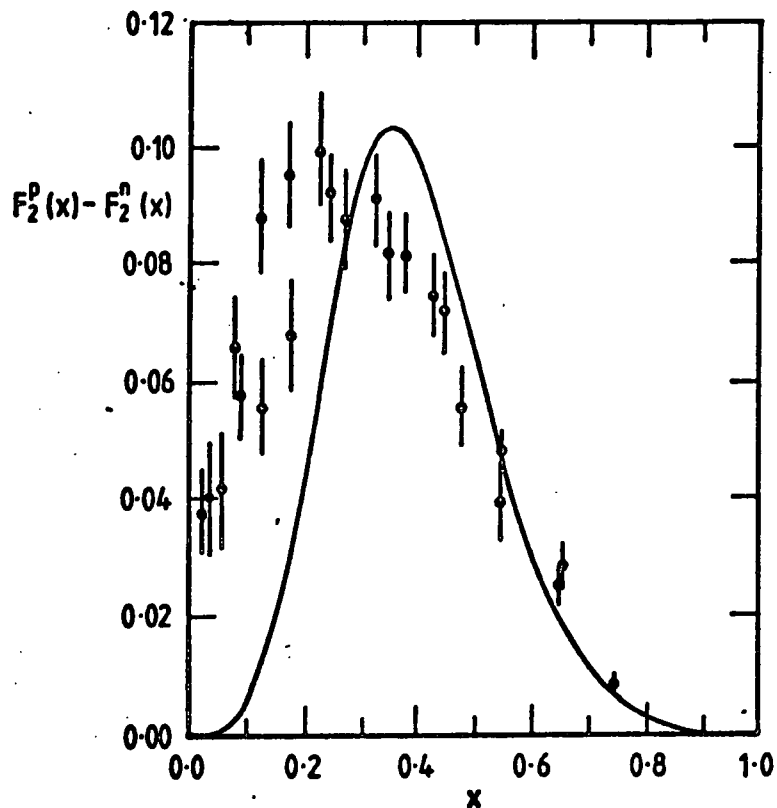


Figure 2.6: Our prediction for $F_2^p(x) - F_2^n(x)$, calculated from (2.7.11) using (2.7.12) and the factor from table 2b, compared with the data⁽²⁶⁾.

discrepancies in figures 2.5 and 2.6 therefore reflect the amount of QCD evolution from Q_0^2 (where the constituent quarks are just resolved) up to the Q^2 at which the distributions are measured; we are not comparing like with like. A much better comparison of our model with experiment comes in the next chapter, when we consider fragmentation functions.

CHAPTER 3

HEAVY QUARK FRAGMENTATION FUNCTIONS

3.1 DISTRIBUTION OF TWO SPINLESS CONSTITUENTS

3.1.1 Introduction

So far we have been considering the x -distributions of quarks inside hadrons, for which the physical region of x is $0 \leq x \leq 1$. We can also consider the possibility of a hadron being produced by a quark with a fraction z of the quark's (light cone) momentum. When the quark fragments, all the resultant hadrons lie in the region $0 \lesssim z (=1/x) \lesssim 1$. If their momenta are large this is a very good approximation, because the interactions between different fragmenting partons will be small by comparison.

When we consider the z -distributions of these hadrons, called fragmentation functions ($D_q^A(z)$), we will need a model of, for example, the distribution of a D-meson inside a D^* , if we are to make comparisons with experimental data. This is because when experimentalists measure the distribution of D-mesons from charmed quarks produced in an e^+e^- -collider, what they really measure is the distribution of D's which come directly from the quarks added to that of D's which come from D^* 's. In principle we could also consider even higher excited states. Clearly then, we shall not only need the fragmentation functions D_c^D and $D_c^{D^*}$, but also a model for the

distribution of D's inside D*'s, $f_{D^*}^D$, in order to make a prediction to compare with the data. With foresight we therefore first construct a model distribution for two spinless constituents inside a hadron.

The idea we use is about the simplest possible. We assume the heavy vector meson consists of a heavy scalar meson and a pion, and that these interact via a four-point interaction, as shown in figure 3.1. Our justification is the most important features of the distribution we need to get correct are the position and width of the peak. The dominant factor determining these is the denominator of the heavy scalar meson propagator. This is present in virtually any model, independent of the other constituents of the vector meson and the dynamics of the interaction, and always has the same effect as long as the other constituents are light by comparison. So, although the behaviour at the limits of x may not be particularly realistic, the distribution should be satisfactory in the region where it matters.

We again employ a photon for our probe, but, as before, the final result will not depend on this choice. Defining our distribution in the same manner as for quarks in a meson, we have

$$16 \pi^3 E_1 \frac{d^3 \sigma(1V \rightarrow 1X)}{d^3 p_1} = \sum_S \int_0^1 dx_S f_V^S(x_S) 16 \pi^3 E_1 \frac{d^3 \sigma(1S \rightarrow 1S)}{d^3 p_1} \quad (3.1.1)$$

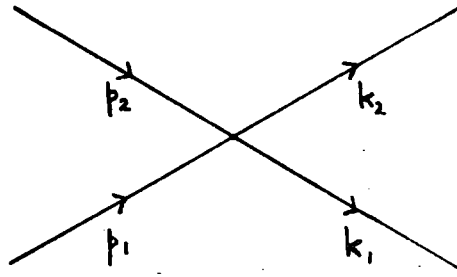


Figure 3.1: The four-point interaction between two spinless particles, showing their four-momenta.

where V is the vector meson, and S a scalar. The summation is over the different constituents of V in this picture. Mueller's theorem, (1.4.7), gives an alternative expression for the left hand side, namely

$$16 \pi^3 E_1 \frac{d^3 \sigma (1V \rightarrow 1X)}{d^3 p_1} = \frac{2}{h'} \text{Disc}(A_{1\bar{1}V \rightarrow 1\bar{1}V}) \quad (3.1.2)$$

where h' is the flux factor and

$$\text{Disc}(A_{1\bar{1}V \rightarrow 1\bar{1}V}) = \text{Disc} \left[\sum_S \right]$$

(3.1.3)

Equating (3.1.1) and (3.1.2), using (3.1.3) and taking just one term in the summation, we obtain

$$\int_0^1 dx_2 f_V^S(x_2) 16 \pi^3 E_1 \frac{d^3 \sigma (1S \rightarrow 1S)}{d^3 p_1} = \frac{2}{h'} \text{Disc}$$

(3.1.4)

We now follow the familiar pattern of modelling Γ_V^S and then calculating f_V^S .

3.1.2 Wavefunction Model and Calculation

Modelling Γ_V^S is easy. We assume the hadronic binding is the same as for quarks inside a hadron. The k_T -dependence is therefore given by (2.5.1). The particles are spinless, so no spinor structure is required, which only leaves a possible x -dependence due to the interaction of figure 3.1. However the vertex is a constant, so we make the very simple choice

$$\Gamma_V^S \equiv C_V G^{\frac{1}{2}}(k_{T1}^2) G^{\frac{1}{2}}(k_{T2}^2) \quad (3.1.5)$$

remembering (2.5.3). C_V is a constant.

The sub-process cross-section in (3.1.4) is similar to (1.6.7). There is one less factor $\frac{1}{2}$ for spin averaging, as one particle is now a scalar, and the photon must couple to this scalar by the correct vertex⁽⁹⁾.

Allowing for these differences we get

$$16 \pi^3 E_1 \frac{d^3 \sigma(1S \rightarrow 1S)}{d^3 p_1} = \frac{e^4 e_2^2}{2hq^4} (2\pi) \theta((k_2+q)^0) \delta((k_2+q)^2 - m_2^2)$$

$$L^{\mu\nu} (2k_2+q)_\mu (2k_2+q)_\nu \quad (3.1.6)$$

If we insert (3.1.5) into (3.1.4), average over the spin of the lepton, and evaluate the discontinuity, it reads

$$\int_0^1 dx_2 f_V^S(x_2) 16\pi^3 E_1 \frac{d^3\sigma}{d^3p_1} (1S+1S) = \frac{1}{h'} \int \frac{d^4k_1 d^4k_2 \delta^4(p_A - k_1 - k_2) e^4 e_2^2}{(2\pi)^4 (k_2^2 - m_2^2 + i\epsilon)(k_2^2 - m_2^2 - i\epsilon)}$$

$$\frac{|C_V|^2 G(k_{T1}^2) G(k_{T2}^2)}{(q^2 + i\epsilon)(q^2 - i\epsilon)} (2\pi)^2 \theta(k_1^0) \delta(k_1^2 - m_1^2) \theta((k_2 + q)^0)$$

$$\delta((k_2 + q)^2 - m_2^2) \frac{1}{4} L^{\mu\nu} (2k_2 + q)_\mu (2k_2 + q)_\nu \quad (3.1.7)$$

As before, we change to light cone variables using (1.5.5) and (2.4.3), equate the integrands, substitute (3.1.6), and cancel all the factors multiplying f_V^S . The result is

$$f_V^S(x_2) = \frac{|C_V|^2 h}{4(2\pi)^3 h'} \int \frac{dx_1}{x_1} d^2\underline{k}_{T1} d^2\underline{k}_{T2} d(k_1^2) d(k_2^2)$$

$$\delta(1 - x_1 - x_2) \delta^2(\underline{k}_{T1} + \underline{k}_{T2}) G(k_{T1}^2) G(k_{T2}^2) \theta(k_1^0) \delta(k_1^2 - m_1^2)$$

$$\delta(x_2 (m_V^2 - \sum_{i=1}^2 \frac{k_i^2 + k_{Ti}^2}{x_i})) \frac{1}{(k_2^2 - m_2^2)^2} \quad (3.1.8)$$

We integrate over the δ -functions in k^2 and use (2.5.8) for the k_T -integrals. Making the definitions

$$V \equiv \frac{\pi |C_V|^2}{4(2\pi)^3 \langle k_T^2 \rangle} \quad ; \quad \alpha_V \equiv \frac{m_V^2}{\langle k_T^2 \rangle} \quad (3.1.9)$$

and employing (2.6.4) and (2.6.5), leads to the final result

$$f_V^S(x_2) = V \int_0^1 dx_1 \frac{\delta(1 - \sum_{i=1}^2 x_i)}{x_1 x_2 (\alpha_V - \sum_{i=1}^2 \frac{\beta_i}{x_i})^2} \quad (3.1.10)$$

As we have already stressed, this simple expression should be good enough for our purposes, because it contains the denominator $(\alpha_V - \sum_{i=1}^2 \frac{\beta_i}{x_i})$, which governs the peak in f_V^S .

We now continue to the region $x > 1$, and consider the reciprocal process of fragmentation.

3.2 FRAGMENTATION FUNCTIONS

A fragmentation function, $D_i^A(z_A)$, is the probability density in z_A of a quark i fragmenting to a hadron A , which carries a fraction z_A of the quark's (light cone) momentum. Thus in $e^+e^- \rightarrow$ hadrons, the defining equation is (27)

$$\frac{1}{\sigma_{\text{tot}}} \frac{d\sigma(e^+e^- \rightarrow AX)}{dz_A} = \frac{1}{\sum_i e_i^2} \sum_i [e_i^2 (D_i^A(z_A) + D_i^A(z_A))] \quad (3.2.1)$$

To derive an expression for $D_i^A(z_A)$ we use the method developed for distribution functions. The relationship between the D 's and f 's will be brought out when we model the wavefunction.

Before starting the calculation, we discuss the inclusion of the word "heavy" in the title of this chapter, for which there is a good reason. If an experiment sets out to measure a fragmentation function of a quark i to a meson A then what will be measured is

$$D_i^A(z_A) \equiv \sum_m D_i^{Am}(z_A) \quad (3.2.2)$$

where $D_i^{Am}(z_A)$ is defined as the fragmentation function for i going to A and $m-1$ other partons, ($m \geq 2$). The summation is not only over m , but all possible sets of partons for each m value as well.

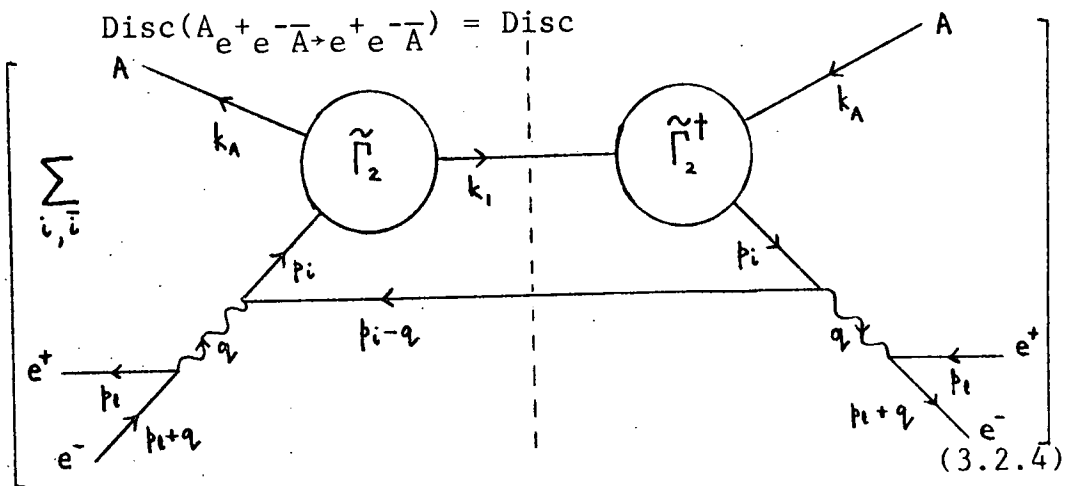
For light quark fragmentation many terms in this summation contribute. However, for a heavy quark fragmenting to a meson containing that heavy quark, the single term with $m=2$ will dominate⁽²⁸⁾. This is because most of the quark momentum carries through to the hadron, due to the large quark and hadron mass. Since $m \geq 3$ for a baryon this predicts that heavy quarks should fragment predominantly to heavy mesons, in agreement with experimental observations.

As valence constituent quark distributions are not measured experimentally, we had difficulty in testing our predictions in Chapter 2. However, providing we consider only heavy quarks, the expression we derive for $D_i^A(z_A)$ will be directly comparable with data.

We begin the derivation by again using (1.4.7),
in the form

$$16 \pi^3 E_A \frac{d^3 \sigma}{d^3 k_A} (e^+ e^- \rightarrow AX) = \frac{2}{h} \text{Disc}(A_{e^+ e^- \bar{A} \rightarrow e^+ e^- \bar{A}}) \quad (3.2.3)$$

where



We only consider $\tilde{\Gamma}_2$ as the quark is heavy. This expression is clearly very similar to (2.1.2), summed just for $m=2$. In (3.2.4) we change the labels $p_A \rightarrow -k_A$, $k_i \rightarrow -p_i$ for the fragmenting quark, and $\Gamma_2 \rightarrow \tilde{\Gamma}_2$, to bring out the fact that we are in an unphysical region as far as (2.1.2) is concerned. Our axis is now given by the three-momentum of the quark, rather than the hadron.

Since z_A is defined by

$$z_A \equiv \frac{k_A^+}{p_i^+} \quad (3.2.5)$$

it follows that

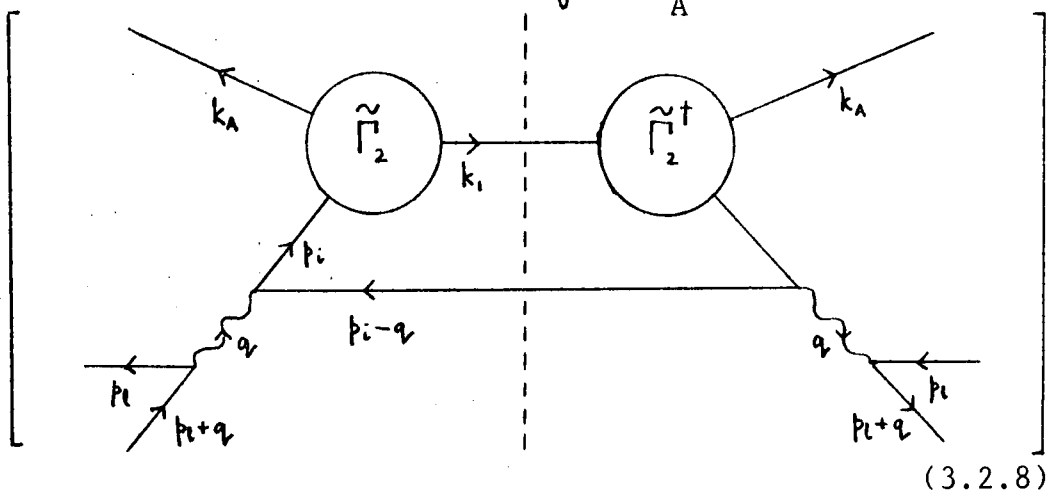
$$\begin{aligned}
 16\pi^3 E_A \frac{d^3\sigma(e^+e^- \rightarrow AX)}{d^3\mathbf{k}_A} &= 16\pi^3 k_A \frac{d^3\sigma(e^+e^- \rightarrow AX)}{dk_A^+ d^2\mathbf{k}_{TA}} \\
 &= 16\pi^3 z_A \frac{d^3\sigma(e^+e^- \rightarrow AX)}{dz_A d^2\mathbf{k}_{TA}} \quad (3.2.6)
 \end{aligned}$$

With this we integrate (3.2.3), obtaining an expression which equates to (3.2.1). Picking the term in the summation where i fragments to A , and using

$$\sigma_{\text{tot}} = \sigma(e^+e^- \rightarrow X) = 3\sigma(e^+e^- \rightarrow \mu^+\mu^-) \sum_i e_i^2 \quad (3.2.7)$$

where the factor 3 is from summing over colours, we get

$$3e_i^2 D_i^A(z_A) \sigma(e^+e^- \rightarrow \mu^+\mu^-) = \int \frac{d^2\mathbf{k}_{TA}}{16\pi^3 z_A} \frac{2}{h} \text{Disc}$$



To proceed further we need a model for $\tilde{\Gamma}_2$.

3.3 WAVEFUNCTION MODEL

$\tilde{\Gamma}_2$ has the same ingredients as Γ_2 , so we define

$$\tilde{\Gamma}_2 \equiv \tilde{C}_2 \tilde{g}_2(z_A, z_1) G^{\frac{1}{2}}(k_{TA}^2) G^{\frac{1}{2}}(k_{T1}^2) \bar{u}_i(\xi_i k_A) u_l(-\xi_l k_A) \quad (3.3.1)$$

The spinor structure is similar to that of (2.2.1), except hadron A is now a final state particle, so the quark (label i) and antiquark (label l) are out-going. The ξ 's are now the final four-momentum fractions, with $\xi_i + \xi_l = 1$.

\underline{k}_T is defined relative to the three momentum of the fragmenting quark. We assume the function which governs the binding of hadrons and quarks inside a quark is the same as that for quarks inside a hadron, $G(\underline{k}_T)$, and build in (2.5.3) to give the k_T -dependence of (3.3.1).

z_A is defined by (3.2.5), and z_1 by

$$z_1 \equiv \frac{k_1^+}{p_i^+} \quad (3.3.2)$$

To determine $\tilde{g}_2(z_A, z_1)$ we use the fact that (2.1.3) with $n=2$ and (3.2.8) describe the same process in different physical regions, so at the boundary between them the z -dependence of $\tilde{\Gamma}_2$ must be equivalent to the x -dependence of Γ_2 . $D_1^A(z_A)$ is then a smooth continuation of $f_A^i(x_2)$

to an unphysical value of x_2 , and vice versa. This is known as "reciprocity".

We therefore choose

$$|\tilde{g}_2(z_A, z_1)|^2 \equiv -z_A^2 z_1 \quad (3.3.3)$$

which may seem rather odd at first, although since we have a hadron and a quark there is no reason for it to be symmetric. Using light cone momentum conservation, $z_A + z_1 = 1$, (3.3.3) may be written

$$|\tilde{g}_2|^2 = -z_A^2(1-z_A) \quad (3.3.4)$$

and therefore

$$|\tilde{g}_2|^2 \Big|_{z_A=1} = 0 \quad ; \quad \frac{\partial}{\partial z_A} |\tilde{g}_2|^2 \Big|_{z_A=1} = 1 \quad (3.3.5)$$

If we re-write (2.2.4) using $x_1 + x_2 = 1$, it reads

$$|g_2|^2 = x_2(1-x_2) \quad (3.3.6)$$

From (1.5.4) and (3.2.5) it follows that

$$x_2 \equiv \frac{1}{z_A} \quad (3.3.7)$$

and substituting this into (3.3.6) we find

$$|g_2|^2 \Big|_{z_A=1} = 0 \quad ; \quad \frac{\partial}{\partial z_A} |g_2|^2 \Big|_{z_A=1} = 1 \quad (3.3.8)$$

$z_A = \frac{1}{x_2} = 1$ is where the physical regions for $D_i^A(z_A)$ and $f_A^i(x_2)$ meet, so (3.3.5) and (3.3.8) show that our choice for $|\tilde{g}_2|^2$, (3.3.3), does indeed join smoothly to $|g_2|^2$ at this point. This z -dependence will also cancel that of the fermion traces in our calculation, so the result for $D_i^A(z_A)$ will satisfy the dimensional counting rules.

The final ingredient in (3.3.1) to be accounted for is \tilde{C}_2 . This is simply a constant, dependent on the normalization of $D_i^A(z_A)$.

3.4 CALCULATION

We now return to (3.2.8), substitute (3.3.1), evaluate the discontinuity, and average over the spins of the external fermions, obtaining

$$3e_i^2 D_i^A(z_A) \sigma(e^+ e^- \rightarrow \mu^+ \mu^-) = \frac{-3}{h} \int \frac{d^2 k_{TA} d^4 p_i d^4 k_1}{16\pi^3 z_A (2\pi)^4}$$

$$\delta^4(p_i - k_A - k_1) e^4 e_i^2$$

$$\frac{\xi_1 \xi_i |\tilde{C}_2|^2 z_A^2 z_1 G(k_{TA}^2) G(k_{T1}^2) (2\pi)^2 \theta(k_1^0)}{(p_i^2 - m_i^2 + i\epsilon)(p_i^2 - m_i^2 - i\epsilon)}$$

$$\frac{\delta(k_1^2 - m_1^2) \theta((q-p_i)^0) \delta((q-p_i)^2 - m_i^2)}{(q^2 + i\epsilon)(q^2 - i\epsilon)}$$

$$\frac{1}{4} L^{\mu\nu} \frac{1}{4} T_{4\mu\nu}(k_A, p_i, p_i - q, p_i) T_2(-k_A, k_1) \quad (3.4.1)$$

The 3 on the right hand side comes from summing over the colours of i , and the traces are defined by (1.6.4) and (2.4.2).

We write $\sigma(e^+e^- \rightarrow \mu^+\mu^-)$ in the form

$$\sigma(e^+e^- \rightarrow \mu^+\mu^-) = \int \frac{dp_i^+ d^2 p_{T i} e^4 (2\pi) \theta((q-p_i)^0) \delta((q-p_i)^2 - m_i^2)}{16\pi^3 p_i^+ 4hq^4}$$

$$L^{\mu\nu} T_{2\mu\nu}(p_i, p_i - q) \quad (3.4.2)$$

by integrating (1.6.7) using (3.2.6). $T_{2\mu\nu}$ is defined by (1.6.8), and the flux factor h is the same as in (3.4.1). We change to light cone variables by substituting (1.5.5) and (2.4.3) into (3.4.1), along with (3.4.2). Equating the integrands, cancelling, operating with $P^{+\mu} P^{+\nu}$ (defined by (1.5.2)), and cancelling again, we obtain

$$D_i^A(z_A) = \frac{-|\tilde{C}_2|^2 \xi_1 \xi_i}{4(2\pi)^3} \int \frac{dz_1 d^2 \underline{k}_{TA} d^2 \underline{k}_{T1}}{z_A z_1} z_A^2 z_1 \delta(1-z_A-z_1)$$

$$\delta^2(\underline{k}_{TA} + \underline{k}_{T1}) G(k_{TA}^2) G(k_{T1}^2) d(k_1^2) \theta(k_1^0) \delta(k_1^2 - m_1^2) d(p_i^2)$$

$$\delta(p_i^2 - m_A^2 - k_1^2 - 2k_A \cdot k_1) \frac{(-2k_A \cdot k_1 + 2m_A m_1)}{(p_i^2 - m_i^2)^2}$$

$$(2k_A \cdot p_i + 2m_A m_i - z_A (p_i^2 - m_i^2)) \quad (3.4.3)$$

We replace the dot products using (1.5.6), being careful about the axis that defines \underline{k}_T , and integrate over k_1^2 , p_i^2 , and the transverse momenta using (2.5.8), which gives

$$D_i^A(z_A) = \frac{\pi \langle k_T^2 \rangle |\tilde{C}_2|^2 \xi_1 \xi_i}{4(2\pi)^3} \int_0^1 dz_1 \frac{\delta(1-z_1-z_A) z_A^2 z_1}{z_A z_1 (m_i^2 - \frac{\langle m_{TA}^2 \rangle}{z_A} - \frac{\langle m_{T1}^2 \rangle}{z_1})^2}$$

$$\left(\frac{z_1 \langle m_{TA}^2 \rangle + z_A \langle m_{T1}^2 \rangle + 2 \langle k_T^2 \rangle - 2m_A m_1}{z_A z_1} \right) \left(\frac{\langle m_{TA}^2 \rangle}{z_A} + z_A m_i^2 + 2m_A m_i \right) \quad (3.4.4)$$

$\langle m_T^2 \rangle$ is defined by (2.6.2). We tidy (3.4.4) by using some of the definitions from (2.6.5), and making the new ones

$$\tilde{V}_2 \equiv \frac{\pi \langle k_T^2 \rangle |\tilde{C}_2|^2 \xi_1 \xi_i}{4(2\pi)^3} ; \quad \tilde{\alpha} \equiv \frac{\langle m_{TA}^2 \rangle}{\langle k_T^2 \rangle} ; \quad \tilde{\beta}_i \equiv \frac{m_i^2}{\langle k_T^2 \rangle} \quad (3.4.5)$$

The final result is

$$D_i^A(z_A) = \tilde{V}_2 \int_0^1 \frac{dz_1 \delta(1-z_1-z_A) z_A^2 z_1}{z_A z_1 (\tilde{\beta}_i - \frac{\tilde{\alpha}}{z_A} - \frac{\tilde{\beta}_1}{z_1})^2}$$

$$\left(\frac{z_1 \tilde{\alpha}}{z_A} + \frac{z_A \tilde{\beta}_1}{z_1} + 2 - 2\gamma_1 \right) \left(\frac{\tilde{\alpha}}{z_A} + z_A \tilde{\beta}_i + 2\gamma_i \right) \quad (3.4.6)$$

This has a similar structure to the expression for $f_A^2(x_2)$, (2.6.7) with $n=2$. The differences arise because here a quark goes to a hadron and a quark, instead of a hadron going to a quark and an antiquark.

Reciprocity predicts the same dimensional counting behaviour for $D_i^A(z_A)$ and $f_A^2(x_2)$, and from (3.4.6) we see that $D_i^A(z_A) \sim z_A^{-1} (1-z_A)$, as expected. This result contrasts with that of Peterson et al⁽²⁹⁾. They include a factor z_A^{-1} for the hadron phase-space and (presumably) assume the z -dependence of the wavefunction cancels that of the fermion traces, but omit the phase space of the final quark. They have a similar denominator to ours; the full expression is

$$D_i^A(z_A) = \frac{N}{z_A \left(1 - \frac{1}{z_A} - \frac{\epsilon_i}{1-z_A}\right)^2} \quad (3.4.7)$$

where N is a normalization constant, and ϵ_i is roughly the ratio of the light to heavy quark masses squared, ie $\epsilon_i \sim m_q^2/m_i^2$. (3.4.7) gives $D_i^A(z_A) \sim z_A^{-1} (1-z_A)^2$, in conflict with the dimensional counting rules.

We conclude this chapter by confronting (3.4.6) with experimental data.

3.5 COMPARISON WITH EXPERIMENT

The lightest quark for which taking one term in the summation in (3.2.2) is a good approximation is the charmed quark. To date most of the measurements on heavy quark fragmentation are for charm although results for bottom quarks are beginning to appear.

Before we compare (3.4.6) with this data there is a subtlety to consider, as we explained at the start of this chapter. In an experiment where $e^+e^- \rightarrow c\bar{c}$ a final state D-meson can either come from the charmed quark directly, or via a D^* . We therefore plot

$$D_c^D(z, a) \equiv aD_c^D(z) + (1-a) \int_z^1 \frac{dy}{y} D_c^{D^*}(y) f_{D^*}^D\left(\frac{z}{y}\right) \quad (3.5.1)$$

where D_c^D , $D_c^{D^*}$ and $f_{D^*}^D$ are calculated from (3.4.6) and (3.1.10) respectively. The constant "a" lies in the range $0 \leq a \leq 1$. The first term in (3.5.1) is the direct fragmentation of $c \rightarrow D$, and the second is where there is an intermediate D^* ; the integral is a (probability conserving) convolution. The masses used to evaluate (3.5.1) are given in table 2a, with the exception of the hadron transverse masses, which we calculate from the actual masses using (2.6.2).

In figure 3.2 we plot the D-meson data against (3.5.1), for $a=0.25$ and 0.50 . Just counting spin degeneracy predicts $a=0.25$ (ie D^* 's are produced 3

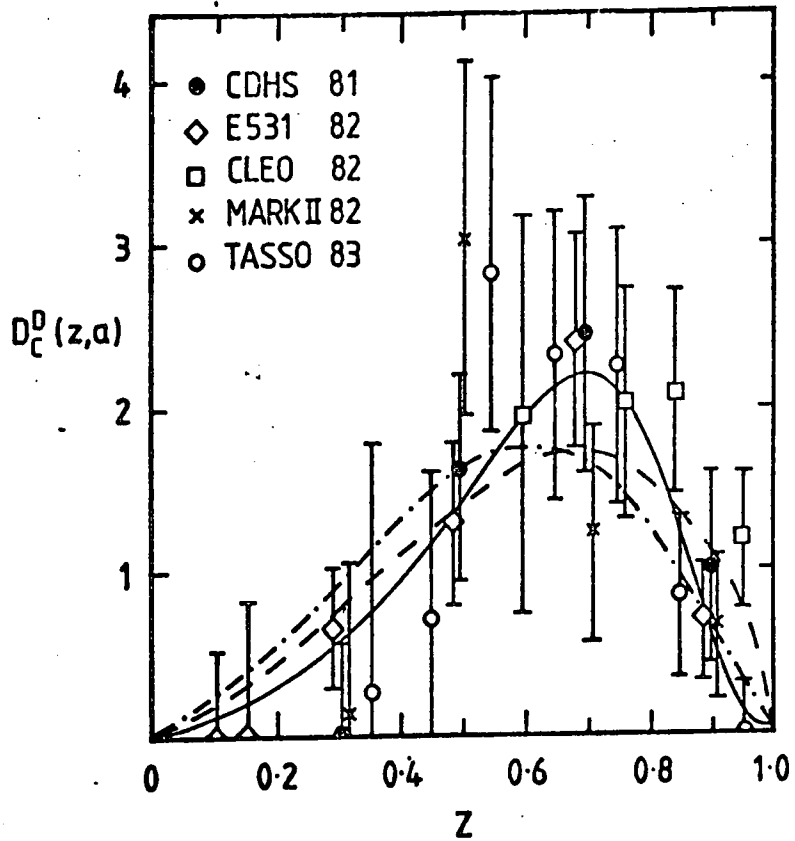


Figure 3.2: Our predictions for D_c^D calculated from (3.5.1) with $a=0.25$ (---) and $a=0.50$ (-----), compared with the data⁽³⁰⁾. Also shown is the prediction of Peterson et al⁽²⁹⁾ (—) calculated from (3.4.7) with $\epsilon_Q=0.10$.

times more often than D's), but unless we suppose there is some suppression of the higher spin (and mass) states there seems little justification for neglecting D**'s etc. The choice $a=0.5$ is probably more realistic, therefore, and this is perhaps borne out in figure 3.2, although given the error bars, either curve is acceptable. The choice $a=0.5$ is definitely preferred in table 3a, though, for the average z-values of the D-(and also B-) mesons.

Experiment	\bar{z}_D	\bar{z}_B
MARK - II	0.59±0.06	0.79±0.09
CLEO	0.68±0.08	
MAC		0.80±0.10
TASSO	0.68±0.08	
MARK-J	0.46±0.05	0.74±0.10
CDHS	0.68±0.08	
HRS	0.56±0.02	
DELCO	0.60±0.10	
JADE	0.55±0.06	
E531	0.62±0.08	
Average	0.60	0.78
Prediction from		
(3.5.1) with $a=0.25$	0.56	0.69
(3.5.1) with $a=0.50$	0.60	0.72
(3.4.7)	0.63	0.79

Table 3a: Our predictions for the average momentum

fractions of D-(B-) mesons produced from c(b) quarks, compared with the measured values⁽³⁰⁾. Also shown are the predictions of Peterson et al⁽²⁹⁾ with $\epsilon_c=0.10$ and $\epsilon_b=m_c^2/m_b^2=0.011$.

We also plot the prediction of Peterson et al⁽²⁹⁾ in figure 3.2, which considering the errors on the data is an acceptable alternative to our model, although it is less attractive from a theoretical viewpoint. Figures 3.3 and 3.4 compare our model with theirs for D_b^B and D_t^T respectively. Our distributions are broader because we consider the possibility of intermediate vector mesons. When data appears care should be taken to compare like with like. Both models predict $\bar{z} \rightarrow 1$ as the mass increases, in agreement with the experimental results in table 3a.

We conclude that our calculations, culminating in (3.5.1), give a good description of the present experimental results. When the data improves, there will clearly be scope for improving the predictions, for example by varying $\langle k_T^2 \rangle$ for a hadron inside a hadron and tuning "a", but at present the experimental errors are just too large.

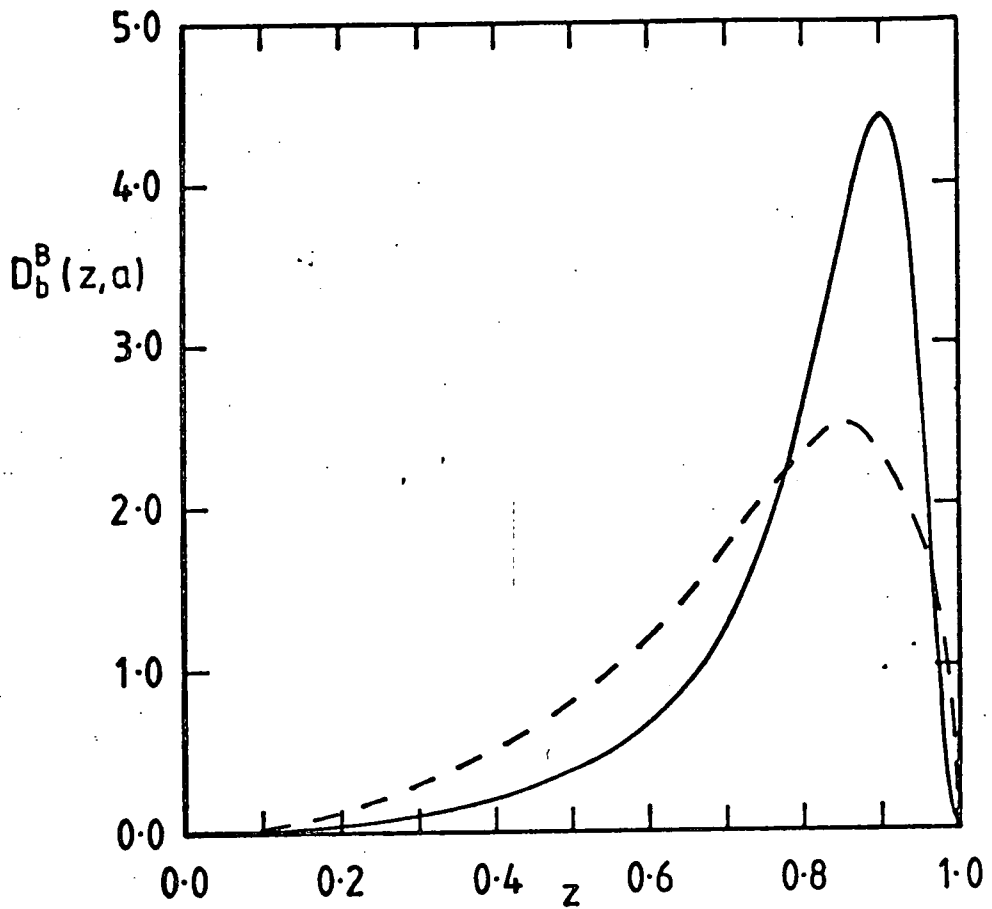


Figure 3.3: Our prediction for D_b^B , calculated from (3.5.1) with $a=0.5$ (---), along with that of Peterson et al⁽²⁹⁾ calculated from (3.4.7) with $\epsilon_Q = 1.1 \times 10^{-2}$ (—).

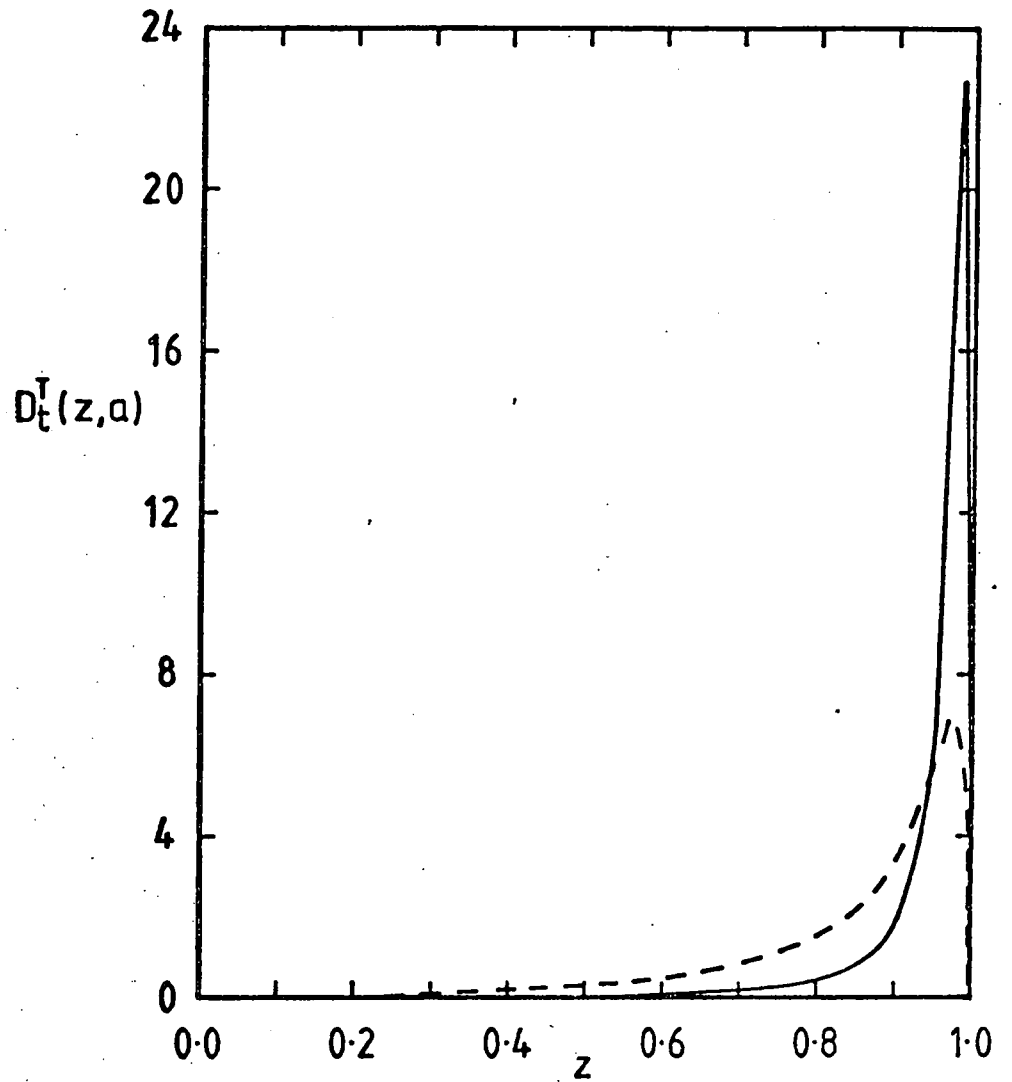


Figure 3.4: Our prediction for D_t^I calculated from (3.5.1) with $a=0.5$ (---) and using $m_t=35$ GeV, along with that of Peterson et al⁽²⁹⁾ calculated from (3.4.7) with $\epsilon_Q=2.3 \times 10^{-4}$ (—).

CHAPTER 4

INTRINSIC HEAVY QUARKS

4.1 INTRODUCTION

In Chapter 1 we suggested that intrinsic heavy quarks may provide an explanation for the forward production of naked heavy flavours in hadron-hadron interactions. In this chapter we construct a model wavefunction which determines their presence in hadrons. This will enable us to calculate heavy quark distributions, in a similar manner to the valence quark distributions of Chapter 2. Finally, for the case of intrinsic charm in a nucleon, we shall compare our results with the EMC deep inelastic scattering data⁽³¹⁾.

In Chapter 2 we considered hadrons to be composed of valence quarks alone, and concluded in such a picture that these have to be constituent, rather than current, quarks ie bare current quarks dressed by a sea of gluons and $q\bar{q}$ pairs.

If a hadron, such as a proton or a pion, is probed hard enough, we know from experiment that occasionally heavy flavours are produced. These have two possible sources; either heavy flavoured quarks are produced in the interaction, or were already inside the hadron and are simply knocked on mass-shell by the probe. In both cases they must then hadronize in some way. (In a sense these contributions are just different time-

orderings of the same diagram.) We return to the former process when comparing our results with experiment, but it is the latter which is the subject of our calculations.

Probing a hadron sufficiently hard, we cannot think of it as being composed just of its valence constituent quarks. Some of the time it will also consist of these plus heavy $Q\bar{Q}$ pairs. For example, a proton may be regarded as being partially in the $|uudQ\bar{Q}\rangle$ Fock state. In this state its momentum is distributed amongst all five quarks, so they are still to be thought of as constituent quarks.

Our aim is to calculate both the x -distributions and normalizations of such heavy $Q\bar{Q}$ pairs inside the light hadrons (ie π, p, n), which form the beams and targets in experiments.

4.2 WAVEFUNCTION MODEL MOTIVATED BY PERTURBATIVE QCD

Our model for the origin of $Q\bar{Q}$ pairs inside a light hadron is that they are created, via a gluon, off one of the valence quarks, as shown in figure 4.1. We again use a photon as our probe, for the purpose of doing the calculations. Figure 4.1 shows the probability of heavy quarks occurring is proportional to α_s^2 , and we incorporate the leading logarithmic

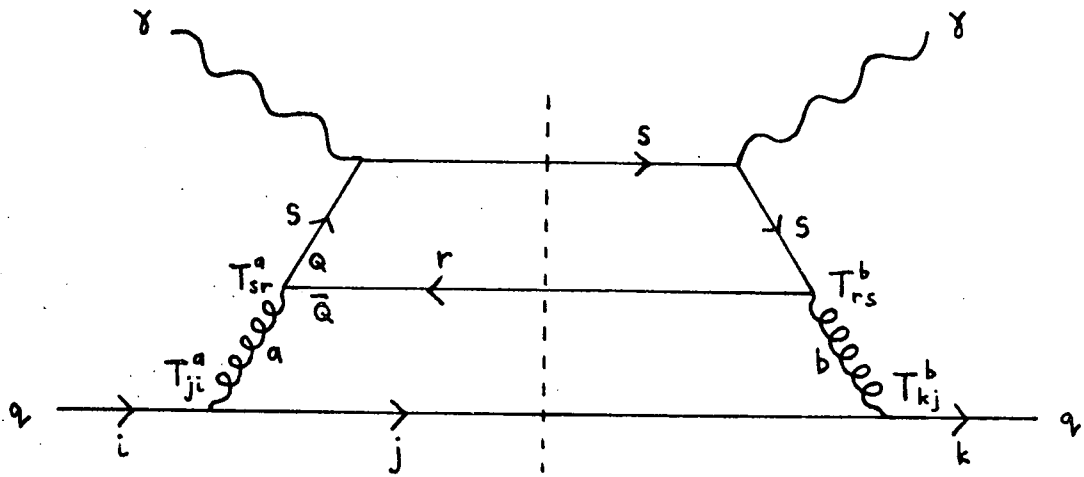


Figure 4.1: The creation of a heavy $Q\bar{Q}$ pair off a light quark q , showing the colour structure. The diagram is for the probability ie the squared modulus of the amplitude.

corrections to all orders by using the running coupling⁽⁴⁾

$$\alpha_s = \frac{12\pi}{(33-2N_f)\log(\frac{Q^2}{\Lambda^2})} \quad (4.2.1)$$

N_f is the number of quark flavours and Λ is the QCD scale parameter. (We take $\Lambda = 0.3$ GeV in all our calculations). Q^2 is the momentum squared scale of the process. We assume $Q^2 = 4\langle m_{TQ}^2 \rangle$ ($\langle m_{TQ}^2 \rangle$ is defined by (2.6.2)), as this is roughly the threshold for the creation of a pair of hadrons containing Q and \bar{Q} . The $Q\bar{Q}$ pair exist virtually at any Q^2 , but if we probe with insufficient Q^2 for them to end up on mass-shell, they must always annihilate back to a gluon.

The colour factor from figure 4.1 is

$$C \equiv \langle T_{kj}^b T_{ji}^a T_{rs}^b T_{sr}^a \rangle = \langle \frac{1}{2} T_{kj}^b T_{ji}^a \delta^{ba} \rangle = \langle \frac{2}{3} \delta_{ki} \rangle = \frac{2}{3} \quad (4.2.2)$$

Since the quark q is in a hadron we have averaged over $k=i$. We do not sum over flavours in the quark loop because we are concerned with a loop of one particular flavour.

4.3 GENERAL CALCULATION

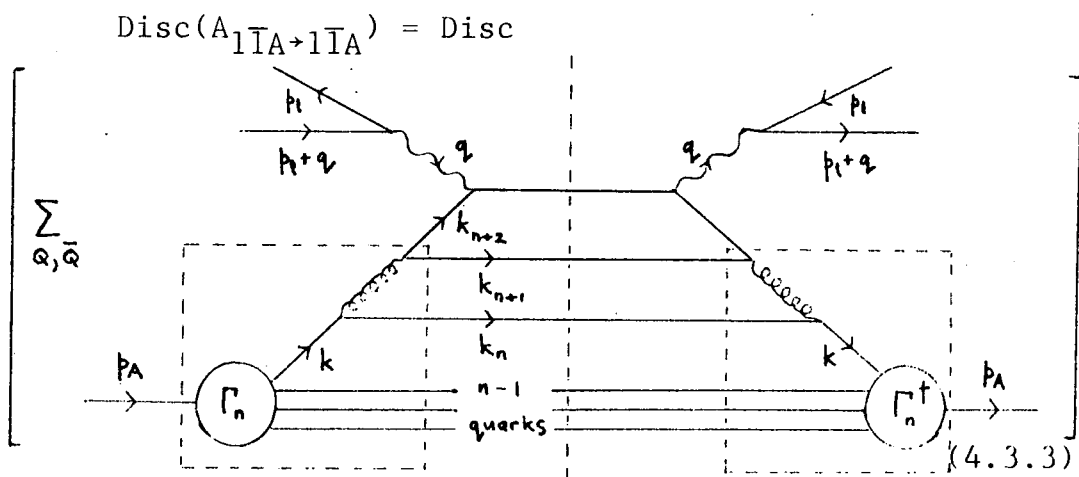
For heavy quark production in deep inelastic scattering the distribution function $f_A^Q(x_Q)$ is defined by

$$16 \pi^3 E_1 \frac{d^3 \sigma(1A \rightarrow 1Q \bar{Q} X)}{d^3 p_1} \equiv \sum_{Q, \bar{Q}} \int_0^1 dx_Q f_A^Q(x_Q) 16 \pi^3 E_1 \frac{d^3 \sigma(1Q \rightarrow 1Q)}{d^3 p_1} \quad (4.3.1)$$

As before, Mueller's theorem, (1.4.7), provides an alternative expression for the left hand side of (4.3.1),

$$16 \pi^3 E_1 \frac{d^3 \sigma(1A \rightarrow 1Q \bar{Q} X)}{d^3 p_1} = \frac{2}{h} \text{Disc}(A_1 \bar{1}A \rightarrow 1 \bar{1}A) \quad (4.3.2)$$

except now



The notation in (4.3.3) is the same as that in (2.1.2).

The calculations will produce not only the form of f_A^Q , but also its normalization relative to the constituent valence distribution, since the valence Γ_n of Chapter 2 appear again. The dotted outlines are drawn around what we consider to be happening inside the hadron, to enforce the idea that the $Q\bar{Q}$ pair is intrinsic. The principle of the calculation is exactly the same as Chapter 2, and most of it may be done for general n . However the arithmetic is rather more complicated.

We begin by equating (4.3.1) and (4.3.2), using (4.3.3) and taking just one term in the summation, to get

$$\int_0^1 dx_{n+2} f_A^{n+2}(x_{n+2}) 16 \pi^3 E_1 \frac{d^3 \sigma(1Q \rightarrow 1Q)}{d^3 p_1} = -\frac{C}{h} \frac{n}{\Sigma}$$

$$\int_{i=1}^{n+1} \Pi \left[\frac{d^4 k_i \theta(k_i^0) \delta(k_i^2 - m_i^2) G(k_{Ti}^2)}{(2\Pi)^3} \right]$$

$$\frac{d^4 k_{n+2} \delta^4(p_A - \sum_{i=1}^{n+2} k_i) (2\Pi) \theta((k_{n+2} + q)^0) \delta((k_{n+2} + q)^2 - m_Q^2)}{(k_{n+2}^2 - m_Q^2 + i\varepsilon)(k_{n+2}^2 - m_Q^2 - i\varepsilon)(k^2 + i\varepsilon)(k^2 - i\varepsilon)((k_{n+2} + k_{n+1})^2 + i\varepsilon)}$$

$$\frac{G(k_{Tn+2}^2) |g_n|^2 |C_n|^2 e^4 e_{n+2}^2 g_s^4}{((k_{n+2} + k_{n+1})^2 - i\varepsilon)(q^2 + i\varepsilon)(q^2 - i\varepsilon)} \frac{1}{4} L^{\mu\nu} \frac{1}{2^n} \prod_{i=1}^{n-1}$$

$$[\xi_i T_2(p_A, k_i)] \xi_n T_4^{\rho\sigma}(p_A, k, k_n, k) T_{4\mu\nu\rho\sigma}(k_{n+2}, k_{n+2} + q, k_{n+2}, -k_{n+1})$$

(4.3.4)

The minus sign comes from the heavy quark loop, C is the colour factor of (4.2.4), \sum_n means sum over the $Q\bar{Q}$ being created off any of the valence quarks, and g_s is the strong interaction coupling, where

$$\alpha_s = \frac{g_s^2}{4\Pi} \quad (4.3.5)$$

We have defined

$$k \equiv k_{n+2} + k_{n+1} + k_n \quad (4.3.6)$$

and used the trace definitions of (1.6.4) and (2.4.2), along with the new one

$$T_{4\mu\nu\rho\sigma}(k_{n+2}, k_{n+2+q}, k_{n+2}, -k_{n+1}) \equiv \text{Tr}\{(k_{n+2}+m_Q) \gamma_\mu (k_{n+2}+q+m_Q) \gamma_\nu (k_{n+2}+m_Q) \gamma_\rho (-k_{n+1}+m_Q) \gamma_\sigma\} \quad (4.3.7)$$

These come from averaging over the spins of the external fermions, using (2.n.1) for Γ_n . We have been careful to get the arguments of the n G 's and g_n correct (as k emerges from Γ_n , not k_n), and then used (2.5.5) to obtain the produce of $n+2$ G 's. Finally we have put the valence quark current masses zero, as this simplifies matters, and is almost true for hadrons made of u and d valence quarks which interest us.

Taking (4.3.4) we substitute for the lepton-quark cross-section, (1.6.7), and change to light cone variables using (1.5.5) and (2.4.3). Equating integrands, cancelling, and applying $P^+ \mu P^{+\nu}$ (defined by (1.5.2)), we obtain

$$f_A^{n+2}(x_{n+2}) = -C \Sigma x_{n+2} |C_n|^2 (4\pi\alpha_s)^2 \int_{i=1}^{n+1} \frac{dx_i d^2k_{-Ti} d(k_i^2)}{2x_i (2\pi)^3}$$

$$\theta(k_i^0) \delta(k_i^2 - m_1^2) G(k_{Ti}^2) \left] \delta\left(1 - \sum_{i=1}^{n+2} x_i\right) |g_n|^2 d^2 k_{Tn+2}\right.$$

$$G(k_{Tn+2}^2) \delta^2\left(\sum_{i=1}^{n+2} k_{Ti}\right) d(k_{n+2}^2) \delta\left(x_{n+2} \left(m_A^2 - \sum_{i=1}^{n+2} \frac{k_i^2 + k_{Ti}^2}{x_i}\right)\right)$$

$$\frac{1}{2} \prod_{i=1}^{n-1} [\xi_i T_2(p_A, k_i)] \frac{\xi_n T_4^{\rho\sigma}(p_A, k, k_n, k)}{(k_{n+2}^2 - m_Q^2)^2 (k_{n+2} + k_{n+1})^4}$$

$$\frac{T_4^{\rho\sigma}(k_{n+2}, k_{n+2+q}, k_{n+2}, -k_{n+1})}{k^4 8k_{n+2}^+(k_{n+2+q})^+} \quad (4.3.8)$$

We have used the analogue of (2.6.4) for the flux factor ratio, and (4.3.5) to remove g_s . The traces in (4.3.8) have already been evaluated in (2.4.5), except for the last one. The calculation of this is straightforward, and gives

$$-T_4^{\rho\sigma}(k_{n+2}, k_{n+2+q}, k_{n+2}, -k_{n+1}) = 4k_{n+2}^+(k_{n+2+q})^+$$

$$\{4(k_{n+2\rho} k_{n+1\sigma} + k_{n+2\sigma} k_{n+1\rho})$$

$$-2g_{\rho\sigma} [2(k_{n+2} \cdot k_{n+1} + m_Q^2) - \frac{x_{n+1}}{x_{n+2}} (k_{n+2}^2 - m_Q^2)]$$

$$-2(P_\rho^+ k_{n+1\sigma} + P_\sigma^+ k_{n+1\rho}) \frac{k_{n+2}^2 - m_Q^2}{k_{n+2}^+} \} \quad (4.3.9)$$

The remaining steps are exactly those at the end of the derivation of $f_A^n(x_n)$. We substitute for the traces in (4.3.8) using (2.4.5) and (4.3.9), and

contract over the indices ρ and σ , obtaining dot products which we replace with (1.5.6). We evaluate the $n+2$ k^2 -integrals over the δ - functions, and the $n+2$ k_T -integrals by the prescription of (2.5.8), leaving the x -integrals. We omit the details, but in the next section we write out the results for $n=2$ and 3 in full.

4.4 EXPLICIT SOLUTIONS FOR PION AND NUCLEON

We use the definitions of (2.6.5), with the addition

$$\beta_{n+2} = \beta_{n+1} \equiv \beta \quad (4.4.1)$$

since the Q and \bar{Q} have equal mass. $\beta_i=1$ for the valence quarks. If $\{x_m\}$ denotes the set $\{x_1, \dots, x_m\}$, for a heavy quark in a light meson we have

$$\int_0^1 \prod_{i=1}^3 [dx_i] \delta(1 - \sum_{i=1}^4 x_i) f_A^4(\{x_4\}) \equiv f_A^4(x_4) = \frac{CV_2}{x_4} \left(\frac{\alpha_s}{2\pi}\right)^2$$

$$\int_0^1 \prod_{i=1}^3 \frac{dx_i}{x_i} \frac{\delta(1 - \sum_{i=1}^4 x_i)}{(\alpha - \sum_{i=1}^4 \frac{\beta_i}{x_i})^2 ((1 - \sum_{i=1}^2 x_i)(\alpha - \sum_{i=1}^2 \frac{1}{x_i}) - \frac{4}{3})^2}$$

$$\left\{ \frac{x_1(1-x_1)(1/x_1 + \alpha x_1)}{((1-x_1)(\alpha - 1/x_1) - 1)^2} \right.$$

$$\begin{aligned}
 & \left[\frac{2\beta^2 x_2}{x_3 x_4} (1-\alpha(1-x_1)^2) + \beta \left(\frac{x_3}{x_4} + \frac{x_4}{x_3} + 4 \right) \left[\alpha \left(\frac{1}{x_2} + \alpha x_2 \right) \right. \right. \\
 & \left. \left. - \left(\frac{x_1}{x_2} + \frac{x_2}{x_1} + \frac{2}{3} \right) (\alpha(1-x_1) + \alpha - \frac{1}{x_1}) \right] - (\alpha(1-x_1) + \alpha - \frac{1}{x_1}) \right. \\
 & \left. \left[\frac{2}{3} \left(\frac{1}{x_3} + \frac{1}{x_4} \right) (x_1 + x_2) - \frac{2}{3} \left(\frac{x_3}{x_4} + \frac{x_4}{x_3} - 2 \left(\frac{x_1}{x_2} + \frac{x_2}{x_1} + \frac{2}{3} \right) \right) \right. \right. \\
 & \left. \left. + \alpha \left[\frac{2}{3} \left(\frac{1}{x_3} + \frac{1}{x_4} \right) - 2 \left(\frac{1}{x_2} + \alpha x_2 \right) \right] \right\} + \left\{ \alpha \left[\frac{2\alpha x_4 x_3}{x_2} + \frac{2\alpha}{3} (x_3 + x_4) \right. \right. \right. \\
 & \left. \left. + \frac{4}{3} \left(\frac{1}{x_2} + \alpha x_2 \right) \right] - (\alpha(1-x_1) + \alpha - \frac{1}{x_1}) \left[\frac{2x_4 x_3}{x_1 x_2} + \frac{2}{3} (x_3 + x_4) \right. \right. \\
 & \left. \left. \left(\frac{1}{x_1} + \frac{1}{x_2} \right) + \frac{4}{3} \left(\frac{x_1}{x_2} + \frac{x_2}{x_1} + \frac{2}{3} \right) + \frac{8}{9} \right] - \frac{10}{3} \left[\alpha \left(\frac{1}{x_2} + \alpha x_2 \right) \right. \right. \\
 & \left. \left. - \left(\frac{x_1}{x_2} + \frac{x_2}{x_1} + \frac{2}{3} \right) (\alpha(1-x_1) + \alpha - \frac{1}{x_1}) \right] \right\} + 1 \leftrightarrow 2 \} \\
 & \hspace{20em} (4.4.2)
 \end{aligned}$$

Clearly the term $1 \leftrightarrow 2$ gives an identical contribution to $f_A^4(x_4)$. However this will not be true when we consider diffractive production of heavy flavour hadrons.

The analogous result for a heavy quark in a light baryon is

$$\int_0^1 \prod_{i=1}^4 [dx_i] \delta(1 - \sum_{i=1}^5 x_i) f_A^5(\{x_i\}) \equiv f_A^5(x_5) = \frac{CV_3}{x_5} \left(\frac{\alpha_S}{2\pi}\right)^2$$

$$\int_0^1 \prod_{i=1}^4 \left[\frac{dx_i}{x_i} \right] \frac{\delta(1 - \sum_{i=1}^5 x_i)}{(\alpha - \sum_{i=1}^5 \frac{\beta_i}{x_i})^2 ((1 - \sum_{i=1}^3 x_i)(\alpha - \sum_{i=1}^3 1/x_i) - 3/2)^2}$$

$$\left\{ \frac{x_1 x_2 (1-x_1-x_2)(1/x_1+\alpha x_1)(1/x_2+\alpha x_2)}{(\alpha - \frac{1}{x_1} - \frac{1}{x_2} - \frac{1}{(1-x_1-x_2)})^2 ((1-x_1-x_2)(\alpha - \frac{1}{x_1} - \frac{1}{x_2}) - \frac{3}{2})^2} \right.$$

$$\left[\frac{2\beta^2 x_3}{x_4 x_5} \left(\frac{3}{2} + \alpha(1-x_1-x_2)^2 \right) + \beta \left(\frac{x_4}{x_5} + \frac{x_5}{x_4} + 4 \right) \right.$$

$$\left[\left(\alpha - \left(\frac{x_1}{x_2} + \frac{x_2}{x_1} + \frac{1}{2} \right) \right) \left(\frac{1}{x_3} + \alpha x_3 \right) - \left(\frac{x_1+x_2}{x_3} + x_3 \left(\frac{1}{x_1} + \frac{1}{x_2} \right) + 1 \right) \right.$$

$$\left. \left(\alpha(1-x_1-x_2) + \alpha - \frac{1}{x_1} - \frac{1}{x_2} \right) \right] - \left(\alpha(1-x_1-x_2) + \alpha - \frac{1}{x_1} - \frac{1}{x_2} \right)$$

$$\left[\frac{1}{2} \left(\frac{1}{x_4} + \frac{1}{x_5} \right) (x_1+x_2+2x_3) - \left(\frac{x_4}{x_5} + \frac{x_5}{x_4} \right) - 2 \left(\frac{x_1+x_2}{x_3} + x_3 \left(\frac{1}{x_1} + \frac{1}{x_2} \right) + 1 \right) \right]$$

$$+ \left(\alpha - \left(\frac{x_1}{x_2} + \frac{x_2}{x_1} + \frac{1}{2} \right) \right) \left[\frac{1}{2} \left(\frac{1}{x_4} + \frac{1}{x_5} \right) - 2 \left(\frac{1}{x_3} + \alpha x_3 \right) \right] + \left(\alpha - \left(\frac{x_1+x_2}{x_2} + \frac{1}{2} \right) \right)$$

$$\left[\frac{2\alpha x_4 x_5}{x_3} + \frac{\alpha(x_4+x_5)}{2} + \frac{3}{2} \left(\frac{1}{x_3} + \alpha x_3 \right) \right] - \left(\alpha(1-x_1-x_2) + \alpha - \frac{1}{x_1} - \frac{1}{x_2} \right)$$

$$\left[\frac{2x_4 x_5}{x_3} \left(\frac{1}{x_1} + \frac{1}{x_2} \right) + \frac{1}{2} (x_4 + x_5) \left(\frac{1}{x_1} + \frac{1}{x_2} + \frac{2}{x_3} \right) + 3 \frac{(x_1 + x_2)}{x_3} + x_3 \left(\frac{1}{x_1} + \frac{1}{x_2} \right) + 1 \right]$$

$$-\frac{7}{2} \left[\left(\alpha - \frac{(x_1 + x_2 + \frac{1}{2})}{x_2 x_1} \right) \left(\frac{1}{x_3} + \alpha x_3 \right) - \frac{(x_1 + x_2)}{x_3} + x_3 \left(\frac{1}{x_1} + \frac{1}{x_2} \right) + 1 \right]$$

$$\left. \left(\alpha(1 - x_1 - x_2) + \alpha - \frac{1}{x_1} - \frac{1}{x_2} \right) \right] \} + 1 \leftrightarrow 3 + 2 \leftrightarrow 3 \} \quad (4.4.3)$$

Again we have put in the terms from Σ^n explicitly, rather than multiplying by 3, so $f_A^5(\{x_5\})$ need not be re-defined later on.

4.5 COMMENTS

The expressions (4.4.2) and (4.4.3) are normalized relative to their corresponding valence distributions (given by (2.6.7)). We can therefore plot them without further assumptions, and do so in figures 4.2 and 4.3 for a pion and a proton respectively. The remaining x-integrals after the one over the δ -function are calculated numerically.

The distributions all diverge in the same way that normal sea distributions do⁽³²⁾, so the amount of momentum carried is finite. The reduction of the magnitude with increasing mass is mainly due to the running coupling, (4.2.1), with the choice of $Q^2 = 4 \langle m_{TQ}^2 \rangle$. The distributions in the pion and proton

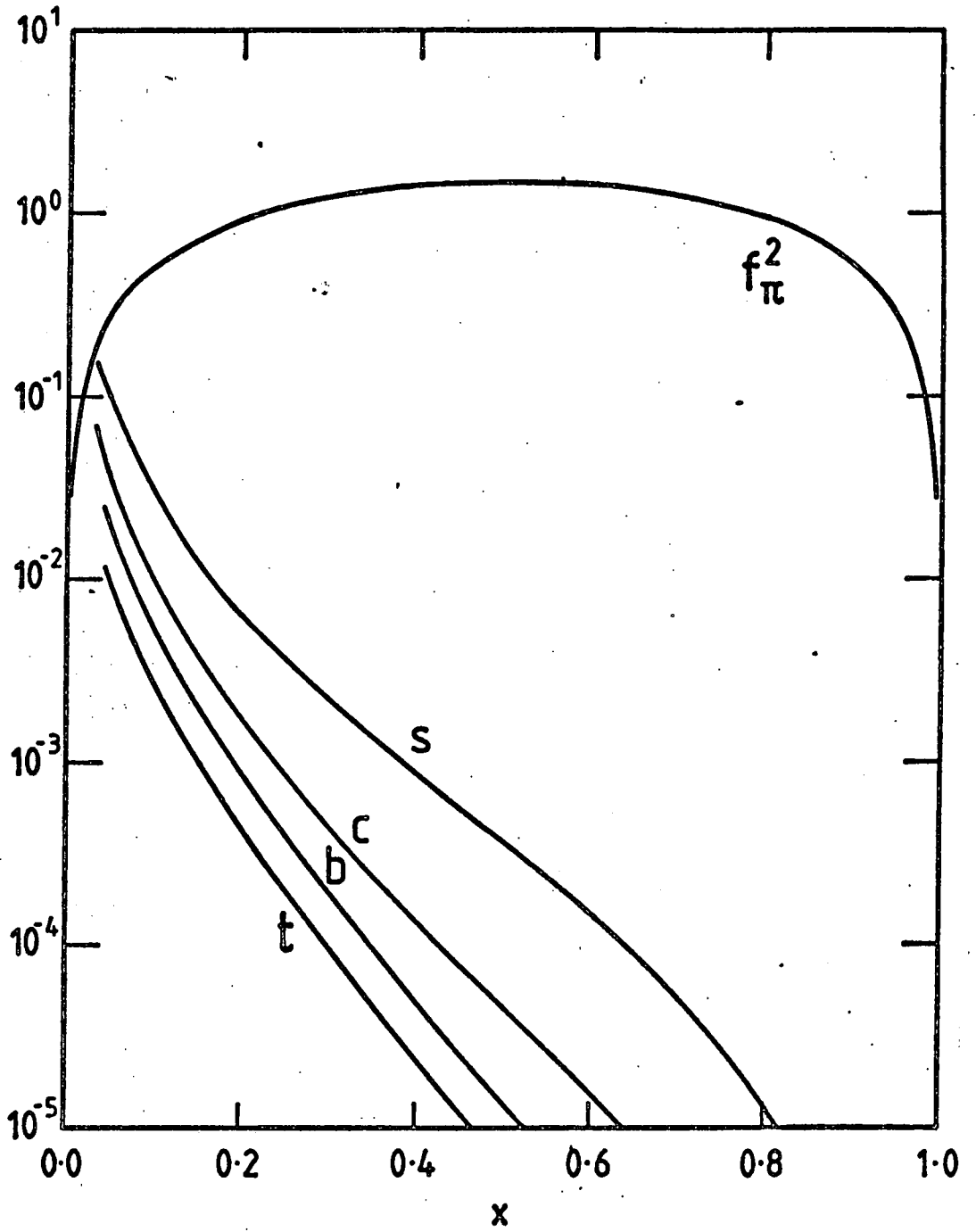


Figure 4.2: The intrinsic heavy quark distributions in a pion, calculated from (4.4.2), for f_{π}^2 (also shown) normalized to unity. The masses are from table 2a, taking only $m_t=35$ GeV.

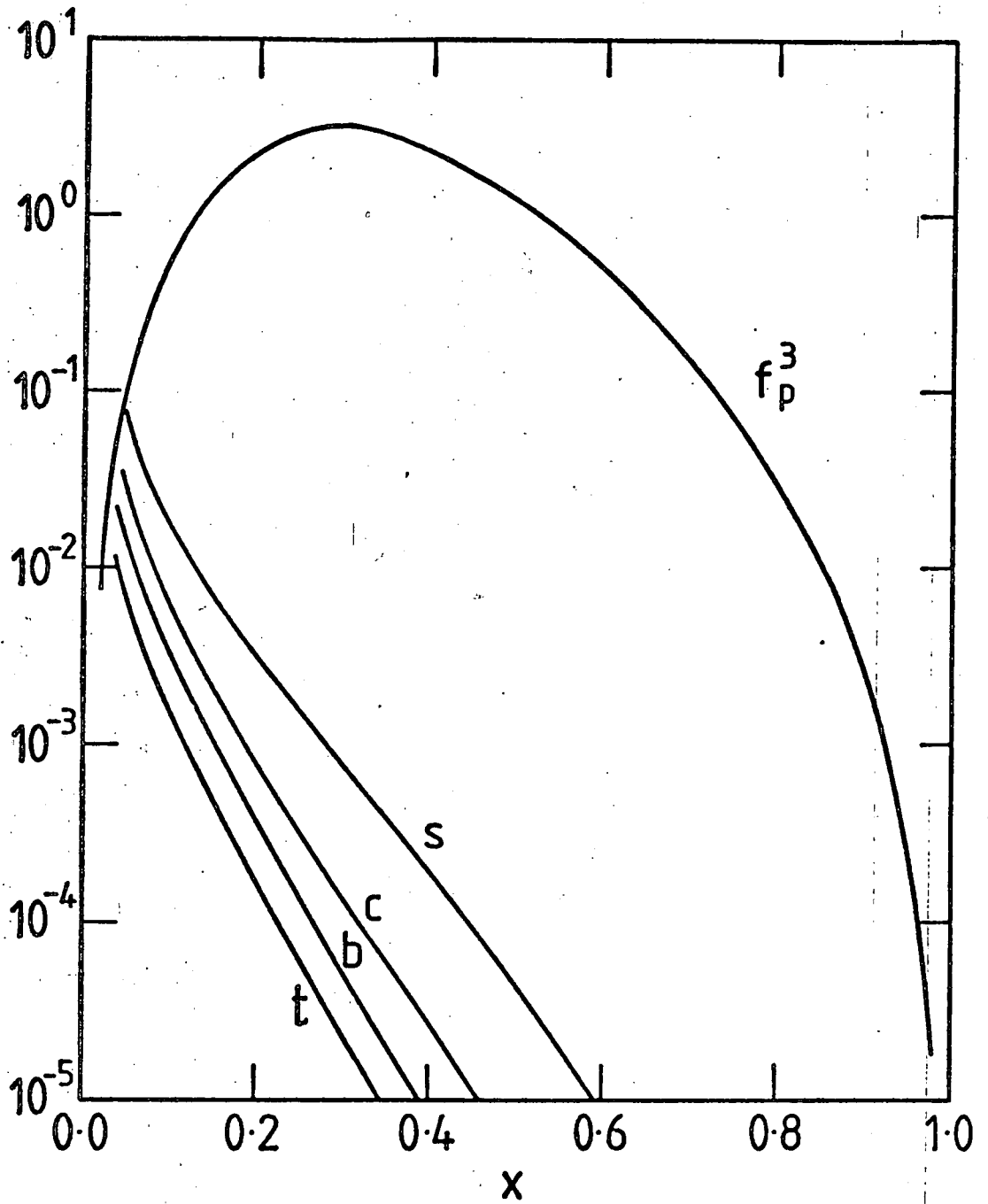


Figure 4.3: The intrinsic heavy quark distributions in a proton, calculated from (4.4.3), for f_p^3 (also shown) normalized to unity. The masses used are from table 2a taking only $m_t = 35$ GeV.

have comparable values near $x=0$ for each flavour, but the proton ones fall faster with increasing x . This is due to the larger number of quarks in the Fock state producing a more suppressed dimensional counting behaviour.

These predictions are in sharp contrast to those of Brodsky et al⁽⁷⁾, who conclude that an intrinsic $Q\bar{Q}$ pair in a light hadron carry most of its momentum. They back their findings up by applying the argument that the quarks should all have the same velocity to hold together in a hadron. However the $Q\bar{Q}$ pairs are being created and annihilated all the time, which suggests that they should favour very small x , as we find.

4.6 RELATION OF DISTRIBUTION FUNCTIONS TO OBSERVABLES

Before we compare our distribution function $f_p^5(x_5)$ with experiment, we must consider its relation to the data. The experimental production process is shown in figure 4.4. At sufficiently large $-q^2$ where all masses squared (including m_Q^2) can be neglected, the analogue of (1.7.16) is

$$\frac{d^2\sigma}{dx dv}(1p \rightarrow 1Q\bar{Q}X) = \sum_{Q,\bar{Q}} e_Q^2 f_P^Q(x) \frac{2\pi\alpha^2}{x} \left[\frac{1}{v^2} - \frac{1}{vm_p E_1'} + \frac{1}{2m_p^2 E_1'^2} \right] \quad (4.6.1)$$

Bjorken- x and v are defined by (1.6.1). Integrating over a range of v gives

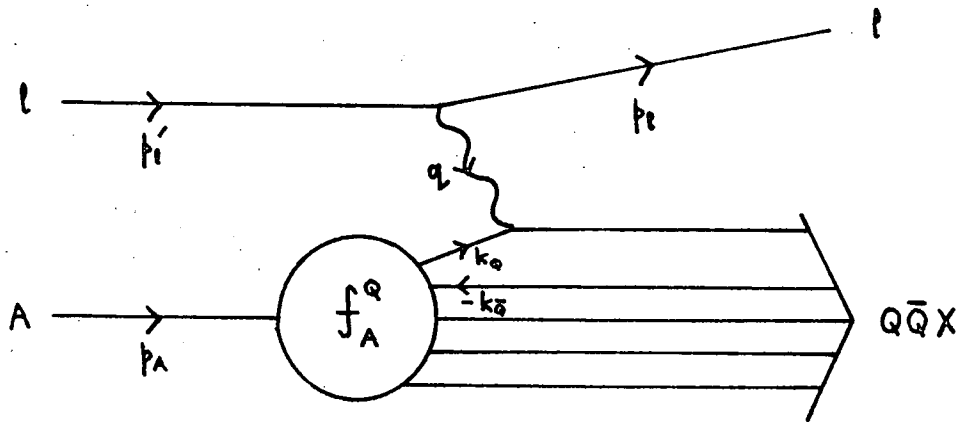


Figure 4.4: The parton diagram for intrinsic heavy flavour production in deep inelastic lepton (l)-hadron (A) scattering, showing the four momenta of the particles.

$$\frac{d\sigma(lp \rightarrow lQ\bar{Q}X)}{dx} = \sum_{Q,\bar{Q}} e^2 f_P^Q(x) \frac{2\pi\alpha^2}{x} \left[\frac{1}{v_{\min}} - \frac{1}{v_{\max}} - \frac{1}{m_p E_l} \right]$$

$$\log \left[\frac{v_{\max}}{v_{\min}} + \frac{(v_{\max} - v_{\min})}{2m_p^2 E_l^2} \right] \quad (4.6.2)$$

This is what we need to compare our distribution function against data, because experiments measure the left hand side, and we can calculate the right hand side.

4.7 NUCLEON INTRINSIC CHARM VERSUS THE DATA

The photon-gluon fusion model⁽³³⁾, where heavy quarks are created in the collision (and so are extrinsic as opposed to intrinsic), is shown in figure 4.5. This is very similar to figure 4.4 (the intrinsic case), since the intrinsic $Q\bar{Q}$ originate from a gluon, as in figure 4.1. The difference between them is the definition of the proton boundary. However, they clearly produce the same final state $lQ\bar{Q}X$, and so must both be considered when looking at data.

For deep inelastic lepto-production of charm, Aubert et al⁽³¹⁾ actually measure $\frac{d\sigma(\mu^+ p \rightarrow \mu^+ \mu X)}{dx}$, where the final μ comes from the decay of a D- or \bar{D} -meson. (4.6.2) therefore requires a slight modification;

$$\frac{d\sigma(\mu^+ p \rightarrow \mu^+ \mu X)}{dx} = 0.389B \sum_{Q,\bar{Q}} e^2 f_P^Q(x) \frac{2\pi\alpha^2}{x} \left[\frac{1}{v_{\min}} - \frac{1}{v_{\max}} \right]$$

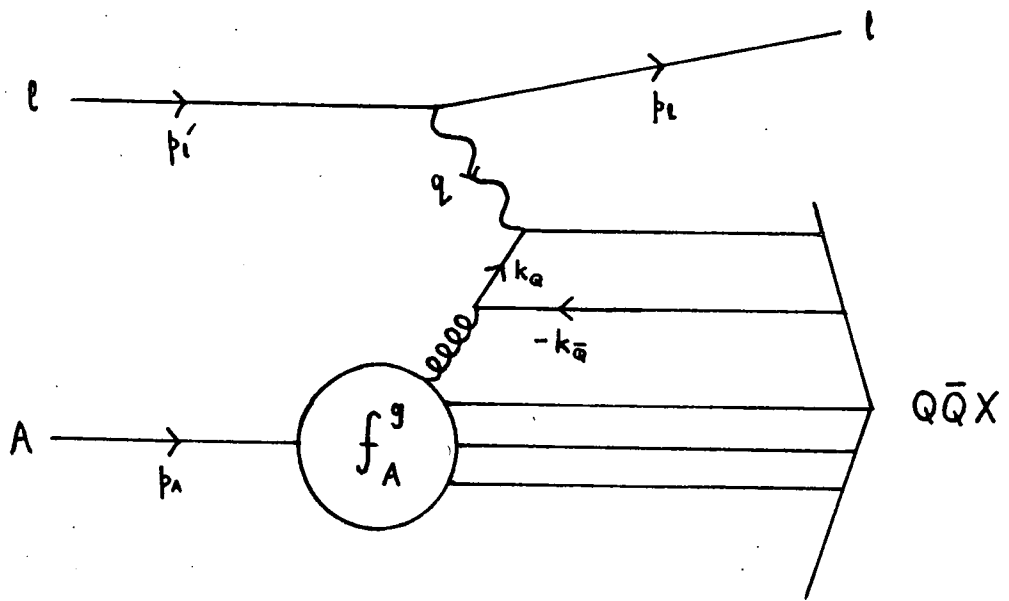


Figure 4.5: The parton diagram for extrinsic heavy flavour production in lepton-hadron scattering, showing the four-momenta of the particles.

$$- \frac{1}{m_p E_1'} \log \left[\frac{v_{\max}}{v_{\min}} \right] + \frac{(v_{\max} - v_{\min})}{2m_p^2 E_1'^2} \Big] \quad \text{mb} \quad (4.7.1)$$

B is the branching ratio for the decay $D \rightarrow \mu x$, and 0.389 converts to mb if the energies are in GeV.

The comparison of (4.7.1) with experiment is shown in figure 4.6. We use (4.4.3) to calculate $f_p^c(x)$, with the value for V_3 which normalizes f_p^3 to unity, and the masses from table 2a. Table 4a contains the values of the other parameters in (4.7.1).

B	$\frac{v_{\min}}{m_p}$ (GeV)	$\frac{v_{\max}}{m_p}$ (GeV)	E_1' (GeV)
0.082	60	220	250

Table 4a: The numbers needed in our calculation for figure 4.6, using (4.7.1).

Clearly the photon-gluon fusion model gives a good description of the data alone, so the additional contribution from intrinsic charm cannot be too large. Our result is, as it stands, compatible with the data. However when comparing f_p^3 with experiment in Section 2.7, we had to normalize it to 0.32 rather than 1, because experiments resolve current quarks, and ours are

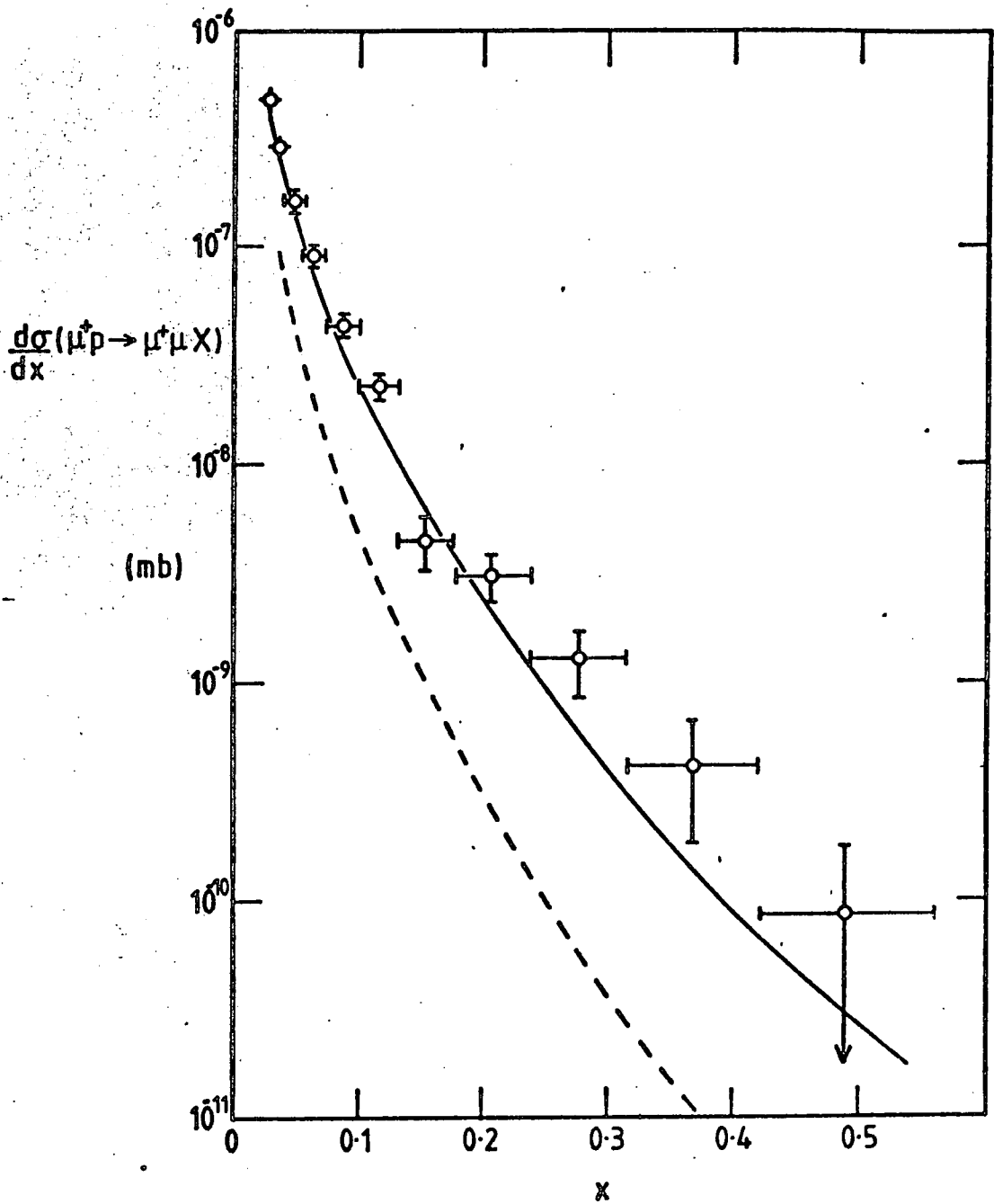


Figure 4.6: The data⁽³¹⁾, compared with the photon-gluon fusion model⁽³³⁾ (—), and our calculation from (4.7.1) (-----).

constituents. This effect may also be present here, along with possible QCD evolution and threshold suppression factors. These three effects contribute in the same direction, to reduce our result, so the curve in figure 4.6 is really an upper limit.

We therefore conclude that our model for the intrinsic charm in a proton is completely consistent with the observed charm production in deep inelastic scattering experiments.



CHAPTER 5

THE SCATTERING PROCESS

5.1 INTRODUCTION

The overall aim of our work is to understand the diffractive production of heavy flavours in hadron-hadron interactions. So far we have derived the distributions of heavy constituent quarks inside hadrons. In this chapter we consider the scattering of these heavy quarks by hadrons, and test our ideas against experiment.

Diffractive high energy hadron-hadron cross-sections are well described by Regge theory⁽⁸⁾, so we begin with a simple discussion of this topic. Figure 5.1 shows the general $2 \rightarrow 2$ scattering processes, which by crossing are described by the same amplitude $A(s,t)$ in different regions of the Mandelstam variables s and t , defined by

$$s \equiv (p_A + p_B)^2 = (p_C + p_D)^2 \quad (5.1.1)$$

$$t \equiv (p_A - p_C)^2 = (p_D - p_B)^2 \quad (5.1.2)$$

This amplitude may be expanded as a t -channel partial wave series

$$A(s,t) = \sum_{l=0}^{\infty} (2l+1) A_l(t) P_l(\cos\theta_t) \quad (5.1.3)$$

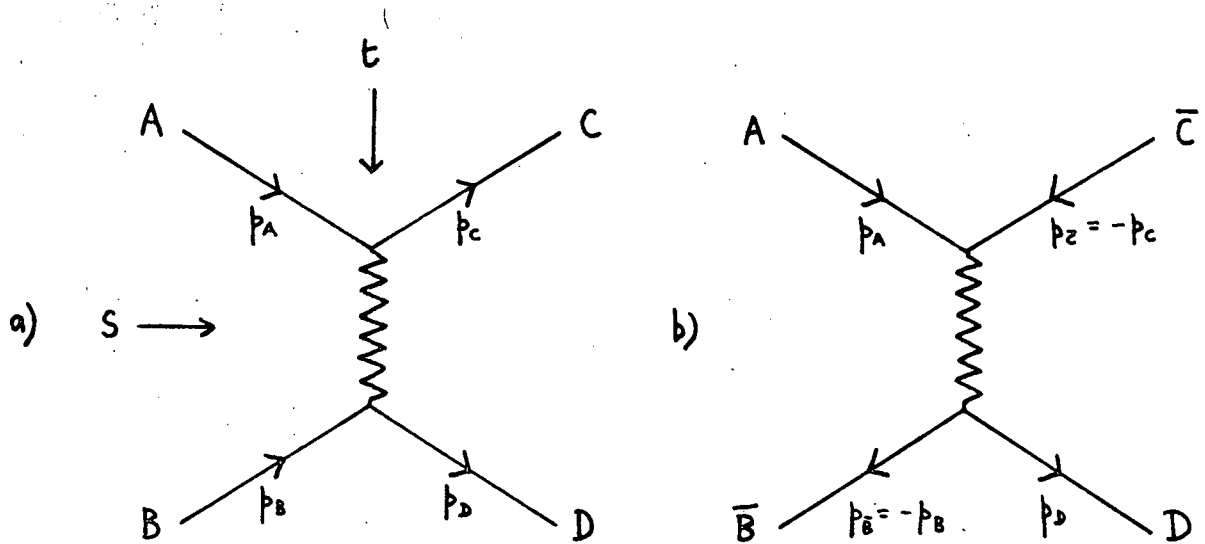


Figure 5.1: The $2 \rightarrow 2$ hadron scattering processes, showing the four momenta. a) $AB \rightarrow CD$; b) $A\bar{C} \rightarrow \bar{B}D$.

where θ_t is the scattering angle in the \overline{AC} COM frame.

In this frame, for the case of equal masses

$$s = (p_A - p_{\overline{B}})^2 = 2m^2 - \frac{t}{2} + 2\left(\frac{t}{4} - m^2\right)\cos\theta_t$$

so

$$\cos\theta_t = 1 + \frac{2s}{t-4m^2} \quad (5.1.4)$$

The intermediate particles produced in the process $\overline{AC} \rightarrow \overline{BD}$, and therefore exchanged in the process $AB \rightarrow CD$, are observed to lie on a Regge trajectory, roughly

$$\alpha(t) = \alpha_0 + \alpha't \quad (5.1.5)$$

where α_0 and α' are constants. $\alpha(t)$ takes the integer value 1 when $t = m_1^2$, m_1 being the mass of the spin 1 particle. The pole due to the propagator of this particle is therefore of the form

$$A_1(t) \cong \frac{\beta(t)}{1-\alpha(t)} \quad (5.1.6)$$

and so (5.1.2) reads

$$A(s,t) \cong \sum_{l=0}^{\infty} (2l+1) \frac{\beta(t)}{1-\alpha(t)} P_l(\cos\theta_t) \quad (5.1.7)$$

From (5.1.4)

$$\cos \theta_t \underset{t \text{ fixed}}{\overset{s \rightarrow \infty}{\sim}} \frac{s}{t-4m^2} \quad (5.1.8)$$

This s-dependence also arises in the case of non-equal masses.

Writing (5.1.7) as a contour integral around the non-negative integers in the complex l-plane, and distorting the contour, we pick up the residue of the Regge pole. For $s \rightarrow \infty$, t fixed, this is the dominant contribution, and using (5.1.8) and the property

$$P_l(\cos \theta_t) \underset{\cos \theta_t \rightarrow \infty}{\sim} (\cos \theta_t)^l \quad (5.1.9)$$

it gives

$$A(s,t) \underset{t \text{ fixed}}{\overset{s \rightarrow \infty}{\sim}} \beta(t) \left(\frac{s_0}{t-4m^2} \right)^{\alpha(t)} \left(\frac{s}{s_0} \right)^{\alpha(t)} \quad (5.1.10)$$

where we have inserted the constant $s_0 \equiv 1 \text{ GeV}^2$.

Substituting (5.1.10) into the optical theorem, (1.4.6), with the flux factor (1.4.3)

$$h = 4 [(p_A \cdot p_B)^2 - m_A^2 m_B^2]^{\frac{1}{2}} \underset{s \rightarrow \infty}{\sim} 2s \quad (5.1.11)$$

we obtain

$$\sigma_{\text{tot}}(AB) \underset{s \rightarrow \infty}{\approx} \sigma_0 \left(\frac{s}{s_0}\right)^{\alpha(0)-1} \quad (5.1.12)$$

where σ_0 is a constant.

We could consider more than one trajectory, but in the limit $s \rightarrow \infty$ the one with the largest value of $\alpha(0)$ dominates. For all hadron-hadron interactions this is the Pomeron, with an effective intercept $\alpha_p(0) = 1.08$. The fact that $\alpha_p(0) > 1$ will lead to an eventual violation of the Froissart bound⁽³⁴⁾ does not affect us, since whatever mechanisms prevent this violation appear to have little effect at present values of s .

As the Pomeron controls all large s interactions, independent of flavour, any particles lying on the trajectory may well be glueballs, although these have yet to be discovered. The Pomeron may not be a simple trajectory, but it certainly behaves like one, and that is all that concerns us here.

5.2 EFFECTIVE HADRON-QUARK CROSS-SECTIONS

The value for $\alpha_p(0)$ comes from the total cross-section measured at the CERN $p\bar{p}$ -Collider⁽³⁵⁾. The result is

$$\sigma_{\text{tot}}(p\bar{p}) \underset{s \rightarrow \infty}{\approx} 22.7 \left(\frac{s}{s_0}\right)^{0.08} \text{ mb} \quad (5.2.1)$$

Using $\alpha_p(0) = 1.08$ to fit the highest energy πp data⁽³⁶⁾ gives

$$\sigma_{\text{tot}}(\pi p) \underset{s \rightarrow \infty}{\cong} 14.7 \left(\frac{s}{s_0} \right)^{0.08} \text{ mb} \quad (5.2.2)$$

The idea of constituent valence quarks enables these to be approximated by

$$\sigma_{\text{tot}}(Ap) \underset{s \rightarrow \infty}{\cong} \sum_{i=1}^n \sigma_{\text{tot}}(q_i p) \quad (5.2.3)$$

with $n=2$ for $A=\pi$, $n=3$ for $A=p$, and where

$$\sigma_{\text{tot}}(q_i p) \cong 7.5 \left(\frac{s}{s_0} \right)^{0.08} \text{ mb} \quad (5.2.4)$$

is the effective asymptotic light (u,d) quark-proton cross-section. The analogous results for scattering on a pion are

$$\sigma_{\text{tot}}(A\pi) \underset{s \rightarrow \infty}{\cong} \sum_{i=1}^n \sigma_{\text{tot}}(q_i \pi) \quad (5.2.5)$$

where

$$\sigma_{\text{tot}}(q_i \pi) \cong 5.0 \left(\frac{s}{s_0} \right)^{0.08} \text{ mb} \quad (5.2.6)$$

We extend this to heavy quarks by invoking the hypothesis of f-dominance of the Pomeron coupling⁽³⁷⁾. If the Pomeron couples to a quark via the relevant f-meson (they have the same quantum numbers), as in

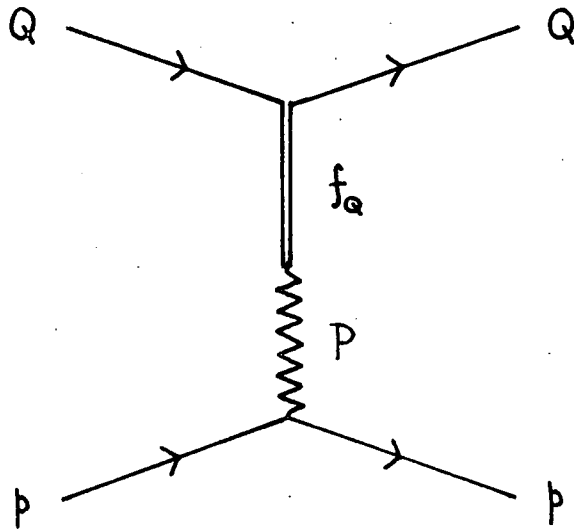


Figure 5.2: The amplitude for $Qp \rightarrow Qp$, assuming f-dominance of the Pomeron(P)-quark coupling.

figure 5.2, (5.1.6) would instead be of the form

$$A_1(t) \cong \frac{\beta_P(t) B_{Pf_Q} \beta_{f_Q}(t)}{(1-\alpha_P(t))(1-\alpha_{f_Q}(t))} \quad (5.2.7)$$

The contour integral now gives a factor $(\alpha_P(t) - \alpha_{f_Q}(t))^{-1}$ from the residue. Assuming quarks couple to their respective f 's with equal strength, the same for f 's to the Pomeron, and remembering that the optical theorem (1.4.6) requires the amplitude at $t=0$, we predict

$$\sigma_{\text{tot}}(\text{QB}) \underset{s \rightarrow \infty}{=} \frac{\alpha_P(0) - \alpha_{f_Q}(0)}{\alpha_P(0) - \alpha_{f_Q}(0)} \sigma_B \left(\frac{s}{s_0}\right)^{0.08} \quad (5.2.8)$$

where $\sigma_B = 7.5$ (5.0) mb for $B = p(\pi)$.

The values of the parameters in the Regge trajectory relevant to us are the solutions of the simultaneous equations

$$1 = \alpha_0 + \alpha' m_{\omega_Q}^2 \quad ; \quad 2 = \alpha_0 + \alpha' m_{f_Q}^2 \quad (5.2.9)$$

which follow from (5.1.5) assuming the mesons lie exactly on the trajectory. Table 5a contains the values of the particle masses we use to calculate these Regge parameters, which are given in table 5b. For the lightest flavours (u,d), a more sophisticated analysis to determine $\alpha_f(t)$ has been performed⁽³⁸⁾, as the masses

of the particles on the trajectory with spin > 2 are known⁽²¹⁾. We use the (u,d) trajectory parameters from reference 38.

Flavour (Q)		$m_{\omega_Q} (1^{--})$	$m_{f_Q} (2^{++})$
u,d		0.783	1.273
s		1.020	1.520
c		3.097	3.556
b		9.456	9.912
(i)	25	49.26 #	49.76 #
t (ii)	35	69.26 #	69.76 #
(iii)	45	89.26 #	89.76 #
		m_t (GeV)	

Table 5a: The known⁽²¹⁾ or assumed[#] masses for the ω_Q^- and f_Q^- -mesons, in GeV.

The unknown ω_t and f_t masses in table 5a are chosen to have a difference of 0.5 GeV, roughly that observed for the lighter pairs. This gives $\alpha'_{m_{Q \rightarrow \infty}} \sim 1/m_Q$ and so $\alpha'_{f_Q} (0) \sim -m_Q$; the results are given in table 5b (a).

Trajectory (i)		α_{0_i}	$\alpha'_i (\text{GeV}^{-2})$
P		1.08	0.22
f		0.49	0.95
f'		0.18	0.79
f _c		-2.17	0.331
f _b		-9.1	0.113
(a) (i)	25	-48	0.0202
f _t (ii)	35	-68	0.0144
(iii)	45	-88	0.0112
(b) (i)	25	-273	0.113
f _t (ii)	35	-541	0.113
(iii)	45	-899	0.113
m _t (GeV)			

Table 5b: The values of the Regge intercepts, calculated from (5.2.9) where appropriate.

The values in table 5b(b) come from assuming α' for top is the same as for bottom, giving $\alpha_{f_Q}(o) \sim -m_Q^2$, and are realistically lower bounds for the trajectory intercept. From (5.2.8) these give lower bounds on $\sigma_{tot}(tB)$.

Using (5.2.8), (5.2.3), and the numbers from table 5b we predict

$$\frac{\sigma_{tot}(Kp)}{\sigma_{tot}(\Pi p)} \underset{s \rightarrow \infty}{=} \frac{(\alpha_p(o) - \alpha_f(o))^{-1} + (\alpha_p(o) - \alpha_{f'}(o))^{-1}}{2(\alpha_p(o) - \alpha_f(o))^{-1}} \approx 0.8 \quad (5.2.10)$$

in good agreement with experiment^(37,14).

Almost all the present data on heavy flavour production is at s values where (5.2.8) cannot be applied; the cross-sections are still rising from threshold. We must therefore model this effect, in order to test (5.2.8) against experiment.

5.3 THRESHOLD RISE

5.3.1 Counting Rule Suppression (Dynamics)

We form our final hadrons by recombining the initial quarks after they scatter. Figure 5.3 shows $pB \rightarrow \Lambda_Q \bar{M}_Q B$ (there is no "X" just above threshold), as an example. It includes the minimum number of gluons required to hold the hadrons together. Just above threshold in

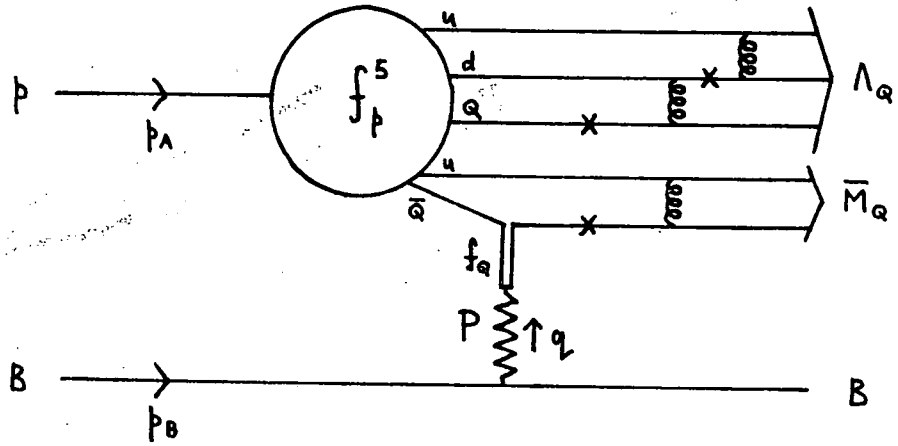


Figure 5.3: The parton diagram for $pB \rightarrow \Lambda_Q \bar{M}_Q B$.

the pB COM frame the Λ_Q and \bar{M}_Q must be almost at rest, so the gluons are needed to "stop" the quarks.

We define a variable x' , (which would equal Bjorken- x if the proton reformed), by

$$(p_A + q)^2 \equiv q^2 \left(1 - \frac{1}{x'}\right) + (m_{\Lambda_Q} + m_{\bar{M}_Q})^2 \quad (5.3.1)$$

Clearly we have an equality of limits;

$$x' \rightarrow 1 \equiv (p_A + q)^2 \rightarrow (m_{\Lambda_Q} + m_{\bar{M}_Q})^2 \equiv s \rightarrow s_{th} \quad (5.3.2)$$

where s is defined by (5.1.1) and s_{th} by

$$s_{th} \equiv (m_B + m_{\Lambda_Q} + m_{\bar{M}_Q})^2 \quad (5.3.3)$$

If the $\Lambda_Q \bar{M}_Q$ system is excited (ie $(p_A + q)^2 > (m_{\Lambda_Q} + m_{\bar{M}_Q})^2$), (5.3.1) gives

$$q^2 \sim (1 - x')^{-1} \quad (5.3.4)$$

In the heavy hadron reformation amplitude, A_r , containing n_g gluons, the fermion traces cancel the gluon propagators, as in Section 1.7. The quarks labelled by $\text{---}x\text{---}$ in figure 5.3 have four momenta squared $\sim q^2$, so $A_r \sim q^{-2n_g}$ from their propagator denominators. From (1.7.6), the reformation probability, P_r , therefore satisfies

$$\frac{dP_r}{dq^2} \sim |A_r|^2 \sim q^{-4n_g} \quad (5.3.5)$$

We assume the $\Lambda_Q \bar{M}_Q$ excited region goes smoothly to threshold, in the same way that we matched-up the scaling and elastic regions to derive the Drell-Yan-West relation in Section 1.7. Using (5.3.4) this gives

$$P_r \sim (1 - x')^{2n_g - 1} \quad (5.3.6)$$

the familiar counting rule behaviour.

From (5.3.2) we obtain the dynamical suppression factor, defined by

$$P(s) \equiv \left(1 - \frac{s_{th}}{s}\right)^{2n_g - 1} \quad (5.3.7)$$

Clearly $P(s) \rightarrow 1$ as $s \rightarrow \infty$, most quickly for the minimum n_g . We use only this value, as in figure 5.3. The real $P(s)$ must be a (normalized) sum over $n_g \geq n_{g_{min}}$, but the higher terms will presumably be down by powers of α_s . For the processes we consider $n_{g_{min}}$ is listed in table 5c. In the case $pB \rightarrow pM_Q \bar{M}_Q B$ we need the final state proton to conserve baryon number, (and assume a light $q\bar{q}$ -pair are created at no cost for this).

Process	$\pi B \rightarrow M_Q \bar{M}_Q B$	$pB \rightarrow \Lambda_Q \bar{M}_Q B$	$pB \rightarrow M_Q \bar{M}_Q pB$
$n_{g_{\min}}$	2	3	4

Table 5c: The relevant values of $n_{g_{\min}}$.

5.3.2 Limited Availability of Phase-space (Kinematics)

Another factor constraining the rise of the cross-section from threshold is the available range of t . This is a kinematical effect, but in order to incorporate it we have to assume some further dynamics.

Consider the process in figure 5.1 a), with

$$p_A^2 = m_A^2 ; \quad p_C^2 = M^2 ; \quad p_B^2 = p_D^2 = m_B^2 \quad (5.3.8)$$

and the definitions

$$p_C^+ \equiv x_C p_A^+ ; \quad p_D^- \equiv x_D p_B^- \quad (5.3.9)$$

We neglect transverse momentum transfer in what follows, in order to find the limits of phase-space. Using (5.3.8), (5.3.9) and (1.5.6), (5.1.2) may be written

$$t = m_B^2 \left(2 - x_D - \frac{1}{x_D} \right) \quad (5.3.10)$$

Clearly for $0 \leq x_D \leq 1$, $-\infty \leq t \leq 0$, but if x_D is further constrained, so is t . We calculate this range as a function of s .

In the COM frame where $p_A^3 + p_B^3 = 0$ and $p_A^3 \equiv > 0$, (5.1.1) gives

$$s^{\frac{1}{2}} = (p_B^3 + m_A^2)^{\frac{1}{2}} + (p_B^3 + m_B^2)^{\frac{1}{2}} \quad (5.3.11)$$

Solving this for p_B^3 , and using (5.3.9) with $p_D^3 = 0$ (which minimizes x_D) we get

$$x_{D \min} = \frac{m_B}{p_B^-} \quad (5.3.12)$$

where

$$p_B^- = \frac{(s+m_B^2-m_A^2)}{2s^{\frac{1}{2}}} + \left[\frac{(s+m_B^2-m_A^2)^2}{4s} - m_B^2 \right]^{\frac{1}{2}} \quad (5.3.13)$$

To find $x_{D \max}$ we again expand (5.1.1), using (5.1.6), obtaining

$$s = m_B^2 + M^2 + \frac{m_B^2 M^2}{x_C x_D p_A^+ p_B^-} + x_C x_D p_A^+ p_B^- \quad (5.3.14)$$

This gives

$$x_C x_D = \frac{w}{p_A^+ p_B^-} \quad (5.3.15)$$

where w is defined by

$$w \equiv \frac{1}{2} \left[(s - m_B^2 - M^2) + \left[(s - m_B^2 - M^2)^2 - 4m_B^2 M^2 \right]^{\frac{1}{2}} \right] \quad (5.3.16)$$

From (5.3.9)

$$x_C p_A^+ = (M^2 + p_C^3)^{\frac{1}{2}} + p_C^3 \quad ; \quad x_D p_B^- = (m_B^2 + p_C^3)^{\frac{1}{2}} + p_C^3 \quad (5.3.17)$$

so

$$p_C^3 = \frac{p_B^- x_{D \max}^2 - m_B^2}{2 p_B^- x_{D \max}} \quad (5.3.18)$$

Eliminating x_C from (5.3.15) and (5.3.17), and using (5.3.18) on the result to remove p_C^3 , we obtain

$$x_{D \max} \left[\left(M^2 + \frac{p_B^- x_{D \max}^2 - m_B^2}{2 p_B^- x_{D \max}} \right)^2 + \frac{p_B^- x_{D \max}^2 - m_B^2}{2 p_B^- x_{D \max}} \right] = \frac{w}{p_B^-} \quad (5.3.19)$$

Solving this we get

$$x_{D \max} = \frac{1}{p_B^-} \left[\frac{w(w + m_B^2)}{w + M^2} \right]^{\frac{1}{2}} \quad (5.3.20)$$

As a check, $s \rightarrow \infty$ implies $x_{D \min} \rightarrow 0$, $x_{D \max} \rightarrow 1$, and $s = s_{th} = (m_B + M)^2$ implies $x_{D \min} = x_{D \max}$.

We therefore define our kinematical threshold rise factor by

$$T(s) \equiv \frac{\int_{t_{\min}}^{t_{\max}} dt \frac{d\sigma}{dt}}{\int_{-\infty}^0 dt \frac{d\sigma}{dt}} \quad (5.3.21)$$

where t_{\max} and t_{\min} come from (5.3.10) using (5.3.20) and (5.3.12) respectively.

To calculate $T(s)$ we need a model for $\frac{d\sigma}{dt}$, which, rewriting (1.7.6), is given by

$$\frac{d\sigma}{dt} \sim \frac{1}{s^2} |A(s,t)|^2 \quad (5.3.22)$$

Regge theory suggests exponential behaviour. Substituting (5.1.5) and (5.1.19) into (5.3.22) gives

$$\frac{d\sigma}{dt} \sim F(t) \left(\frac{s}{s_0}\right)^{2\alpha} s_0^{-2} \exp[2\alpha' t \log(\frac{s}{s_0})] \quad (5.3.23)$$

where $F(t)$ contains the remaining t -dependence. The large s cross-sections for Np and pp elastic scattering can be well fitted by considering just the Pomeron trajectory, but with a sum of exponentials in the amplitude⁽³⁹⁾, giving

$$\frac{d\sigma_{el}}{dt} \propto e^{2C_P t} ((1-X) + X e^{a_1 t})^2 \quad (5.3.24)$$

where C_P is defined by

$$C_P \equiv a_P + \alpha'_P \log\left(\frac{s}{s_0}\right) \quad (5.3.25)$$

We assume (5.3.24) also gives a reasonable description of $\frac{d\sigma}{dt}$ when the π or p are diffractively excited. Using (5.3.24), (5.3.21) integrates to

$$T(s) = \left[\frac{(1-X)^2}{2C_P} + \frac{2X(1-X)}{(2C_P+a_1)} + \frac{X^2}{2(C_P+a_1)} \right]^{-1} \left[\frac{(1-X)^2}{2C_P} (e^{2C_P t_{\max}} - e^{2C_P t_{\min}}) \right. \\ \left. + \frac{2X(1-X)}{(2C_P+a_1)} (e^{(2C_P+a_1)t_{\max}} - e^{(2C_P+a_1)t_{\min}}) \right. \\ \left. + \frac{X^2}{2(C_P+a_1)} (e^{2(C_P+a_1)t_{\max}} - e^{2(C_P+a_1)t_{\min}}) \right] \quad (5.3.26)$$

The values of the parameters are given in table 5d.

Process	X	a_p (GeV ⁻²)	a'_p (GeV ⁻²)	a_1 (GeV ⁻²)
πp	0.66	1.00	0.22	3.20
pp	0.65	2.05	0.22	3.39

Table 5d: The values of the parameters⁽³⁹⁾ used in (5.3.26).

There is one more point to consider, the choice of M . In principle we should average (5.3.26) over all possible M -values with some assumed distribution, as

t_{\max} is a function of M . However we simplify this, and just replace M^2 in (5.3.20) by \bar{M}^2 , where \bar{M}^2 is defined by

$$\bar{M}^2 \equiv \frac{\int_{M_{\min}^2}^{M_{\max}^2} dM^2 \frac{d\sigma_{\text{diff}}}{dM^2}}{\int_{M_{\min}^2}^{M_{\max}^2} \frac{d\sigma_{\text{diff}}}{dM^2}} \quad (5.3.27)$$

with

$$M_{\max}^2 \equiv (s^{\frac{1}{2}} - m_B)^2 ; \quad M_{\min}^2 \equiv (s_{\text{th}}^{\frac{1}{2}} - m_B)^2 \quad (5.3.28)$$

Using the empirical observation⁽⁴⁰⁾ that for $M^2 \gtrsim 2 \text{ GeV}^2$

$$\frac{d\sigma_{\text{diff}}}{dM^2} \sim \frac{1}{M^2} \quad (5.3.29)$$

the dependence expected from the triple Pomeron model⁽⁴¹⁾, (5.3.27) integrates to give

$$\bar{M}^2 = \frac{M_{\max}^2 - M_{\min}^2}{\log \left[\frac{M_{\max}^2}{M_{\min}^2} \right]} \quad (5.3.30)$$

With \bar{M}^2 in (5.3.26) rather than, for example, M_{\min}^2 , $T(s)$ still $\rightarrow 1$ as $s \rightarrow \infty$, but takes longer. This is because, in a simplified way, we are allowing for the production of $\Lambda_Q \bar{M}_Q X$, and not just $\Lambda_Q \bar{M}_Q$, to use our

counting rule example.

We end this section with the new version of (5.2.8), valid for all s ,

$$\sigma_{\text{tot}}(\text{QB}) = P(s)T(s) \left(\frac{\alpha_P^{(0)} - \alpha_f^{(0)}}{\alpha_P^{(0)} - \alpha_{f_Q}^{(0)}} \right) \sigma_B \left(\frac{s}{s_0} \right)^{0.08} \quad (5.3.31)$$

$P(s)$ and $T(s)$ are given by (5.3.7) and (5.3.26) respectively and $\sigma_B = 7.5$ (5.0) mb for $B = p(\pi)$.

5.4 CHARM PRODUCTION IN γp INTERACTIONS

Since there is no data on heavy particle scattering cross-sections, we test (5.3.31) against experiment by predicting the total cross-section for heavy particle production in γp interactions. A nice feature of this test is that it doesn't depend on our distribution functions from Chapters 2 or 4.

Generalized vector dominance⁽⁴²⁾ says the total γp cross-section may be written

$$\sigma_{\text{tot}}(\gamma p) = \sum_V |A_{\gamma V}|^2 \sigma_{\text{tot}}(V p) \quad (5.4.1)$$

The sum runs over all vector mesons having the same quantum numbers as γ , and $|A_{\gamma V}|^2$ is the probability for $\gamma \rightarrow V$.

This is related to the width $\Gamma_{V \rightarrow e^+ e^-}$, for the vector meson going to a virtual photon which decays to $e^+ e^-$, as in figure 5.4. In the V rest frame, (1.4.2) gives

$$\Gamma_{V \rightarrow e^+ e^-} = \frac{1}{2m_V} \int \frac{d^3 p_1}{2E_1 (2\pi)^3} \frac{d^3 p_2}{2E_2 (2\pi)^3} (2\pi)^4 \delta^4(p_V - p_1 - p_2) \frac{e^2 |A_{\gamma V}|^2}{3} \left(g^{\mu\nu} - \frac{p_V^\mu p_V^\nu}{m_V^2} \right) T_{2\mu\nu}(p_1, -p_2) \quad (5.4.2)$$

We have averaged over the initial spin, and summed over final ones; $T_{2\mu\nu}$ is defined by (1.6.8). Neglecting the lepton masses and remembering (1.6.5), we integrate over p_2 to get

$$\Gamma_{V \rightarrow e^+ e^-} = \frac{\alpha}{12\pi m_V} \int \frac{d^3 p_1}{E_1} \delta(m_V^2 - 2p_V \cdot p_1) |A_{\gamma V}|^2 \left(g^{\mu\nu} - \frac{p_V^\mu p_V^\nu}{m_V^2} \right) T_{2\mu\nu}(p_1, p_1 - p_V) \quad (5.4.3)$$

Using

$$d^3 p_1 = E_1^2 dE_1 d\Omega \quad ; \quad \delta(m_V^2 - 2p_V \cdot p_1) = \frac{1}{2m_V} \delta\left(\frac{m_V}{2} - E_1\right) \quad (5.4.4)$$

and substituting for $T_{2\mu\nu}$ from (1.6.9), the remaining integrals give

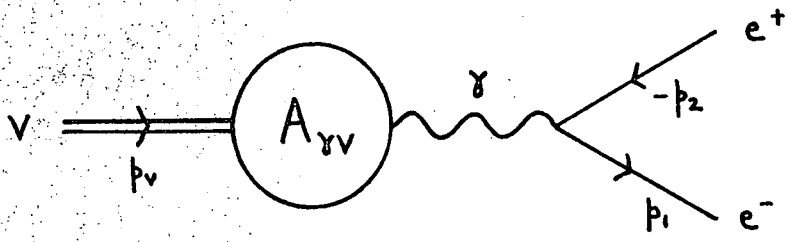


Figure 5.4: The decay $V \rightarrow e^+e^-$, showing the four momenta of the particles.

$$\begin{aligned} \Gamma_{V \rightarrow e^+ e^-} &= \frac{\alpha |A_{\gamma V}|^2}{3m_V} P_1 \cdot P_V \left[1 - \frac{2(p_1 - p_V) \cdot p_V}{m_V^2} \right]_{E_1 = \frac{m_V}{2}} \\ &= \frac{\alpha |A_{\gamma V}|^2}{3m_V} \end{aligned} \quad (5.4.5)$$

Using this (5.4.1) becomes

$$\sigma_{\text{tot}}(\gamma p) = \sum_V \frac{3\Gamma_{V \rightarrow e^+ e^-}}{\alpha m_V} \sigma_{\text{tot}}(Vp) \quad (5.4.6)$$

where $\sigma_{\text{tot}}(Vp)$ is given by Pomeron exchange, assuming f-dominance for the coupling.

This has been tested against experiment⁽⁴³⁾, and gives good results. The Reggeon-photon coupling analogy^(38,44), which incorporates (5.4.1) in its basic assumptions, also gives good predictions for $\frac{d\sigma}{dt}(\gamma p \rightarrow \rho p)$ and $\frac{d\sigma}{dt}(\gamma p \rightarrow \phi p)$ (amongst other things), as shown in reference 43, so we conclude (5.4.6) is on solid ground.

Assuming charm production comes from the single term $V = \psi$ gives

$$\sigma(\gamma p \rightarrow c\bar{c}X) \approx \frac{3\Gamma_{\psi \rightarrow e^+ e^-}}{\alpha m_\psi} \sigma_{\text{tot}}(\psi p) \quad (5.4.7)$$

This neglects the higher mass versions of the ψ , and

any intrinsic charm in all the vector mesons and the proton. We also assume all the charm produced is naked (in the form of charmed mesons). Substituting (5.2.3) into (5.4.7), we obtain

$$\sigma(\gamma p \rightarrow c\bar{c}X) \approx \frac{6\Gamma_{\psi \rightarrow e^+e^-} \sigma_{\text{tot}}(\text{cp})}{\alpha m_\psi} \quad (5.4.8)$$

which is calculable using (5.3.31) for $\sigma_{\text{tot}}(\text{cp})$.

5.5 COMPARISON WITH THE DATA

In figure 5.5 we plot the prediction (5.4.8) against the data, having used

$$E_\gamma = \frac{s - m_p^2}{2m_p} \quad (5.5.1)$$

where E_γ is the photon energy in the proton rest frame, to change the argument of (5.3.31). The numbers needed come from tables 2a, 5b and 5d, with the exception of $\Gamma_{\psi \rightarrow e^+e^-}$ and m_ψ (21). We take $n_g=2$, assuming light $q\bar{q}$ pairs form at no cost, two gluons then being necessary to form a D and \bar{D} (or excited versions). The agreement between theory and experiment is rather good. Our approximation of ignoring hidden charm production is clearly justifiable, since at $E_\gamma \sim 105$ GeV, $\sigma(\gamma p \rightarrow \psi X) \sim 20$ nb⁽⁴⁶⁾, giving

$$\frac{\sigma(\gamma p \rightarrow \psi X)}{\sigma(\gamma p \rightarrow c\bar{c}X)} \sim \frac{1}{30}$$

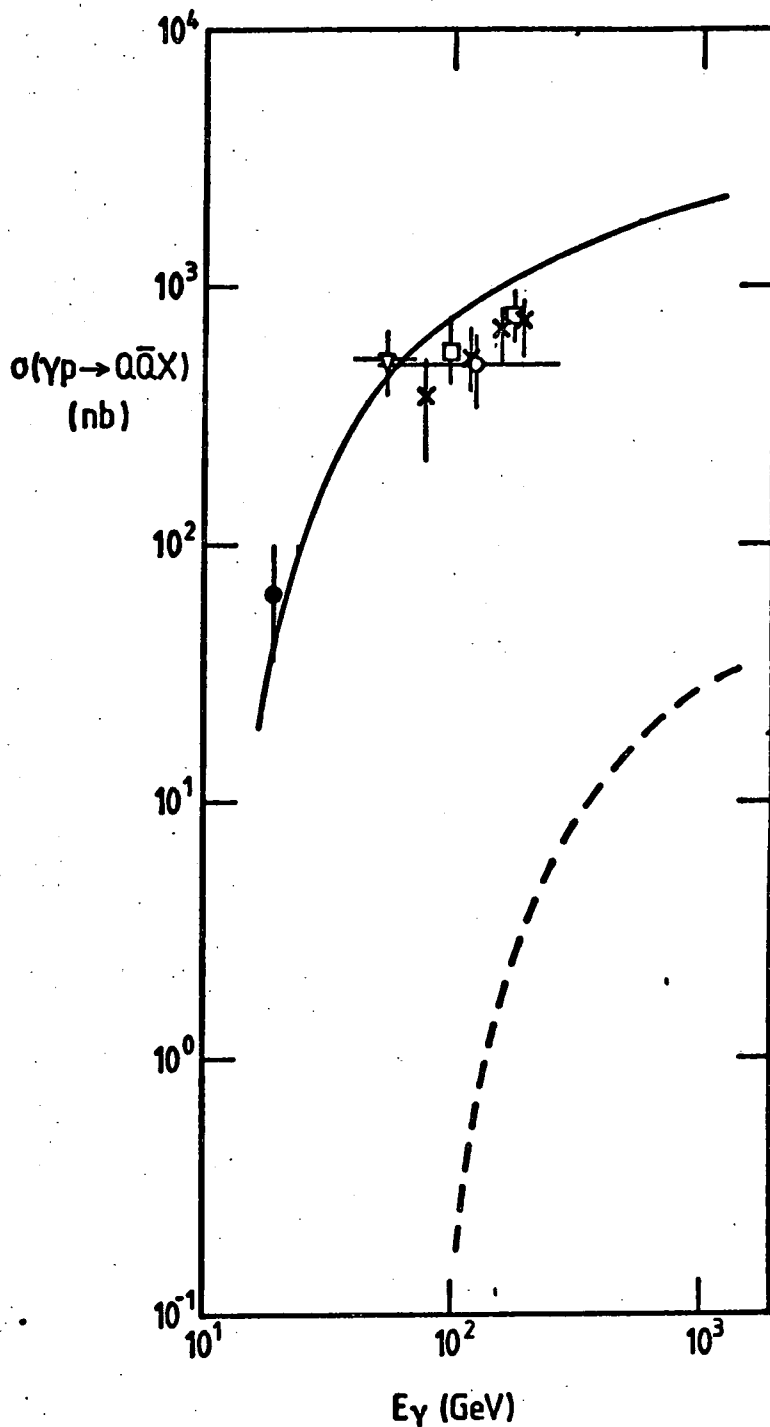


Figure 5.5: $\sigma(\gamma p \rightarrow c\bar{c}X)$ (—), calculated from (5.4.8), compared with the data⁽⁴⁵⁾; ● SHF Photon Collaboration, ▼ CERN $\Omega(\gamma p \rightarrow \bar{D}^0 X)$, ○ FNAL Broad Band ($\gamma p \rightarrow D^0 X$), × EMC, ■ BFP Collaboration. Also shown is $\sigma(\gamma p \rightarrow b\bar{b}X)$ (---), calculated from (5.4.8).

Also shown in figure 5.5 is the prediction for $\sigma(\gamma p \rightarrow b\bar{b}X)$.

We plot the predicted distributions of D^{*-} and D -mesons in figure 5.6, assuming that the charmed quarks fragment after the interaction, and using (2.6.7) and (3.4.6) to calculate

$$f_{\psi}^{D^{*}/D}(z) = \int_z^1 \frac{dx}{x} f_{\psi}^c(x) D_c^{D^{*}/D}\left(\frac{z}{x}\right) \quad (5.5.2)$$

As in (3.5.1), the observed distribution of D -mesons will be of the form

$$f_{\psi}^D(z, a') \equiv a' f_{\psi}^D(z) + (1-a') \int_z^1 \frac{dy}{y} f_{\psi}^{D^{*}}(y) f_{D^{*}}^D\left(\frac{z}{y}\right) \quad (5.5.3)$$

where $0 \leq a' \leq 1$. There is not yet any good z -distribution data, so we cannot determine a' to compare with a ~ 0.5 from Section 3.5. However the trend of the data so far⁽⁴⁷⁾, for D^{*} 's, is that they generally carry a sizeable fraction of E_{γ} , and don't form a distribution sharply peaked at the origin. This is in qualitative agreement with our predictions of figure 5.6. Figure 5.7 shows the analogous predictions for bottom production.

We conclude that our model for heavy quark-proton scattering, (5.3.31), when used in conjunction with generalized vector dominance, gives a good description of the existing data on the photo-production of heavy flavours.

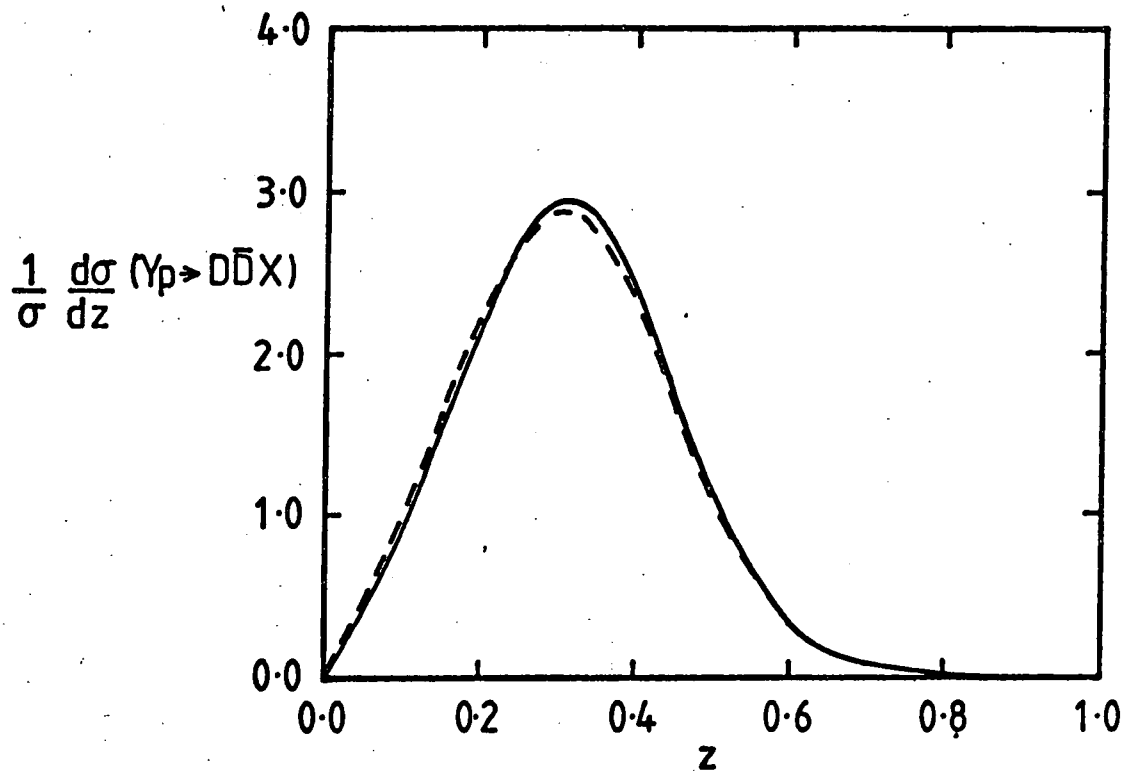


Figure 5.6: The predicted z -distributions of D^* (---) and D (—)-mesons produced in γp interactions, calculated from (5.5.2).

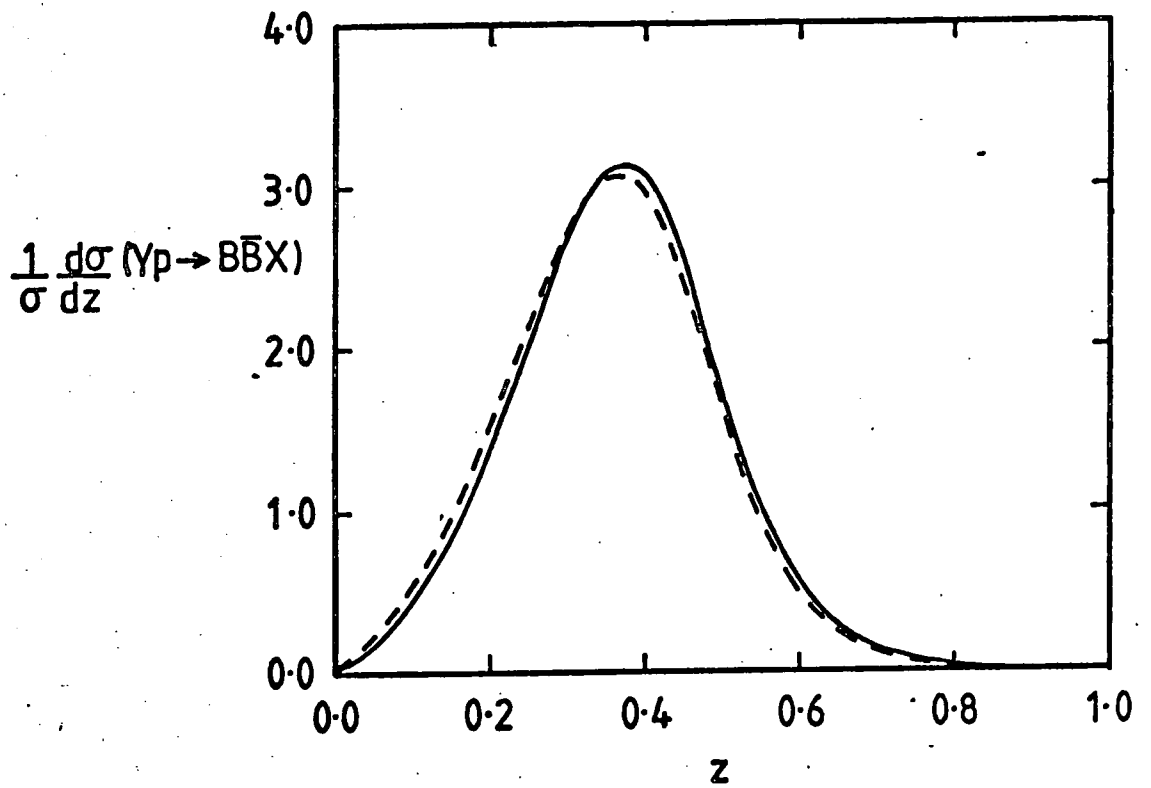


Figure 5.7: The predicted z -distributions of B^* (---) and B (—)-mesons produced in γp interactions, calculated from (5.5.2).

CHAPTER 6

HADRONIC HEAVY FLAVOUR PRODUCTION

6.1 THE MODEL

We now have all the ingredients to calculate hadronic production of heavy flavours. Figure 6.1 shows an example of our model, for Λ_Q production from a proton. Hadron B scatters on the \bar{Q} in the $|uudQ\bar{Q}\rangle$ Fock state of the proton, from which udQ then reform into a Λ_Q .

For the sub-process (boxed by --- in figure 6.1)

$$p_B^+ + x_4 p_A^+ = p_B'^+ + x_4' p_A^+ \quad (6.1.1)$$

Our definition of p_A^+ , (1.5.1), gives $p_A^+ \gg p_B^+$ in any frame where $|p_i^3| \gg m_i$ for $i = A$ and B , and for diffractive scattering the momentum transfer is small so $p_A^+ \gg p_B'^+$ as well. From (6.1.1), therefore, $x_4 \approx x_4'$. As the heavy quark receives only a glancing blow, hadron B can scatter on the Q or \bar{Q} , independent of which one then goes into the reformation.

The Λ_Q production cross-section is given by

$$\sigma(p_B \rightarrow \Lambda_Q^M X) \equiv \int_0^1 dx \Lambda_Q \int_0^1 \prod_{i=1}^5 [dx_i] \delta(1 - \sum_{i=1}^5 x_i) f_p^5(\{x_5\}) \sigma_{tot}(\bar{Q}B) R_5^{\Lambda_Q}(x_1, x_2, x_5) \delta(x_{\Lambda_Q} - x_1 - x_2 - x_5) \quad (6.1.2)$$

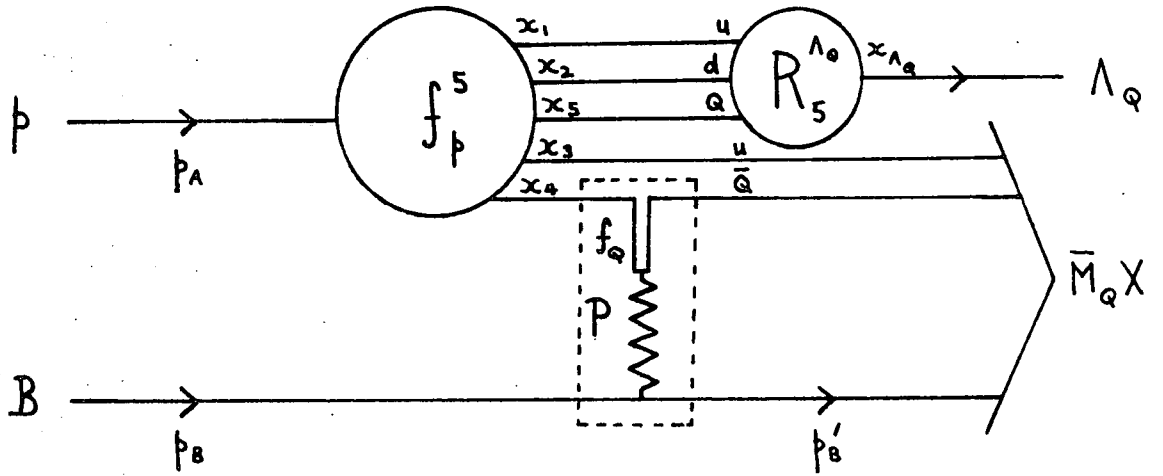


Figure 6.1: The parton diagram for $pB \rightarrow \Lambda_Q \bar{M}_Q X$ with four-momenta and x's labelled.

$f_p^5(\{x_5\})$ (defined by (4.4.3)) is the initial x -distribution of the $|uudQ\bar{Q}\rangle$ Fock state, and $R_5^{\Lambda_Q}(x_1, x_2, x_5)$ is the Λ_Q recombination function, with $\delta(x_{\Lambda_Q} - x_1 - x_2 - x_5)$ fixing its quark content. $R_5^{\Lambda_Q}$ is essentially the valence distribution of the Λ_Q . We discuss this fully in Section 6.2. The integrals evaluate the overlap between these functions, giving the probability of reforming a Λ_Q with light cone momentum fraction x_{Λ_Q} from the initial quark distribution, summed over all x_{Λ_Q} . $\sigma_{\text{tot}}(\bar{Q}B)$ is the hadron-quark cross-section of (5.3.31), which gives the scattering probability and contains the s -dependence.

The diffractive cross-section, defined as $\sigma_d(p \rightarrow \Lambda_Q \bar{Q} X)$, is calculated by summing (6.1.2) over the Pomeron coupling to the Q or the \bar{Q} , and the possible combinations from $|uudQ\bar{Q}\rangle$ which can form a Λ_Q .

For charm and heavier flavours we assume all these possibilities produce Λ_Q 's, if not immediately, then via a decay. For example Σ_c^{++} (uuc) decays to Λ_c^+ (udc). In principle the reformation function is a sum over all heavy baryons which can form, but in the absence of any information on the relative weights of the terms, we approximate to just one, $R_5^{\Lambda_Q}$. Consequently we neglect any smearing of the Λ_Q distribution to smaller x_{Λ_Q} from intermediate states. However Σ_s^+ (uus) doesn't decay to Λ_s^0 (uds), although Σ_s^0 (uds) does, so in our

picture 1/3 of the strange baryons produced are Σ_s^+ 's, and 2/3 Λ_s^0 's.

Using the same notation we define

$$\sigma(p \rightarrow \bar{M}_Q M_Q X) \equiv \int_0^1 dx_{\bar{M}_Q} \int_0^1 \prod_{i=1}^5 [dx_i] \delta(1 - \sum_{i=1}^5 x_i) f_p^5(\{x_5\}) \sigma_{\text{tot}}(\bar{Q}B) R_5^{M_Q^*}(x_3, x_4) \delta(x_{\bar{M}_Q} - x_3 - x_4) \quad (6.1.3)$$

$$\sigma(\pi \rightarrow M_Q \bar{M}_Q X) \equiv \int_0^1 dx_{M_Q} \int_0^1 \prod_{i=1}^4 [dx_i] \delta(1 - \sum_{i=1}^4 x_i) f_\pi^4(\{x_4\}) \sigma_{\text{tot}}(\bar{Q}B) R_4^{M_Q^*}(x_2, x_4) \delta(x_{M_Q} - x_2 - x_4) \quad (6.1.4)$$

and again the diffractive cross-sections, σ_d , are calculated by summing these for the Pomeron scattering on the Q or \bar{Q} , and over the different quark combinations which can form the final hadron. $R^{M_Q^*}$ is a single term approximation for the meson reformation function. Our mechanism cannot produce diffractive Λ_Q 's from π 's.

In each case the heavy quark which doesn't recombine will produce a heavy hadron (probably a meson) at low x, either by fragmenting or recombining with sea quarks. We assume that if heavy hadron production does not occur, the heavy quarks annihilate each other.

"Hidden" heavy flavour (J/ψ , T etc) production is

not calculable without further assumptions, but is clearly suppressed by the need to get the colour and invariant mass correct, since the $Q\bar{Q}$ pair in our picture are created in a colour octet state. It is observed to be very small compared to "open" heavy flavour production.

The diffractive heavy flavour production cross-sections are calculated by adding the contributions from both the initial particles, giving

$$\begin{aligned} \sigma_d(pp \rightarrow \Lambda_Q \bar{M}_Q X) &= 2\sigma_d(p \rightarrow \Lambda_Q \bar{M}_Q X) = \sigma_d(p\bar{p} \rightarrow \Lambda_Q \bar{M}_Q X / \bar{\Lambda}_Q M_Q X) \\ &= \sigma_d(p \rightarrow \Lambda_Q \bar{M}_Q X) + \sigma_d(\bar{p} \rightarrow \bar{\Lambda}_Q M_Q X) \end{aligned} \quad (6.1.5)$$

$$\begin{aligned} \sigma_d(pp \rightarrow M_Q \bar{M}_Q X) &= 2\sigma_d(p \rightarrow M_Q \bar{M}_Q X) = \sigma_d(p\bar{p} \rightarrow M_Q \bar{M}_Q X) \\ &= \sigma_d(p \rightarrow M_Q \bar{M}_Q X) + \sigma_d(\bar{p} \rightarrow M_Q \bar{M}_Q X) \end{aligned} \quad (6.1.6)$$

$$\sigma_d(\Pi p \rightarrow \Lambda_Q \bar{M}_Q X) = \sigma_d(p_{\bar{H}} \rightarrow \Lambda_Q \bar{M}_Q X) \quad (6.1.7)$$

$$\sigma_d(\Pi p \rightarrow M_Q \bar{M}_Q X) = \sigma_d(\Pi \rightarrow M_Q \bar{M}_Q X) + \sigma_d(p_{\bar{H}} \rightarrow M_Q \bar{M}_Q X) \quad (6.1.8)$$

6.2 RECOMBINATION FUNCTIONS

In the $|uudQ\bar{Q}\rangle$ Fock state of a proton the Q is at very low x , whereas in a Λ_Q valence distribution it carries most of the momentum, and the light quarks are at low x .

Λ_Q production from the initial distribution must be suppressed by this mis-match. We take

$$R_5^{\Lambda_Q}(x_1, x_2, x_5) = N_5^{\Lambda_Q} f_{\Lambda_Q}^3 \left(\frac{x_1}{x_{\Lambda_Q}}, \frac{x_2}{x_{\Lambda_Q}}, \frac{x_5}{x_{\Lambda_Q}} \right) \quad (6.2.1)$$

where $f_{\Lambda_Q}^3$ (defined by (2.6.7)) gives the distribution of the valence quarks in a Λ_Q .

The normalization constant $N_5^{\Lambda_Q}$ is chosen so that the overlap integral is unity if we consider all possible final states in the reverse process $\Lambda_Q \bar{Q} u \rightarrow X$, ie

$$\int_0^1 dx_{\Lambda_Q} \int_0^1 \prod_{i=1}^5 [dx_i] \delta(1 - \sum_{i=1}^5 x_i) N_5^{\Lambda_Q} f_{\Lambda_Q}^3 \left(\frac{x_1}{x_{\Lambda_Q}}, \frac{x_2}{x_{\Lambda_Q}}, \frac{x_5}{x_{\Lambda_Q}} \right) \delta(x_{\Lambda_Q} - x_1 - x_2 - x_5) = 1 \quad ((6.2.2))$$

Inserting the normalization condition for $f_{\Lambda_Q}^3$, which may be written

$$\int_0^1 \frac{dx_1 dx_2 dx_5}{x_{\Lambda_Q}^3} f_{\Lambda_Q}^3 \left(\frac{x_1}{x_{\Lambda_Q}}, \frac{x_2}{x_{\Lambda_Q}}, \frac{x_5}{x_{\Lambda_Q}} \right) \delta(1 - \frac{x_1}{x_{\Lambda_Q}} - \frac{x_2}{x_{\Lambda_Q}} - \frac{x_5}{x_{\Lambda_Q}}) = 1 \quad (6.2.3)$$

we obtain

$$\int_0^1 dx_{\Lambda_Q} x_{\Lambda_Q}^2 \int_0^1 dx_3 dx_4 \delta(1 - x_{\Lambda_Q} - x_3 - x_4) N_5^{\Lambda_Q} = 1$$

which gives

$$\int_0^1 dx_{\Lambda_Q} x_{\Lambda_Q}^2 (1-x_{\Lambda_Q}) N_5^{\Lambda_Q} = 1 \quad (6.2.4)$$

This implies

$$N_5^{\Lambda_Q} = 12 \quad (6.2.5)$$

Writing

$$R_5^{\bar{M}_Q^*}(x_3, x_4) = N_5^{\bar{M}_Q^*} f_{\bar{M}_Q^*}^2 \left(\frac{x_3}{x_{\bar{M}_Q}}, \frac{x_4}{x_{\bar{M}_Q}} \right) \quad (6.2.6)$$

$$R_4^{M_Q^*}(x_2, x_4) = N_4^{M_Q^*} f_{M_Q^*}^2 \left(\frac{x_2}{x_{M_Q}}, \frac{x_4}{x_{M_Q}} \right) \quad (6.2.7)$$

similar arguments give

$$\int_0^1 dx_{\bar{M}_Q} \int_0^1 \prod_{i=1}^5 [dx_i] \delta(1 - \sum_{i=1}^5 x_i) N_5^{\bar{M}_Q^*} f_{\bar{M}_Q^*}^2 \left(\frac{x_3}{x_{\bar{M}_Q}}, \frac{x_4}{x_{\bar{M}_Q}} \right)$$

$$\delta(x_{\bar{M}_Q} - x_3 - x_4) = 1 \quad (6.2.8)$$

$$\int_0^1 dx_{M_Q} \int_0^1 \prod_{i=1}^4 [dx_i] \delta(1 - \sum_{i=1}^4 x_i) N_4^{M_Q^*} f_{M_Q^*}^2 \left(\frac{x_2}{x_{M_Q}}, \frac{x_4}{x_{M_Q}} \right)$$

$$\delta(x_{M_Q} - x_2 - x_4) = 1 \quad (6.2.9)$$

which we again evaluate using the normalization conditions

for the f's. The results are listed in table 6a.

$N_5^{\Lambda Q}$	$N_5^{\bar{M}^* Q}$	$N_4^{M^* Q}$
12	24	6

Table 6a: The reformation function normalization factors.

6.3 RESULTS AND COMPARISON WITH EXPERIMENT

In this section we present the predictions of our model, (6.1.2)-(6.1.4), and compare them with the data using (6.1.5)-(6.1.8). All the integrals, after those over the δ -functions, are calculated numerically.

We begin by considering the differential forms of (6.1.2)-(6.1.4) with respect to the x of the heavy flavoured hadron at fixed $s^{\frac{1}{2}}$, in figures 6.2 to 6.12. We choose values of $s^{\frac{1}{2}}$ for which data exists, or is likely to in the future. Where there is data the agreement between theory and experiment is quite good at large $|x|$, while at small $|x|$ the data lies well above our predictions.

This is due to central production, which is not predicted by our model. Perturbative QCD does not really explain this either; (see Section 1.2). When a better model exists, the sum of its predictions and ours will hopefully account for the data at all values of x . We

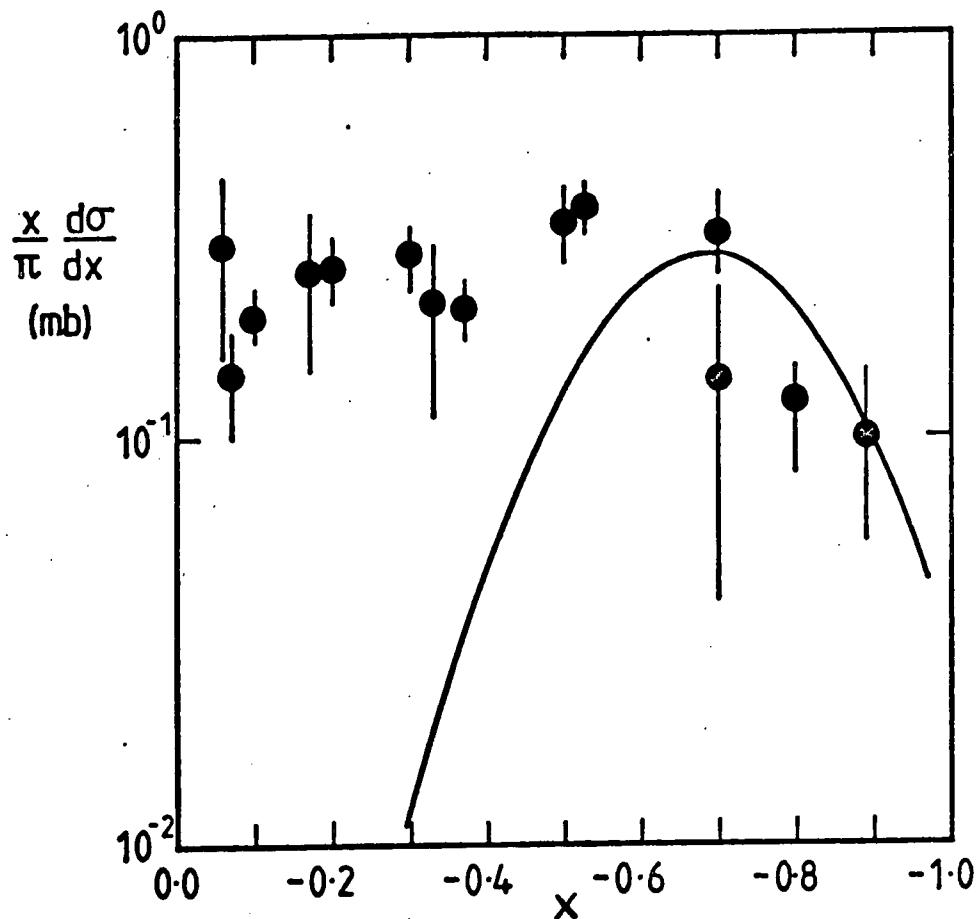


Figure 6.2: Our prediction for $\frac{x}{\pi} \frac{d\sigma}{dx}$ ($pp \rightarrow \Lambda_s^0 \bar{K} X$) at $s^{\frac{1}{2}} = 20$ GeV, compared with the data in a small $s^{\frac{1}{2}}$ -range centred on this value⁽⁴⁸⁾.

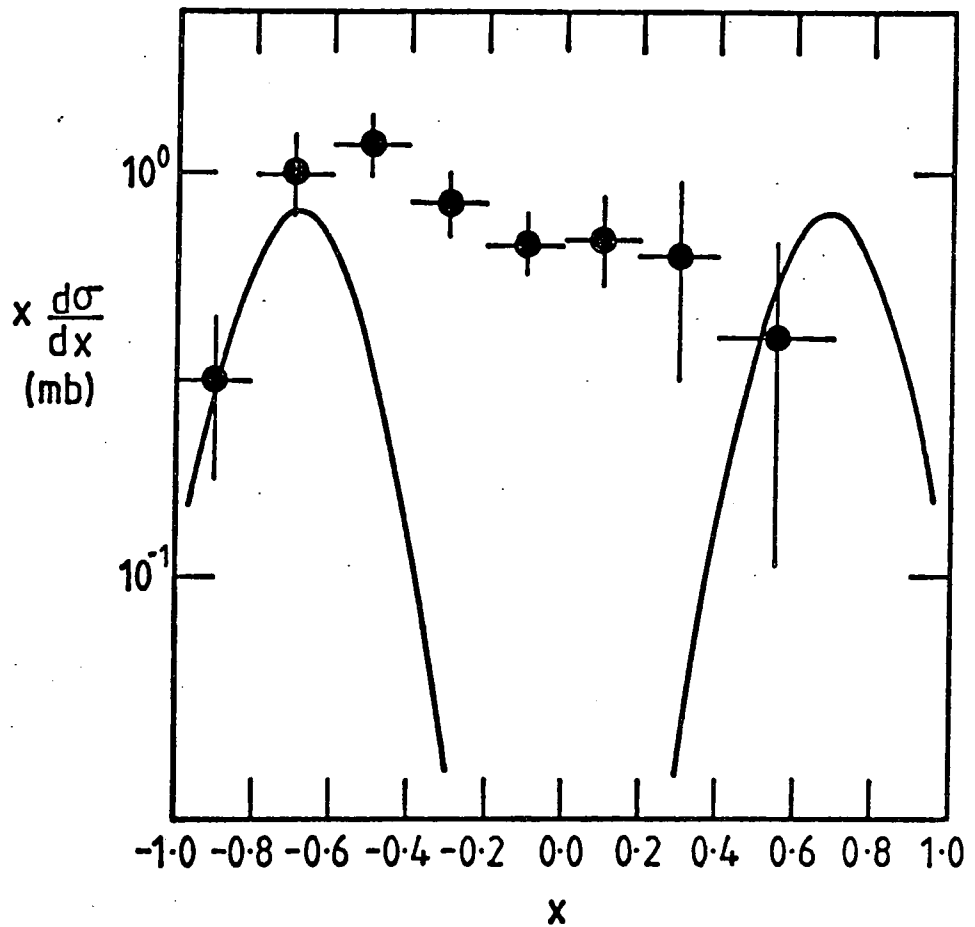


Figure 6.3: Our prediction for $x \frac{d\sigma}{dx}(pp \rightarrow \Lambda_S^0 \bar{K} X)$ at $s^{\frac{1}{2}} = 16.6$ GeV, compared with the data at this $s^{\frac{1}{2}}$ value (48). The experiment in reference 48 has a bias against fast forward ($x \rightarrow 1$) particles, hence the (unexpected) asymmetry in the data.

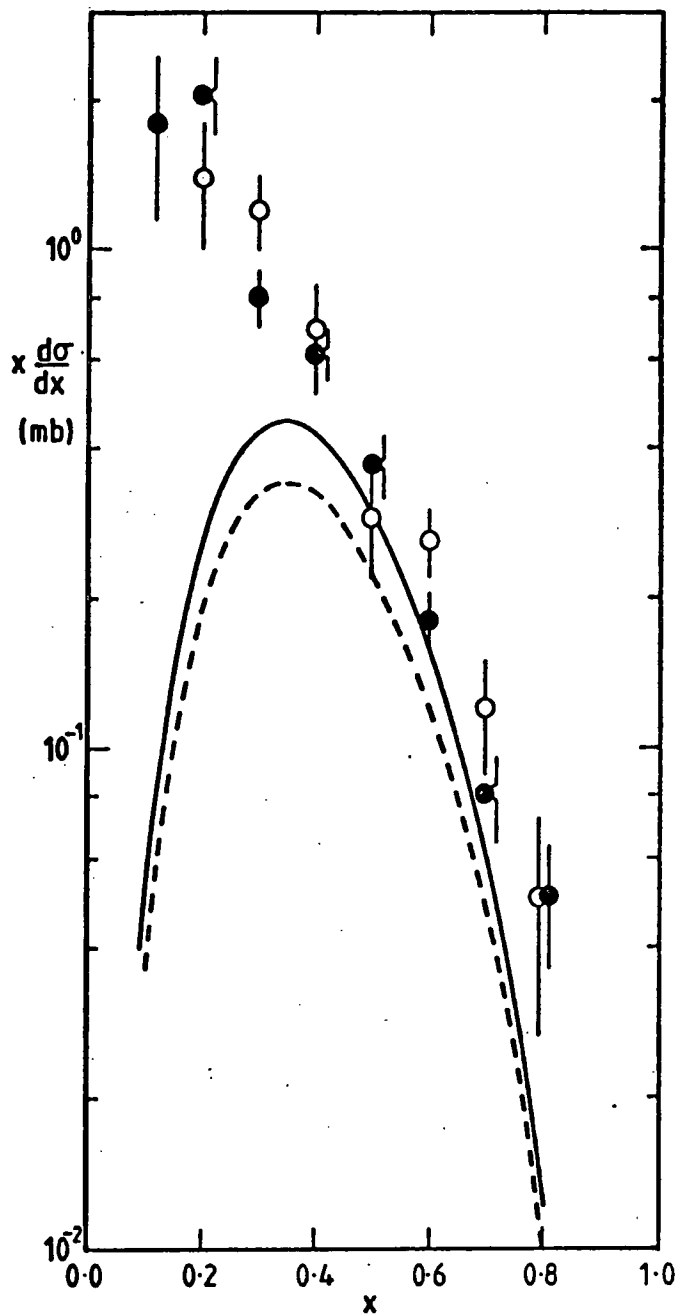


Figure 6.4: Our prediction for $x \frac{d\sigma}{dx}(pp \rightarrow K^+ K X)$ at $s^{\frac{1}{2}} = 13.7$ GeV (---) and 18.1 GeV (—), compared with the data at these values⁽⁴⁹⁾, o and • respectively. We assume 2/3 of the $\bar{K}K$ production is K^+K , considering the possibilities out of $|uuds\bar{s}\rangle$ which can form a K^+ .

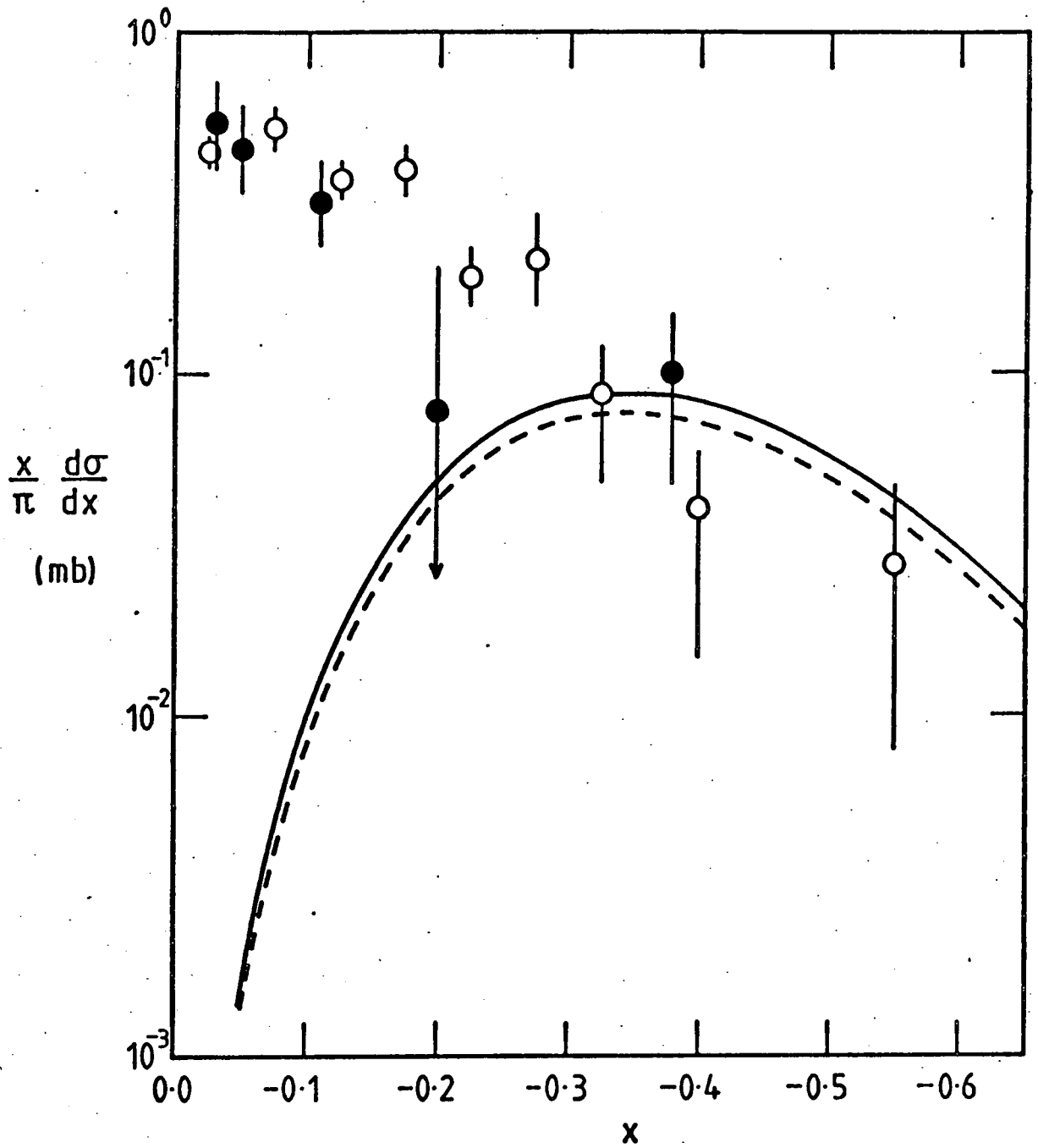


Figure 6.5: Our prediction for $\frac{x}{\pi} \frac{d\sigma}{dx}(pp \rightarrow K^0 K X)$ at $s^{1/2} = 19.6$ GeV (---) and 23.8 GeV (—), compared with the data at these values⁽⁴⁸⁾, o and • respectively. We assume 1/3 of the $\bar{K}K$ production is $K^0 K$, considering the possibilities out of $|uuds\bar{s}\rangle$ which can form a K^0 .

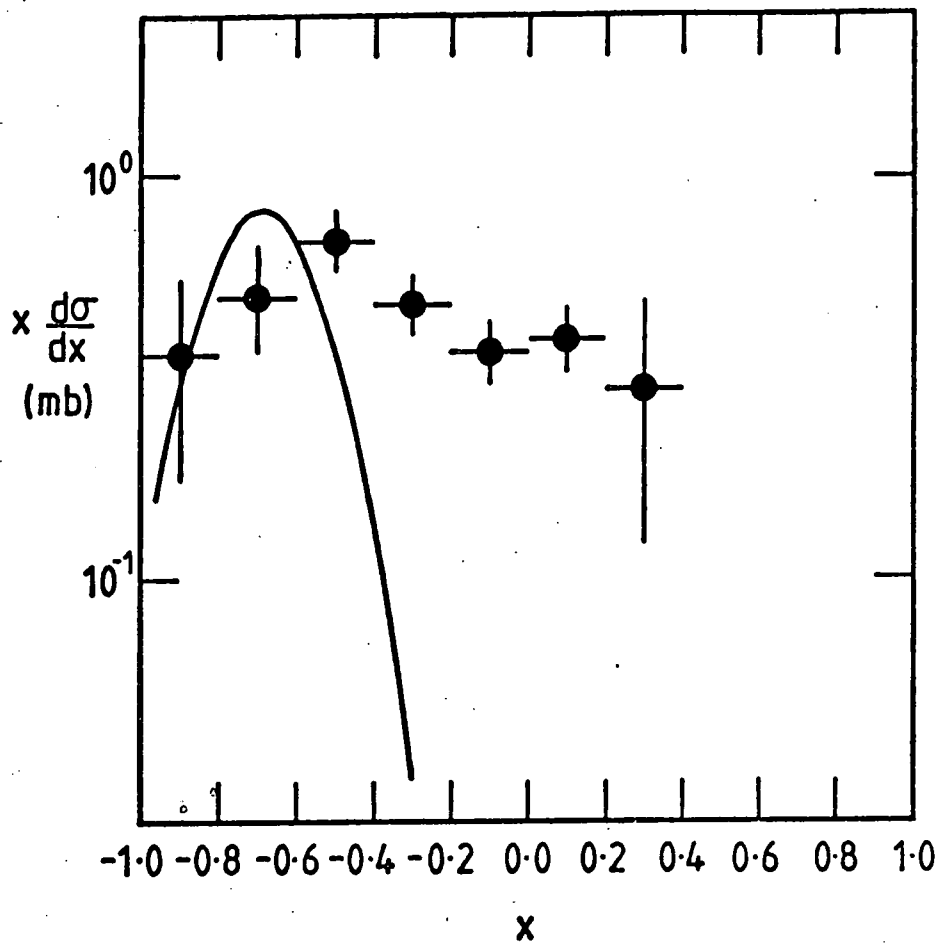


Figure 6.6: Our prediction for $x \frac{d\sigma}{dx}(\pi p \rightarrow \Lambda_S^0 \bar{K}X)$ at $s^{\frac{1}{2}}=16.6$ GeV, compared with the data at this $s^{\frac{1}{2}}$ value⁽⁴⁸⁾.

$x > 0$ is the pion direction.

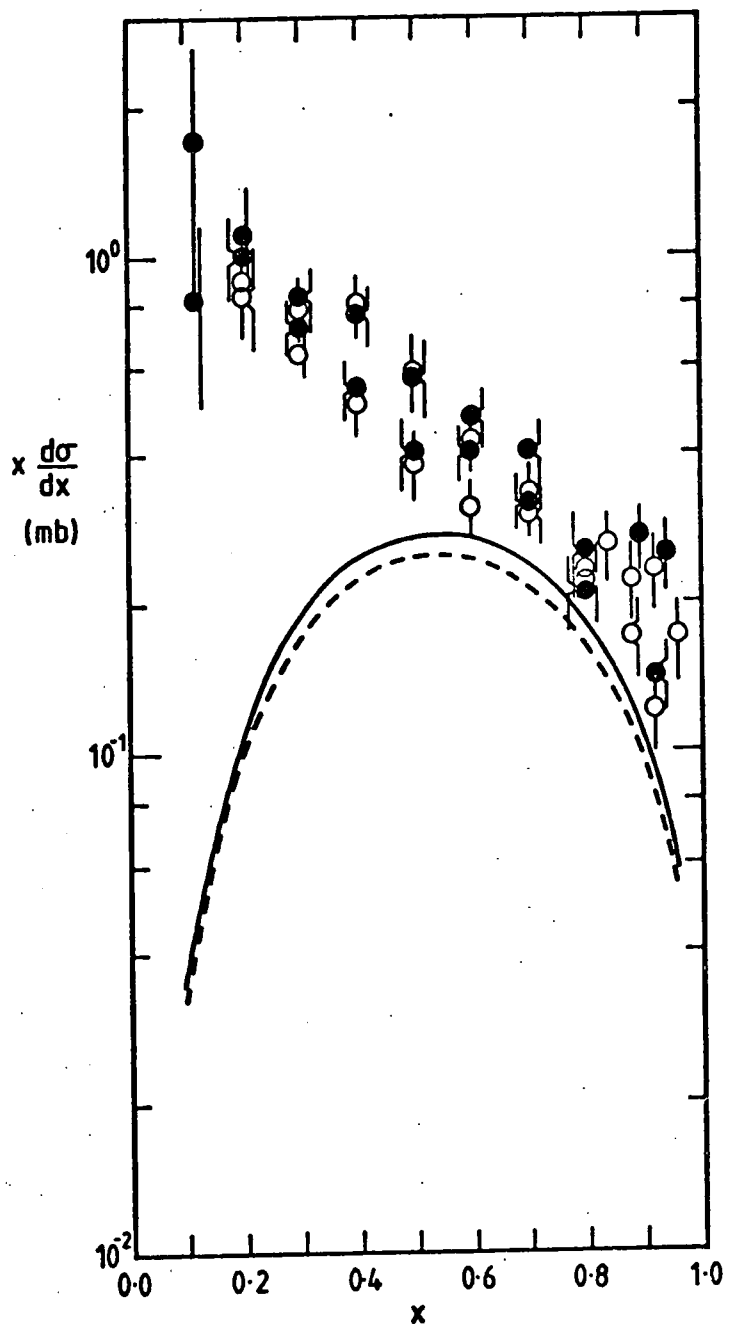


Figure 6.7: Our prediction for $x \frac{d\sigma}{dx}(\pi^- p \rightarrow K^- K^+ X)$ at $s^{1/2} = 13.7$ GeV (---) and 18.1 GeV (—) compared with the data at these values⁽⁴⁹⁾, o and ● respectively. $x > 0$ is the pion direction.

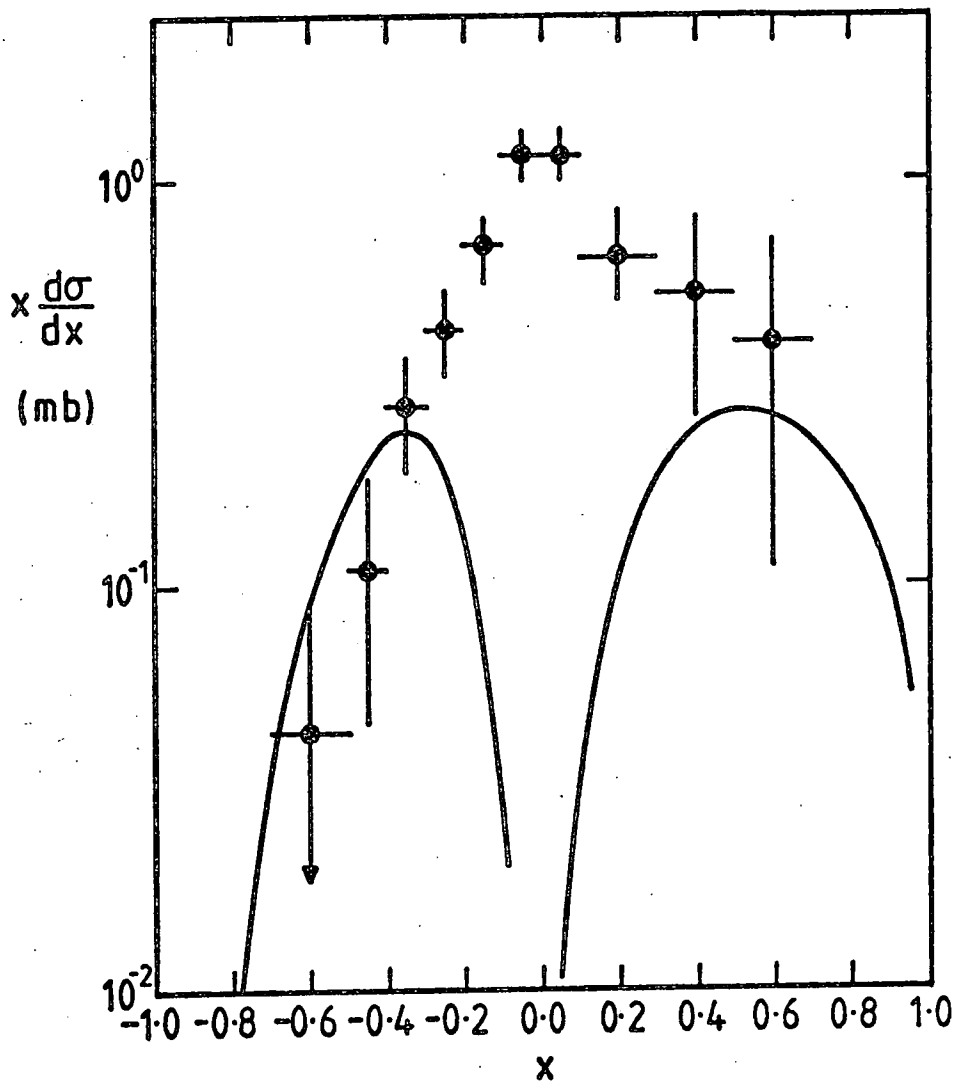


Figure 6.8: Our prediction for $x \frac{d\sigma}{dx}(\pi p \rightarrow K^0 K X)$ at $s^{\frac{1}{2}}=16.6$ GeV compared with the data at this $s^{\frac{1}{2}}$ value⁽⁴⁸⁾. $x > 0$ is the pion direction, and we again assume 1/3 of the $\bar{K}K$ production from the proton is $K^0 K$.

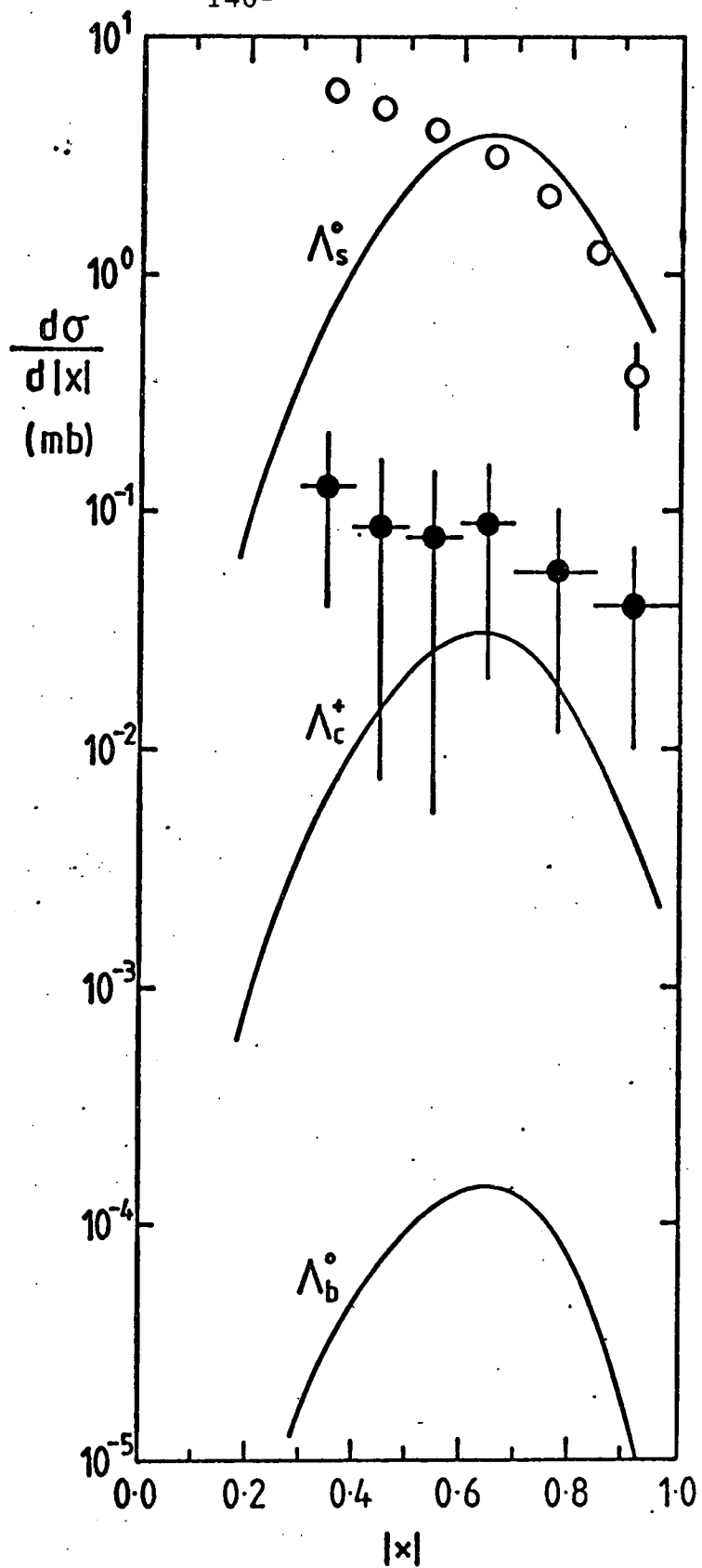


Figure 6.9: Our predictions for $\frac{d\sigma}{d|x|}$ ($pp \rightarrow \Lambda_Q \bar{M}_Q X$) at $s^{\frac{1}{2}}=53$ GeV for $Q=s$, and $s^{\frac{1}{2}}=64$ GeV for $Q=c, b$, compared with the $\Lambda_s^0(50)$ (o) and $\Lambda_c^+(51)$ (●) data at these respective energies.

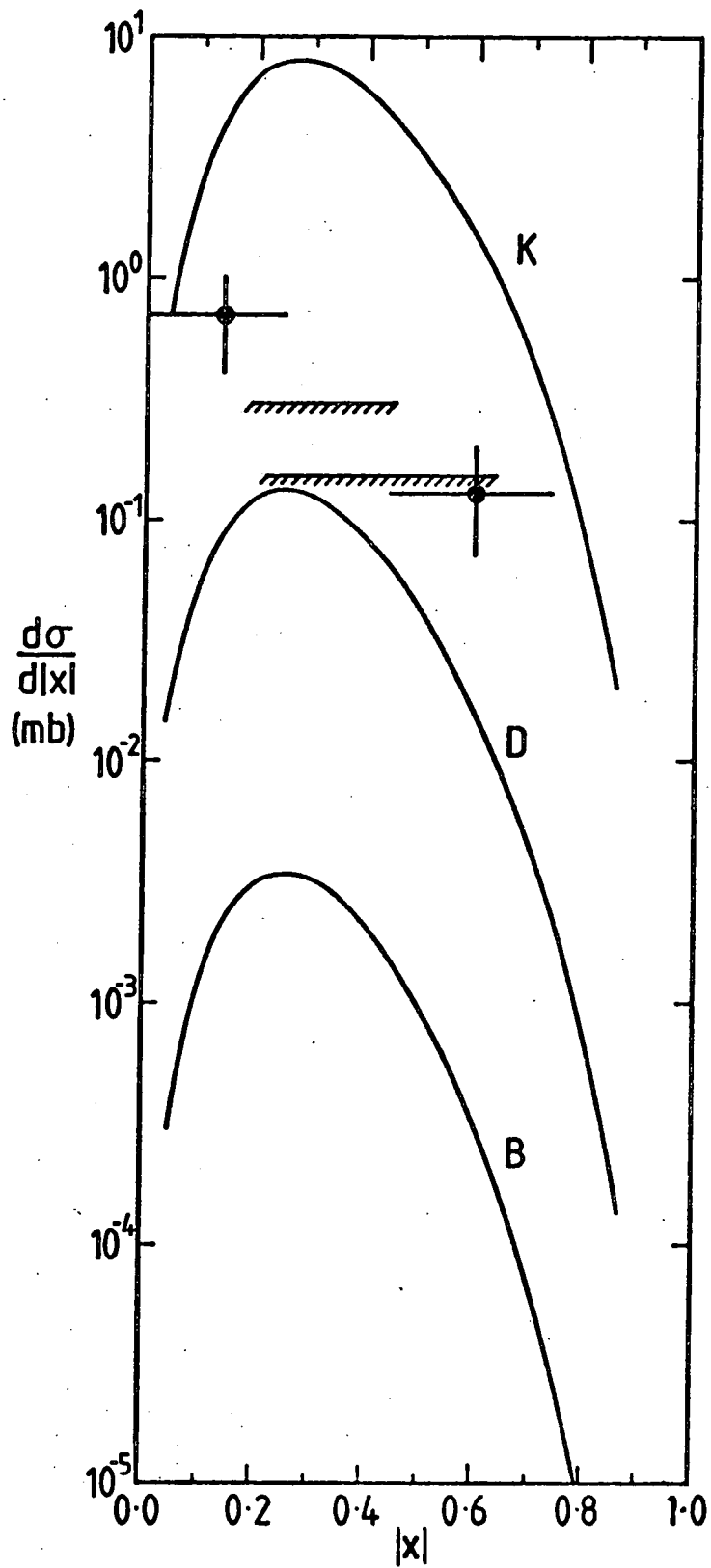


Figure 6.10: Our predictions for $\frac{d\sigma_d}{d|x|}$ ($pp \rightarrow \bar{M}_Q M_Q X$) at $s^{\frac{1}{2}} = 64$ GeV for $Q = s, c, b$, compared with the D-meson data⁽⁵¹⁾ at this value of $s^{\frac{1}{2}}$.

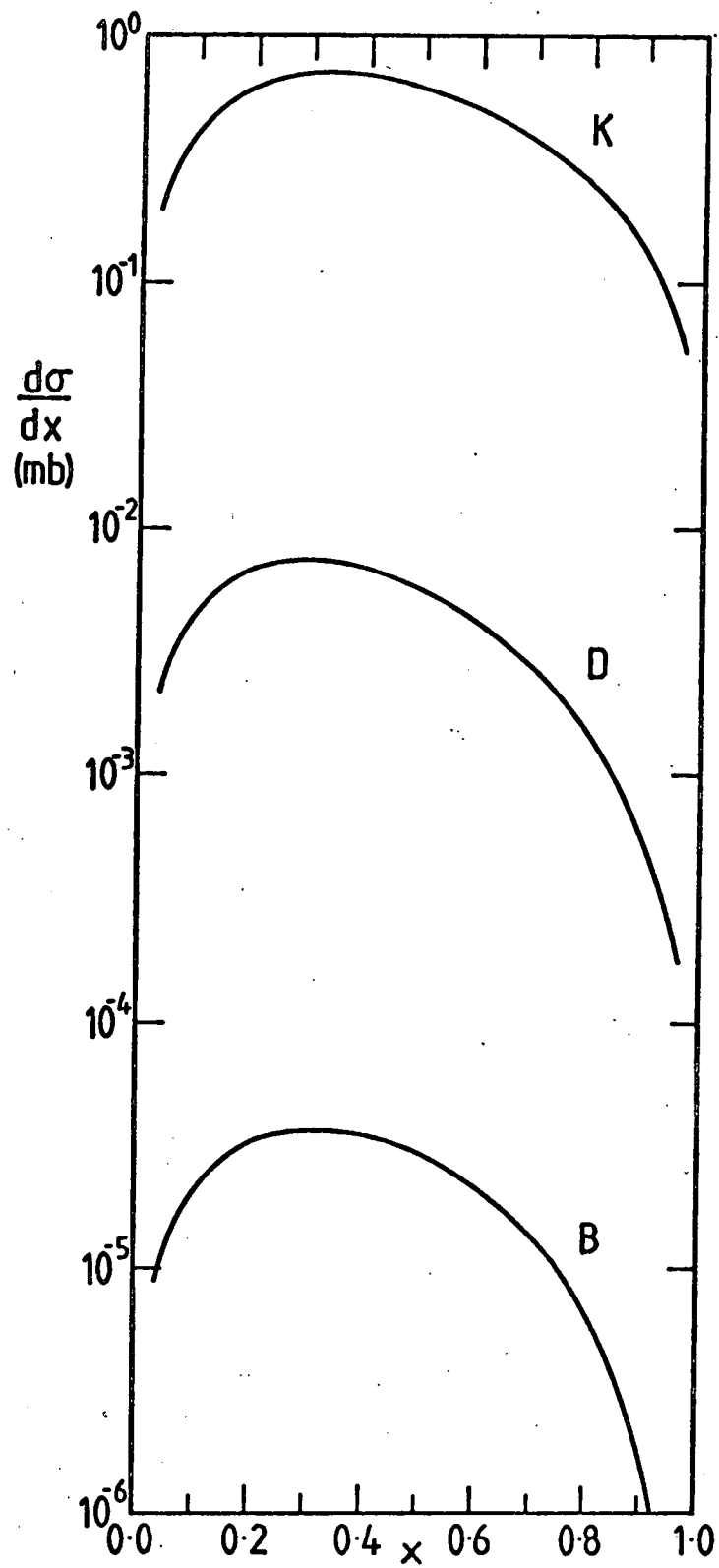


Figure 6.11: Our predictions for $\frac{d\sigma}{dx}(\pi p \rightarrow M_Q \bar{M}_Q X)$ at $s^{\frac{1}{2}}=26$ GeV for $Q=s,c,b$. $x>0$ is the pion direction.

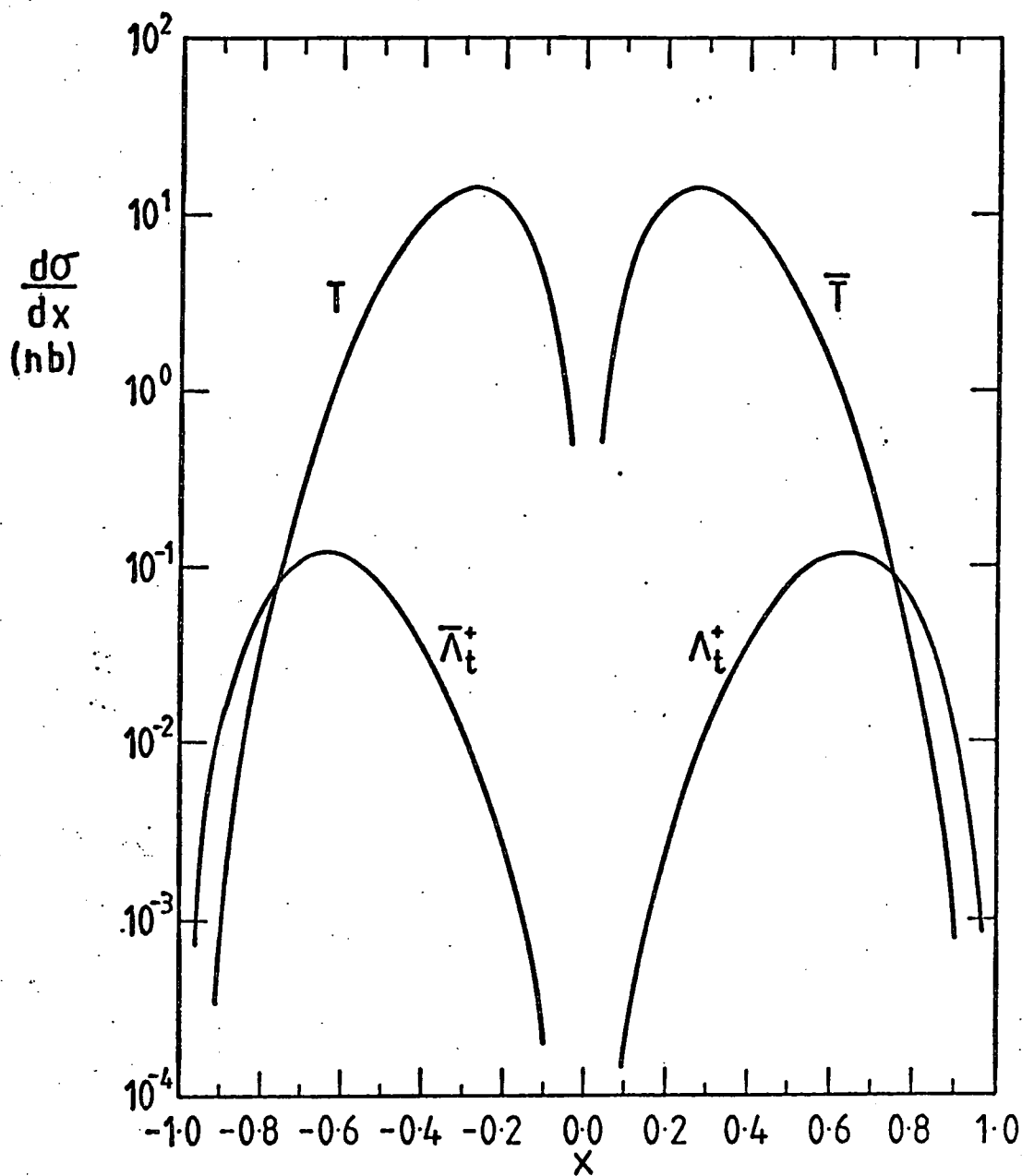


Figure 6.12: Our predictions for $\frac{d\sigma}{dx}(\bar{p}p \rightarrow T\bar{T}X)$ and $\frac{d\sigma}{dx}(\bar{p}p \rightarrow \Lambda_t^+ \bar{T}X / \bar{\Lambda}_t^+ TX)$ at $s^{\frac{1}{2}}=540$ GeV, for $m_t=35$ GeV and the lower α_{f_t} (o) from table 5b(b). With the higher intercept from table 5b(a) these curves should be multiplied by 8, and for the other choices of m_t may be scaled by the ratios of the cross-sections in tables 6b and 6c. $x>0$ is the proton direction.

estimate that our diffractive contribution is about 1/5 of the total production cross-section well above threshold.

Figure 6.12 shows our predictions for top production at the $\bar{p}p$ -Collider, as a function of x .

Our x -distributions are similar in shape to those of Brodsky et al⁽⁷⁾ and Barger et al⁽⁵⁾, but we also predict the normalization, rather than fitting to the charm data and assuming $(m_c/m_Q)^2$ scaling for heavier flavours.

Our suppression is somewhat greater (for the lower choice of the unknown heavy flavour Regge trajectory intercept), as shown in figure 6.13. This is due to the increasing difficulty of forming the heavy hadrons as m_Q increases. We also predict a decrease in the production ratio $\Lambda_Q \bar{M}_Q : \bar{M}_Q M_Q$ as m_Q increases, because to reform a Λ_Q requires two light valence quarks at progressively lower x , whereas an \bar{M}_Q requires only one.

We now consider the predictions of (6.1.2)-(6.1.4), as a function of $s^{\frac{1}{2}}$. The measured cross-sections for heavy flavour production, after rising from threshold, seem to tend to a constant fraction of the total cross-section. Our diffractive model predicts this behaviour, and so presumably the other (central) contribution has it as well.

To compare our predictions with experiment as a

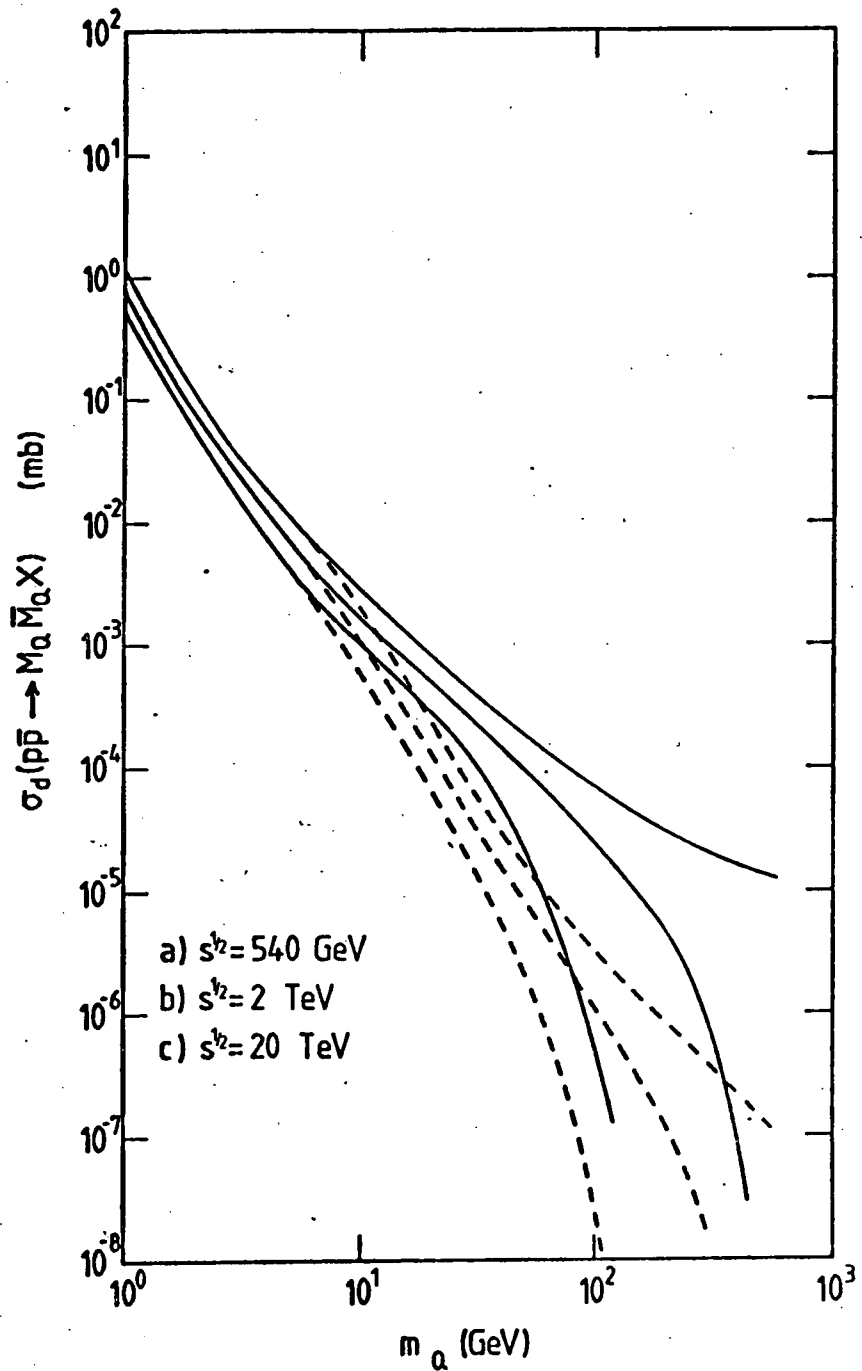


Figure 6.13: Our prediction for $\sigma_d(p\bar{p} \rightarrow \bar{M}_Q M_Q X)$ as a function of m_Q , for three values of $s^{1/2}$. At the branching the solid curve is for the higher Regge intercept model (ie $\alpha_{f_Q}(0) \propto -m_Q$), and the dotted curve for the lower ($\alpha_{f_Q}(0) \propto -m_Q^2$).

Figure 6.14: Our predictions for $\sigma_d(pp \rightarrow \bar{M}_Q M_Q X)$ or $\sigma_d(p\bar{p} \rightarrow \bar{M}_Q M_Q X)$ (—), and $\sigma_d(pp \rightarrow \Lambda_Q \bar{M}_Q X)$ or $\sigma_d(p\bar{p} \rightarrow \Lambda_Q \bar{M}_Q X / \bar{\Lambda}_Q M_Q X)$ (---), as functions of $s^{\frac{1}{2}}$, multiplied by 5 to allow for central production. Also shown is the pp (inelastic) data⁽⁵²⁾ (●), and that for strange⁽⁵³⁾ (∇), charm⁽⁵⁴⁾ (□) and bottom^(55,56) (○) production, with solid points for mesons and open points for baryons. Top production is shown for the lower α_{f_t} (o) from table 5b(b), and may be scaled to the higher values in table 5b(a) by multiplying by 6, 8, 10 for $m_t=25, 35, 45$ GeV respectively. The charm and bottom data is plotted assuming an $A^{2/3}$ dependence for the cross-section as a function of atomic mass number A , which is thought to be a better approximation than an A^1 dependence⁽⁵⁷⁾.

Figure 6.15: Our predictions for $\sigma_d(\Pi p \rightarrow M_Q \bar{M}_Q X)$ (—) and $\sigma_d(\Pi p \rightarrow \Lambda_Q \bar{M}_Q X)$ (---), as functions of $s^{\frac{1}{2}}$, multiplied by 5 to allow for central production. Also shown is the Πp (inelastic) data⁽³⁶⁾ (●), and that for strange^(36,53) (∇), charm⁽⁵⁸⁾ (□) and bottom⁽⁵⁹⁾ (○) production, with solid points for mesons and open ones for baryons. Λ_Q production is for $x < 0$, and D and B production is for $x > 0$ only, as this is what is measured experimentally. $x > 0$ is the pion direction. As in figure 6.14 the charm and bottom data is plotted assuming an $A^{2/3}$ dependence for the cross-section.

Figure 6.14.

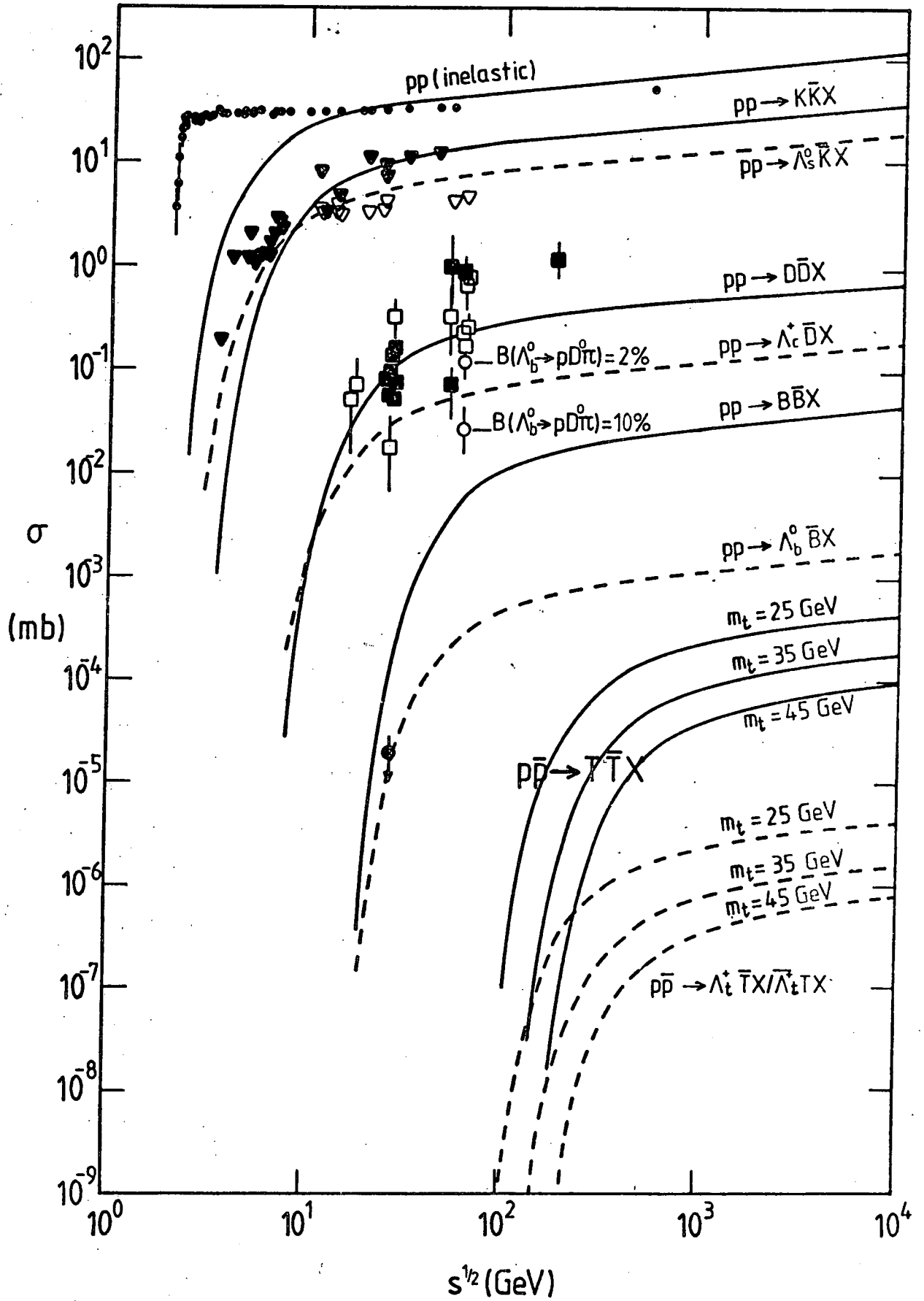
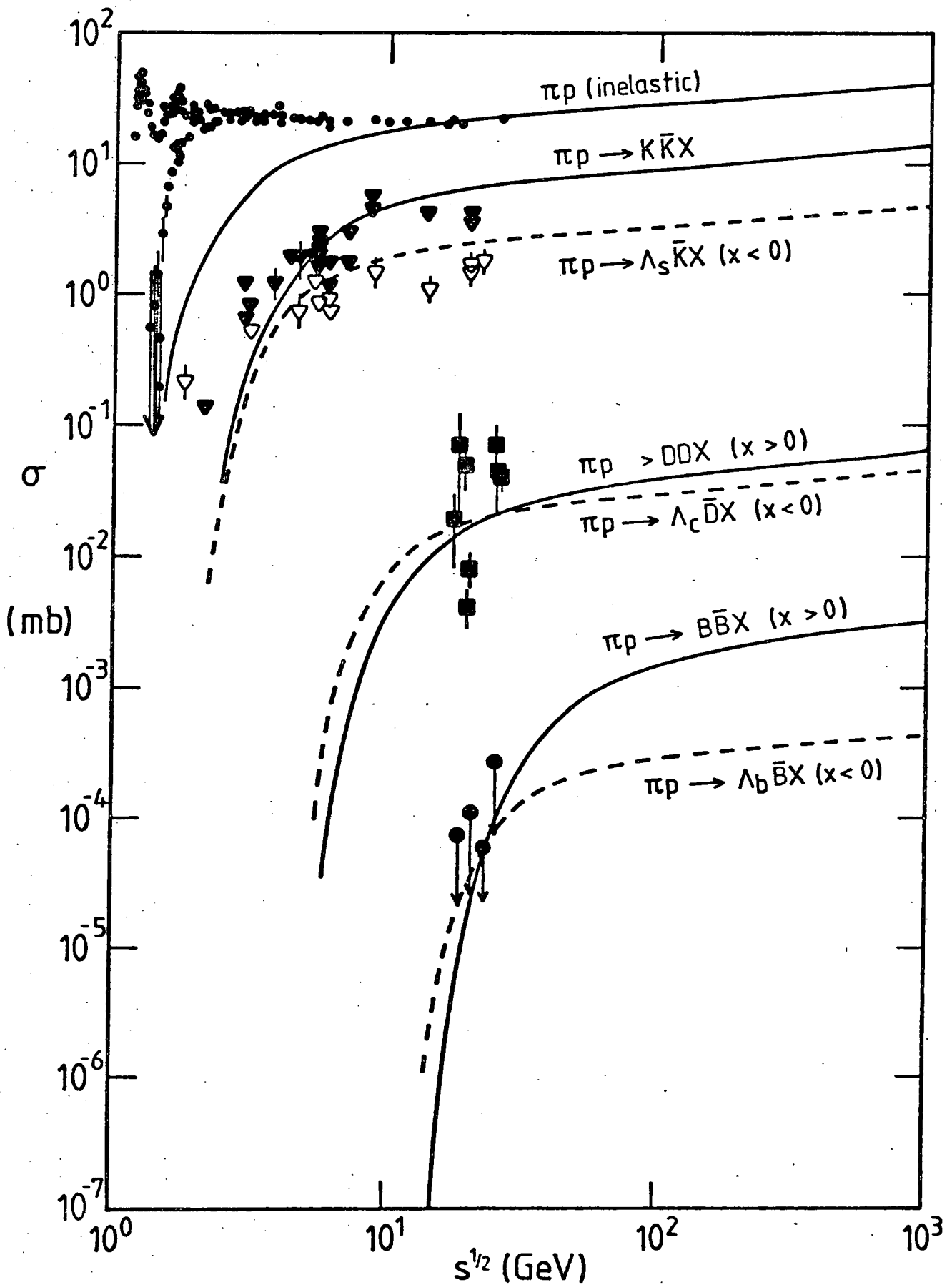


Figure 6.15



function of $s^{\frac{1}{2}}$ we therefore multiply by 5 to allow for central production. The results are shown in figures 6.14 and 6.15.

We extrapolate back to light (u,d) flavour production, to see how far the model may be pushed, being careful to avoid double counting (which is a negligible effect for the heavier flavour production). Figure 6.16 shows the various contributions to a total hadronic cross-section, and using that notation our calculated cross-sections are

$$\sigma_d(A \rightarrow B X) = g_{dA}(g_{eB} + g_{dB}) \quad (6.3.1)$$

$$\sigma_d(B \rightarrow A X) = g_{dB}(g_{eA} + g_{dA})$$

We require $\sigma_d(AB \rightarrow X)$, given by

$$\sigma_d(AB \rightarrow X) = g_{dA}g_{eB} + g_{eA}g_{dB} + g_{dA}g_{dB} \quad (6.3.2)$$

and, assuming $g_{dA}, g_{dB} > g_{eA}, g_{eB}$ (which is observed experimentally), make the approximation

$$\sigma_d(AB \rightarrow X) \approx \frac{1}{2}(\sigma_d(A \rightarrow B X) + \sigma_d(B \rightarrow A X)) \quad (6.3.3)$$

It is this quantity which is plotted in figures 6.14 and 6.15, again multiplied by 5 to allow for the central production.

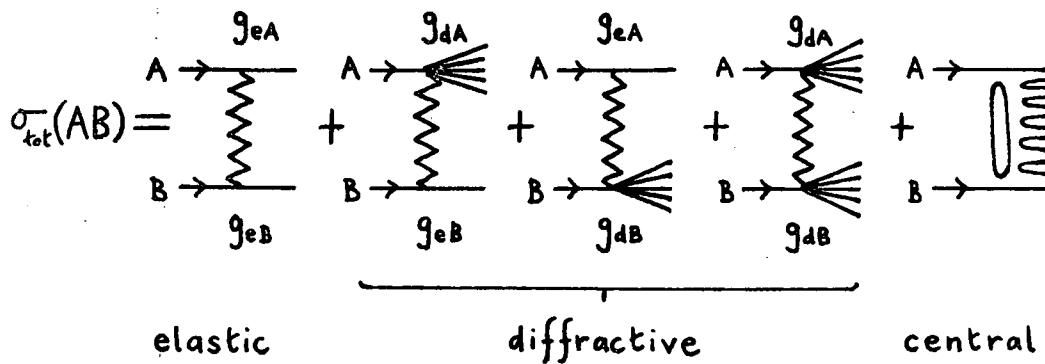


Figure 6.16: The different contributions making up $\sigma_{\text{tot}}(AB)$. The g 's are defined so that $\sigma_e(AB \rightarrow AB) = g_{eA}g_{eB}$ and $\sigma_d(AB \rightarrow X) = g_{dA}g_{eB} + g_{eA}g_{dB} + g_{dA}g_{dB}$.

The agreement between our predictions and the data is reasonably good, considering we have simply extrapolated our model to a region of m_Q for which it was not originally designed. It is also possible that the central and diffractive contributions have different m_Q -dependence, and so multiplying our predictions by 5 independent of m_Q is inaccurate. Improved data on charm and bottom production is required to examine this.

Figure 6.14 and 6.15 show that the threshold rise for u,d and s production is too slow. This is presumably because the central component rises faster than the diffractive one. Our naive method of allowing for central production is then only valid for $s^{\frac{1}{2}} \gg s_{th}^{\frac{1}{2}}$.

In figure 6.14 our prediction for total $B\bar{B}$ production is in conflict with the one data point⁽⁵⁵⁾, but as it is so near to threshold this does not unduly worry us. Our prediction for Λ_b^0 production is well below the (disputed) data⁽⁵⁶⁾.

All these calculations are done with $\langle k_T^2 \rangle^{\frac{1}{2}} = 0.45$ GeV and $\Lambda = 0.30$ GeV, which are essentially the only parameters in our model. These values are chosen to give the best overall agreement with the data, although for the heaviest quarks the results are insensitive to these choices.

Considering the range of both $s^{\frac{1}{2}}$ and m_Q over which we are predicting, and the quality of the present data, the agreement between theory and experiment is quite good.

6.4 LEPTONS FROM TOP QUARKS AT THE COLLIDER

Top quarks produced at the $p\bar{p}$ -Collider should reveal themselves through their leptonic decay^(60,61), shown in figure 6.17. The final state muons (electrons) can be detected if $k_{T1} \gtrsim 5(15)$ GeV, provided $\theta \gtrsim 10^\circ$. Leptons from the decay of diffractive top hadrons will mostly have $\theta < 10^\circ$ for any k_{T1} , because of the longitudinal momentum spectrum of figure 6.12.

However each diffractive top hadron leaves behind another top quark, whose x-distribution is calculable either by undoing the x_4 integral in (6.1.2) or the x_5 integral in (6.1.3). In both cases the result peaks at the origin, with essentially all of the distribution having $|x| < 0.05$, as shown, for example, in figure 6.18. This produces few leptons with $k_{T1} \gtrsim 5$ GeV and $\theta < 10^\circ$, since in the quark rest frame any lepton with $k_{T1} \gtrsim 5$ GeV has $\theta \gtrsim 20^\circ$ (for $m_t \sim 25-45$ GeV).

The hadronization of the top quark before its decay, either by fragmentation or recombination with a low-x sea quark, has a negligible effect on this argument, because the intrinsic k_T is small (~ 0.45 GeV) and

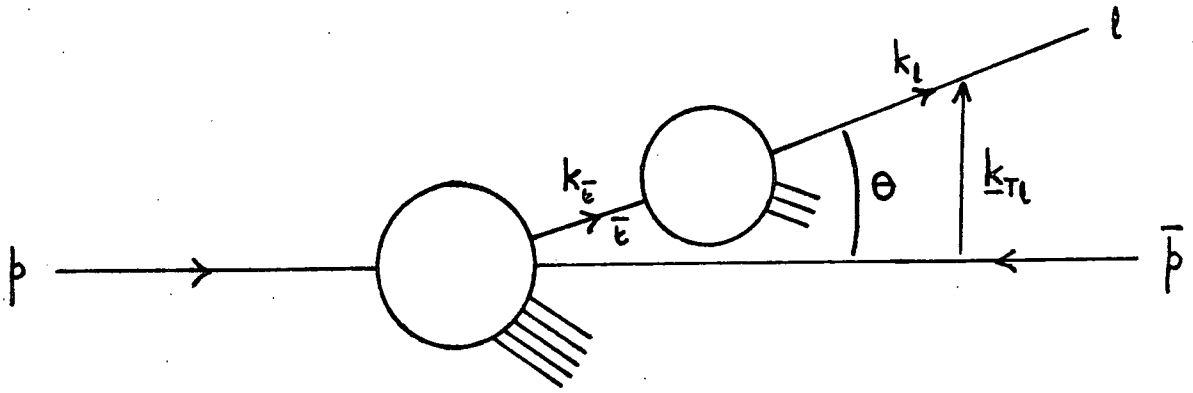


Figure 6.17: The lepton $l(\bar{l})$ from the decay of a top quark $\bar{t}(t)$ produced at the $p\bar{p}$ -Collider, showing the four-momenta. θ is the angle in the $p\bar{p}$ COM frame.

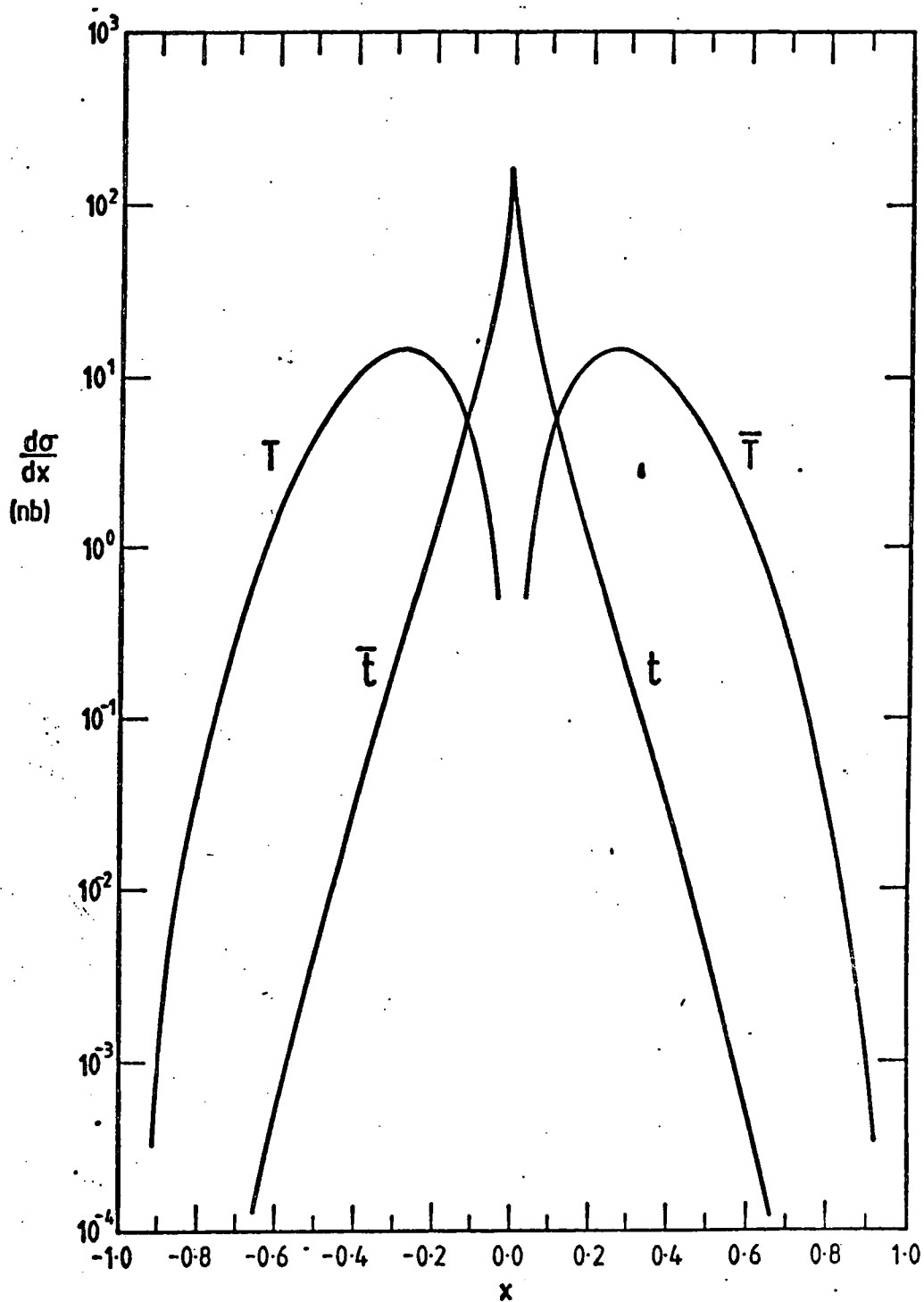


Figure 6.18: Our prediction for $\frac{d\sigma}{dx}d(p\bar{p} \rightarrow T\bar{T}X)$ at $s^{\frac{1}{2}}=540$ GeV, for the x of the diffractive \bar{T}/T , and that of the t/\bar{t} "left behind". $x > 0$ is the proton direction. We have taken $m_t=35$ GeV and the lower α_{f_t} (o) from table 5b(b).

$$m_T \approx m_t.$$

We therefore calculate the fraction of leptons with $k_{T1} \geq k_{TC}$ in the top quark rest frame, and assume all these have $\theta > 10^\circ$ in the $p\bar{p}$ COM frame, for $k_{TC} \geq 5$ GeV. Following Horgan and Jacob⁽⁶⁰⁾, we use the standard V-A weak interaction theory⁽¹⁰⁾ to calculate $\Gamma(t \rightarrow \bar{\nu}_1 b) (= \Gamma(\bar{t} \rightarrow \nu_1 \bar{b}))$, neglecting all final particle masses. The decay is shown in figure 6.19.

The amplitude is

$$A_{t \rightarrow \bar{\nu}_1 b} = 2^{-\frac{1}{2}} G \bar{u}_{\nu_1} \gamma^\alpha (1 + \gamma_5) u_t \bar{u}_b \gamma_\alpha (1 + \gamma_5) u_t \quad (6.4.1)$$

Substituting this into (1.4.2) for $N=3$ gives⁽⁶²⁾

$$\Gamma(t \rightarrow \bar{\nu}_1 b) = \frac{64G^2}{2m_t} \int \frac{d^3 \underline{k}_{\bar{1}}}{2(2\pi)^3 E_{\bar{1}}} \frac{d^3 \underline{k}_b}{2(2\pi)^3 E_b} \frac{d^3 \underline{k}_{\nu_1}}{2(2\pi)^3 E_{\nu_1}}$$

$$(2\pi)^4 \delta^4(k_t - k_{\bar{1}} - k_b - k_{\nu_1}) k_t \cdot k_{\bar{1}} k_b \cdot k_{\nu_1} \quad (6.4.2)$$

and so

$$E_{\bar{1}} \frac{d^3 \Gamma(t \rightarrow \bar{\nu}_1 b)}{d^3 \underline{k}_{\bar{1}}} = \frac{G^2 k_t \cdot k_{\bar{1}}}{4\pi^5 m_t} \int \frac{d^3 \underline{k}_b}{E_b} d^4 k_{\nu_1} \delta^4(k_t - k_{\bar{1}} - k_b - k_{\nu_1})$$

$$\delta(k_{\nu_1}^2) k_b \cdot k_{\nu_1} = \frac{G^2 k_t \cdot k_{\bar{1}}}{4\pi^5 m_t} \int dE_b d\Omega_b E_b \delta((k_t - k_{\bar{1}})^2 - 2k_b \cdot (k_t - k_{\bar{1}}))$$

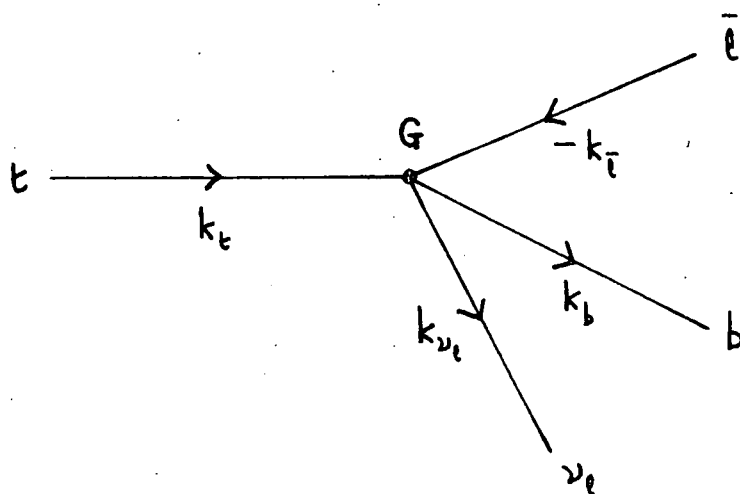


Figure 6.19: The leptonic decay of a top quark, showing the four-momenta. G is the weak coupling.

$$k_b \cdot (k_t - k_{\bar{1}}) \quad (6.4.3)$$

In the bv_1 COM frame

$$\delta((k_t - k_{\bar{1}})^2 - 2k_b \cdot (k_t - k_{\bar{1}})) k_b \cdot (k_t - k_{\bar{1}}) = \delta\left(\frac{(E_t - E_{\bar{1}})^2}{2} - E_b\right) \frac{E_b}{2} \quad (6.4.4)$$

Using this the remaining integrals in (6.4.3) are easy, with the result (written in invariant form)

$$E_{\bar{1}} \frac{d^3 \Gamma(t \rightarrow \bar{1} v_1 b)}{d^3 \underline{k}_{\bar{1}}} = \frac{G^2 k_t \cdot k_{\bar{1}} (k_t - k_{\bar{1}})^2}{8\pi^4 m_t} \quad (6.4.5)$$

We define the variables y , z , and the axis direction by

$$k_{\bar{1}}^+ \equiv z k_t^+ ; \quad m_t^2 y \equiv k_{\bar{1}T}^2 ; \quad \underline{k}_{Tt} \equiv \underline{0} \quad (6.4.6)$$

These give

$$\frac{d^3 \underline{k}_{\bar{1}}}{E_{\bar{1}}} = \frac{m_t^2 dz dy d\phi}{2z} \quad (6.4.7)$$

where ϕ is the angle defining $\underline{k}_{T\bar{1}}$. We introduce the branching ratio for $t \rightarrow \bar{1} v_1 b$,

$$B(t \rightarrow \bar{1} v_1 b) \equiv \frac{\Gamma(t \rightarrow \bar{1} v_1 b)}{\Gamma_{tot}} \quad (6.4.8)$$

Γ_{tot} being the total top quark width. Using these definitions in (6.4.5), with (1.5.6) for the dot products, we integrate over ϕ to get

$$\frac{d^2B}{dzdy}(t \rightarrow \bar{l} \nu_1 b) = \frac{G^2 m_t^5}{16 \pi^3 \Gamma_{\text{tot}} z} \left(z + \frac{y}{z}\right) \left(1 - z - \frac{y}{z}\right) \quad (6.4.9)$$

$k_{T\bar{l}}$ (and therefore, from (6.4.6), y) maximizes when the b -quark and ν_1 are collinear. Expanding $k_t^2 = (k_{T\bar{l}} + k_b + k_{\nu_1})^2$ for this situation, and using (1.5.6) for the dot products gives

$$m_t^2 = k_{T\bar{l}}^2 \left(\frac{z}{1-z} + \frac{1-z}{z} + 2 \right)$$

and so, using (6.4.6)

$$y = z(1 - z) \quad (6.4.10)$$

For leptons with $k_{T\bar{l}} \geq k_{TC}$ (ie $y \geq y_C \equiv \frac{k_{TC}^2}{m_t^2}$), the allowed region of yz space is shown in figure 6.20.

We define the dimensionless constant B_0 by

$$B_0 \equiv \frac{G^2 m_t^5}{16 \pi^3 \Gamma_{\text{tot}}} \quad (6.4.11)$$

and δB as the branching ratio for $b \rightarrow \bar{l} \nu_1 b$ with $k_{T\bar{l}} \geq k_{TC}$,

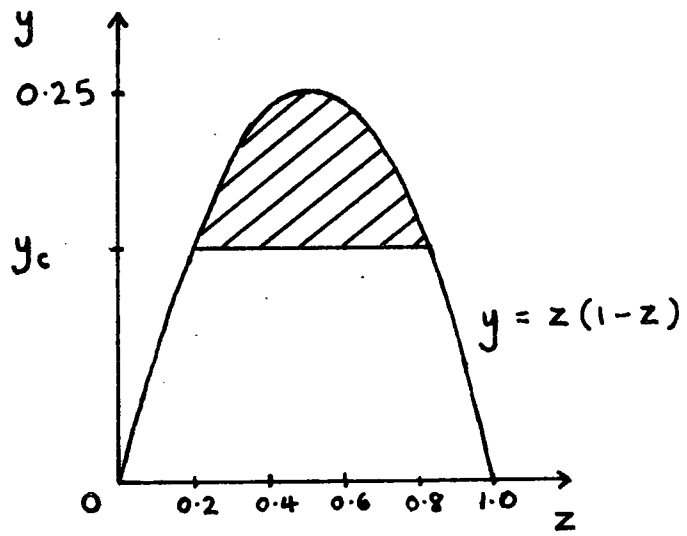


Figure 6.20: The yz plane, with the allowed region for leptons with $y \geq y_c$ shaded.

which is the subject of this calculation. Substituting (6.4.11) into (6.4.9), and integrating over the allowed area, we obtain

$$\delta B = B_0 \int_{\sqrt{\frac{1}{2} - (\frac{1}{4} - y_C)^{\frac{1}{2}}}}^{\sqrt{\frac{1}{2} + (\frac{1}{4} - y_C)^{\frac{1}{2}}}} dz \int_{y_C}^{z(1-z)} dy \quad (1 + \frac{y}{z^2})(1 - z - \frac{y}{z})$$

$$= B_0 \left[\frac{z}{6} - \frac{z^3}{6} + \frac{z^4}{12} - y_C z + \frac{y_C z^2}{2} + \frac{y_C^2}{2z} + y_C^2 \log z - \frac{y_C^3}{6z^2} \right]_{\sqrt{\frac{1}{2} - (\frac{1}{4} - y_C)^{\frac{1}{2}}}}^{\sqrt{\frac{1}{2} + (\frac{1}{4} - y_C)^{\frac{1}{2}}}}$$

(6.4.12)

which gives δB as a function of y_C . For the calculations we choose $B(t \rightarrow \bar{\nu}_1 b) = 0.1$. In the limit $y_C \rightarrow 0$, $\delta B \rightarrow B(t \rightarrow \bar{\nu}_1 b)$, so this choice fixes $B_0 = 1.2$.

Table 6b contains our predicted lepton yields from diffractive $T\bar{T}$ production at the $p\bar{p}$ -Collider, for three possible top quark masses. δB is calculated from (6.4.12), and the predicted numbers of leptons are for an assumed integrated luminosity of 100 nb^{-1} . The cross-sections are from figure 6.14, without the central production factor of 5. Remember these are for the smaller Regge intercepts from table 5b(b), and the larger intercepts from table 5b(a) give results bigger by 6, 8, 10 for $m_t = 25, 35, 45 \text{ GeV}$ respectively. If central production at the Collider really is 4 times larger than diffractive production, and these events

k_{TC} (GeV)	m_t (GeV)	25	35	45
		σ (nb)	30	9.1
5	$\sigma_{\delta B}$ (nb)	1.8	0.71	0.29
	No of leptons	180	71	29
8	$\sigma_{\delta B}$ (nb)	0.71	0.47	0.23
	No of leptons	71	47	23
15	$\sigma_{\delta B}$ (nb)	0	2.8×10^{-2}	6.8×10^{-2}
	No of leptons	0	3	7
20	$\sigma_{\delta B}$ (nb)	0	0	5.8×10^{-3}
	No of leptons	0	0	~ 0 or 1

Table 6b: The predicted lepton yields from $p\bar{p} \rightarrow T\bar{T}X$ at $s^{\frac{1}{2}}=540$ GeV.

produce a visible lepton with roughly the same probability as the diffractive ones, then all these results should be multiplied by 5 for the total (diffractive and central) lepton yields. We also consider the larger cut-off $k_{TC} = 8(20)$ GeV for muons (electrons).

Table 6c contains the corresponding predictions for leptons from diffractive $\Lambda_t \bar{T} / \bar{\Lambda}_t T$ production at the Collider.

k_{TC} (GeV)	m_t (GeV)	25	35	45
		σ (nb)	3.0×10^{-1}	8.5×10^{-2}
5	$\sigma \delta B$ (nb)	1.9×10^{-2}	6.7×10^{-3}	2.6×10^{-3}
	No of leptons	~ 2	~ 1	~ 0 or 1
8	$\sigma \delta B$ (nb)	7.3×10^{-3}	4.4×10^{-3}	2.0×10^{-3}
	No of leptons	~ 1	~ 0 or 1	~ 0 or 1
15	$\sigma \delta B$ (nb)	0	2.6×10^{-4}	6.1×10^{-4}
	No of leptons	0	0	0
20	$\sigma \delta B$ (nb)	0	0	5.1×10^{-5}
	No of leptons	0	0	0

Table 6c: The predicted lepton yields from $p\bar{p} \rightarrow \Lambda_t \bar{T} X / \bar{\Lambda}_t T X$ at $s^{\frac{1}{2}} = 540$ GeV.

From these numbers we conclude that if the top quark has a mass in the range we have considered, it

should be visible at the $p\bar{p}$ -Collider via its muonic,
and also possibly its electronic, decay, for an integrated
luminosity of $\sim 100 \text{ nb}^{-1}$.

CHAPTER 7

SUMMARY AND CONCLUSIONS

The aim of this work has been to develop a model for the diffractive production of heavy flavours in hadron scattering, predicting both the normalization and x -dependence of the production cross-sections.

Our model contains three ingredients; the initial distribution of intrinsic heavy quarks in the incident hadron, the heavy quark-hadron total cross-section, and the recombination function for producing heavy flavoured hadrons from the scattered quarks. In an interaction a hadron scatters on one of the intrinsic heavy quarks in the other hadron, with very little disruption of its initial x -distribution. The probability of the heavy quarks forming heavy hadrons is given by the overlap of this distribution with the recombination function, which is essentially the heavy hadron valence distribution. If the $Q\bar{Q}$ pair do not hadronize in this way, we assume they annihilate each other.

In Chapter 2 we modelled constituent valence quark distributions for all types of hadron. They are needed to calculate the heavy flavoured hadron recombination functions, and the $Q\bar{Q}$ distributions in light hadrons. For pions and nucleons we compared these valence

distributions with deep inelastic scattering data, and in each case found discrepancies, the theoretical peak being at larger x . This is expected because the data is for current quarks whereas our distributions are of constituent quarks, which are current quarks surrounded by a sea of $q\bar{q}$ pairs and gluons. If our distributions are probed by larger momentum transfers (in order to resolve the current quarks), they will be suppressed to smaller x by QCD evolution. This moves the theoretical curves in figures 2.5 and 2.6 towards the data, thus, one may suppose, resolving the discrepancies.

These valence distributions obey the dimensional counting rules as $x \rightarrow 1$, and by reciprocity should match up with their corresponding fragmentation functions as $z \rightarrow 1$. We investigated this in Chapter 3, where we modelled the fragmentation functions. For heavy quarks the dominant fragmentation process is $Q \rightarrow M_Q q$, so our predictions compare directly with experiment. Figure 3.2 and table 3a indicate the good agreement obtained for both charm and bottom fragmentation. We also give predictions for top quark fragmentation.

In Chapter 4 we calculated the intrinsic heavy quark distributions in light hadrons, assuming that the $Q\bar{Q}$ pair are created by a gluon emitted from one of the valence constituent quarks. Our prediction for charm production in deep inelastic scattering due to

intrinsic charmed quarks is under the data, even without a possible QCD evolution, as shown in figure 4.6. Since the data is already well described by the photon-gluon fusion model, this is necessary to avoid any conflict.

The remaining ingredient, the heavy quark-hadron total cross-section, was considered in Chapter 5. We modelled total hadronic cross-sections by introducing the idea of a light (valence) quark-hadron cross-section, dominated by Pomeron exchange at large s . We extended this to heavy quarks using the f -dominance hypothesis for the Pomeron-quark coupling. The rise of these cross-sections from threshold is limited both by dynamics ie the difficulty of forming the final state hadrons in the exclusive threshold process, and by kinematics ie the restricted range of t available at low s . Correcting for these effects, and using the hypothesis of generalized vector dominance enabled us to predict the cross-section for the photo-production of heavy flavours. Figure 5.5 shows the good agreement with the data for charm production.

We used these successes as the basis for our model of diffractive hadronic heavy flavour production, assuming the intrinsic heavy quarks in one hadron are scattered by the other, before reforming heavy flavoured hadrons. We constructed this model, and tested it against experiment, in Chapter 6. Figures 6.2 to 6.10

show good agreement with the data at large x , whereas at small x the data lies above our predictions because of central production. This presumably occurs through a quite different mechanism, and when a good model exists, its predictions added to ours should be able to account for the data at all x .

Central production appears to constitute about $4/5$ of the total cross-section, and so we multiplied our diffractive results by 5 before plotting them against the total cross-section data as a function of $s^{1/2}$ in figures 6.14 and 6.15. These figures also contain our predictions of the total cross-sections for bottom and top production. The data support the threshold rise built into the model, but suggest that central production rises faster than the diffractive component, at least for light flavours. (It is also possible that our threshold rise for the diffractive component is too slow for the lightest flavours; it was derived with heavy flavours in mind). We have extrapolated the model to light (u,d) flavour production, and obtain agreement with the data to better than a factor of 2 at large s . This is the most one should expect, since the assumptions in our model, (particularly the use of lowest order QCD to create the intrinsic $Q\bar{Q}$), cannot really be justified for light quark production.

The production of top quarks at the $p\bar{p}$ -Collider

is of particular interest at the moment, so we devoted Section 6.4 to calculating the large k_T lepton yield from our diffractive top production, for a range of m_t . The backgrounds to these leptons have been considered by various authors^(61,63), and the top signal should be clearly visible above them. There should also be associated jet activity from the bottom quark decay. We considered two possible top quark-proton cross-sections; the smaller of these is really a lower bound, so failure to observe leptons at or above the rate predicted using this would cast serious doubt on the existence of the top quark with a mass in the range $25 \lesssim m_t \lesssim 45$ GeV.

We discussed other models for hadronic production of heavy flavours in Section 1.2. The x -dependence we predict for the cross-sections is in sharp contrast to those from QCD perturbation theory models⁽³⁾, calculated using (1.2.1). These peak at $x=0$, but are unable to account for the observed magnitudes of central heavy flavour production. Our x -distributions of heavy flavoured hadrons are similar to those predicted by Barger et al⁽⁵⁾, Brodsky et al⁽⁷⁾ and Donnachie⁽⁶⁾, despite the rather different picture we adopt. However we predict the magnitudes of the diffractive cross-sections, rather than normalizing to the data, which is very important for extrapolating to top production.

We conclude, finally, that our diffractive model accounts for the present large x hadronic heavy flavour production data, and that all aspects of the model separately compare well with experiment. Hopefully more data will appear soon, adding further support; in particular if the top quark has $25 \lesssim m_t \lesssim 45$ GeV it should be visible at the $p\bar{p}$ -Collider.

REFERENCES

1. Hagedorn, R., CERN Report 71-12.
2. Peterson, C., Proc. of the Topical workshop on Forward Production of High Mass Flavours at Collider Energies, College de France, Paris (1979).
3. Jones, L.M., and Wyld, H.W., Phys. Rev. D17, 1782 (1978), Babcock, J., Sivers, D., and Wolfram, S., Phys. Rev. D18, 162 (1978), Carlson, C.E., and Suaya, R., Phys. Rev. D18, 760 (1978), Georgi, H.M., et al., Ann. of Phys. 114, 273 (1978), Hagiwara, K., and Yoshino, T., Phys. Lett. 80B, 282 (1979), Combridge, B.L., Nucl. Phys. B151, 429 (1979), Carlson, C.E., and Suaya, R., Phys. Lett. 81B, 329 (1979), Michael, C., and Winder, R., Nucl. Phys. B173, 59 (1980).
4. Reya, E., Physics Reports 69C, 3 (1981), Pennington, M.R., Reports on Progress in Physics 46, 393 (1983), and references therein.
5. Barger, V., Halzen, F., and Keung, W.Y., Phys. Rev. D24, 1428 (1981); D25, 112 (1982).
6. Donnachie, A., Z. Phys. C4, 161 (1980).
7. Brodsky, S.J., Peterson, C., and Sakai, N., Phys. Rev. D23, 2745 (1981).
8. Collins, P.D.B., An Introduction to Regge Theory and High Energy Physics, Cambridge University Press (1977).
9. e.g. Itzykson, C., and Zuber, J-B., Quantum Field Theory, McGraw-Hill (1980).
10. e.g. Okun, L.B., Leptons and Quarks, North-Holland (1982).

11. Mueller, A.H., Phys. Rev. D2, 2963 (1970), and ref. 8, Section 10.4.
12. Cutkosky, R.E., J. Math. Phys. 1, 429 (1960); Rev. Mod. Phys. 33, 446 (1961), and ref. 9, Section 6-3-4.
13. Close, F.E., An Introduction to Quarks and Partons, Academic Press (1979).
14. Collins, P.D.B., and Martin, A.D., Reports on Progress in Physics 45, 335 (1982).
15. Ref. 13, Section 9.1.3.
16. Callan, C., and Gross, D., Phys. Rev. Lett. 22, 156 (1969), Bjorken, J.D., and Paschos, E.A., Phys. Rev. 185, 1975 (1969).
17. Brodsky, S.J., and Farrar, G.R., Phys. Rev. Lett. 31, 1153 (1973), Matveev, V.A., Muradyan, R.M., and Tavkhelidze, A.N., Lett. al Nuovo Cimento 7, 719 (1973).
18. Gunion, J.F., Phys. Lett. 88B, 150 (1979).
19. Gilman, F.J., Physics Reports 4C, 95 (1972).
20. Drell, S.D., and Yan, T.M., Phys. Rev. Lett. 24, 181 (1970), West, G.B., Phys. Rev. Lett. 24, 1206 (1970).
21. Particle Data Group, Review of Particle Properties, Phys. Lett. 111B (1982). Chaveau, J., University of Rochester Pre-print COO-3065-362.
22. Quigg, C., and Rosner, J.L., Phys. Lett. 71B, 153 (1977); Physics Reports 56C, 167 (1979).

23. Kenyon, I.R., Reports on Progress in Physics 44, 1261 (1982).
24. de Groot, J.G.H., et al., Phys. Lett. 82B, 456 (1979), Steinberger, J., (CDHS collab.), Proc. of XX International Conference on High Energy Physics, Madison (1980).
25. Altarelli, G., and Parisi, G., Nucl. Phys. B126, 298 (1977).
26. Rith, K., Proc. of the International Europhysics Conference on High Energy Physics, Brighton, 80 (1983).
27. Ref. 13, Section 12.2.
28. Bjorken, J.D., Phys. Rev. D17, 171 (1978), Suzuki, M., Phys. Lett. 71B, 189 (1977).
29. Peterson, C., et al., Phys. Rev. D27, 105 (1983).
30. Söding, P., Proc. of the International Europhysics Conference on High Energy Physics, Brighton, 567 (1983).
31. Aubert, J.J., et al., Phys. Lett. 110B, 73 (1982).
32. e.g. Barger. V. and Phillips, R.J.N., Nucl. Phys. B73, 269 (1974).
33. Glück, M. and Reya, E., Phys. Lett. 79B, 453 (1978); Phys. Lett. 83B, 98 (1979), Leveille, J.P., and Weiler, T., Nucl. Phys. B147, 147 (1979).
34. Froissart, M., Phys. Rev. 123, 1053 (1961).
35. Donnachie, A., and Landshoff, P.V., Nucl. Phys. B231, 189 (1984).
36. Flaminio, V., et al., CERN-HERA 83-01 (1983).
37. Carlitz. R., Green, M.B., and Zee, A., Phys. Rev. D4, 3439 (1971).

38. Collins, P.D.B. and Wright, A.D.M., J. Phys. G: Nucl. Phys. 4, 1223 (1978).
39. Collins, P.D.B. and Gault, F.D., Nucl. Phys. B80, 135 (1974),
Collins, P.D.B., Gault, F.D., and Martin, A., Nucl. Phys. B83, 241 (1974).
40. Albrow, M.G., et al., Nucl. Phys. B108, 1 (1976).
41. Ref. 8, Section 10.8.
42. Sakurai, J.J., Ann. Phys. 11, 1 (1960).
43. Collins, P.D.B. and Wright, A.D.M., J. Phys. G: Nucl. Phys. 4, L201 (1978).
44. Collins, P.D.B. and Gault, F.D., Nucl. Phys. B112, 483 (1976); Nucl. Phys. B113, 34 (1976),
Collins, P.D.B., Gault, F.D., and Wright, A.D.M., J. Phys. G: Nucl. Phys. 4, 471 (1978).
45. Abe, K., et al., Phys. Rev. Lett. 51, 156 (1983).
46. Denby, B.H., et al., Phys. Rev. Lett. 52, 795 (1984).
47. Avery, P., et al., Phys. Rev. Lett. 44, 1309 (1980).
48. Brick, D., et al., Nucl. Phys. B164, 1 (1980).
49. Brenner, A.E., et al., Phys. Rev. D26, 1497 (1982).
50. Erhan, S., et al., Phys. Lett. 85B, 447 (1979).
51. Drijard, D., et al., Phys. Lett. 81B, 250 (1979),
Giboni, K.L., et al., Phys. Lett. 85B, 437 (1979),
Lockman, W., et al., Phys. Lett. 85B, 443 (1979),
Basile, M., et al., Lett. al Nuovo Cimento 30, 487 (1981),
Wojcicki, S., Proc. XXth International Conference on High Energy Physics, AIP, 68, 1430 (1981).

52. Flaminio, V., et al., CERN-HERA 79-03 (1979).
53. Whitmore, J., Physics Reports 10C, 273 (1974);
Physics Reports 27C, 187 (1976), and refs. 50 and 52.
54. Basile, M., et al., Il Nuovo Cimento 63A, 230 (1981);
65A, 457 (1981); 67A, 40 (1982),
Drijard, D., et al., Phys. Lett. 85B, 452 (1979),
Lockman, W., et al., Phys. Lett. 85B, 443 (1979),
Giboni, K., et al., Phys. Lett. 85B, 437 (1979),
Sajot, G., Proc. of XX International Conference on
High Energy Physics, Madison, 192 (1980),
Muller, F., Proc. of XX International Conference
on High Energy Physics, Madison, 193 (1980),
Irion, K., et al., Phys. Lett. 99B, 495 (1981),
Aguilar-Benitez, M., et al., Phys. Lett. 123B, 103 (1983),
Ushida, N., et al., Lett. al Nuovo Cimento 23, 577 (1978),
Clark, A.G., et al., Phys. Lett. 77B, 339 (1978),
Drijard, D., et al., Phys. Lett. 81B, 250 (1979),
Sandweiss, J., et al., Phys. Rev. Lett. 44, 1104 (1980),
Chilingarov, A., et al., Phys. Lett. 83B, 136 (1979),
Aziz, T., et al., Nucl. Phys. B199, 424 (1982),
Fuchi, H., et al., Proc. of 16th International Cosmic
Ray Conference, Kyoto, 6, 112 (1979),
Ritchie, J.L., et al., Phys. Rev. Lett. 44, 230 (1980),
Diamant-Berger, A., et al., Phys. Rev. Lett. 43,
1774 (1979),
Daum, C., et al., Proc. of XXI International
Conference on High Energy Physics, Paris, (1982),
Ball, R.C., et al., Phys. Rev. Lett. 51, 743 (1983).

55. Diamant-Berger, A., et al., Phys. Rev. Lett. 44, 507 (1980).
56. Basile, M., et al., Il Nuovo Cimento 65A, 391 (1981).
57. Halzen, F., Proc. of XXI International Conference on High Energy Physics, Paris, C3-381 (1982).
58. Fuchi, H., et al., Lett. al Nuovo Cimento 31, 199 (1981),
Fitch, V.L., et al., Phys. Rev. Lett. 46, 761 (1981),
Badertscher, A., et al., Phys. Lett. 123B, 471 (1983),
Aguilar-Benitez, M., et al., Phys. Lett. 123B, 98 (1983),
Koester, L.J., et al., Proc. of XX International Conference on High Energy Physics, Madison, 190 (1980),
Barloutaud, R., et al., Nucl. Phys. B172, 25 (1980),
Daum, C., et al., Proc. of XXI International Conference on High Energy Physics, Paris, (1982),
Buchholz, D., et al., Proc. of XVII Recontre de Moriond, 377 (1982).
59. Badier, J., et al., Phys. Lett. 124B, 535 (1983),
Barate, R., et al., Phys. Lett. 121B, 449 (1983),
Albanese, J.P., et al., Phys. Lett, 122B, 197 (1983),
Coleman, R.N., et al., Phys. Rev. Lett. 44, 1313 (1980).
60. Horgan, R., and Jacob, M., Phys. Lett. 107B, 395 (1981);
TH.3682-CERN (1983).
61. Barger, V., Martin, A.D., and Phillips, R.J.N.,
Phys. Lett. 125B, 339, 343 (1983); Phys. Rev. D28, 145 (1983).
62. Ref. 10, Section 3.1.
63. Baer, H., Barger, V., Martin, A.D., and Phillips, R.J.N.,
Madison preprint MAD/PH/133 (1983).
64. Odorico R., Phys. Lett. 107B, 231; 118B, 425.

